CONTROLLING THE SPATIAL DEPOSITION OF ELECTROSPUN FIBRE

A Dissertation

Presented to

The Department of Mechanical Engineering

College of Engineering

University of Canterbury

In Partial Fulfilment

of the Requirements for the Degree

Doctor of Philosophy

Nurfaizey Abdul Hamid

2014

ACKNOWLEDGEMENTS

I would like to express my greatest appreciation to my supervisor Dr. Mark P. Staiger, co-supervisor Dr. Nick Tucker, assistant supervisors Dr. Alan Wood and Neil Buunk for their constant guidance, remarks and engagement through the learning process of this project. Without their encouragement and support, this manuscript would not have materialized.

A heartfelt thanks to the staff at Plant and Food Research Lincoln for their kind help and support; especially Dr. Nigel Larsen, Dr. Hussam Razzaq, Andrew Wallace, Alasdair Noble, Donna Gibson, Robert Lamberts, Naomi Shaw and Tom Finger. Also I would like to thank the staff at the Department of Mechanical Engineering, University of Canterbury; especially Kevin Stobbs, Mike Flaws, Julian Phillips, Scott Amies, and David Read. A special thanks to Electrospinz Ltd, Blenheim who kindly loaned certain pieces of equipment throughout the study.

Special appreciation goes to my sponsors, the Department of Higher Education Malaysia (MOHE) and Universiti Teknikal Malaysia Melaka (UTeM) for their financial support. I also appreciate the personal and professional support received from my colleagues and friends especially Dr. Jon Stanger, Pablo Lepe, Dr. Deborah Le Corre, and members of the Malaysian Postgraduates Association of Canterbury (MPAC) and their families.

Apart from the above mentioned individuals, the success of this study partly depended on the support and encouragement received from my loved ones. For this, a heartfelt thank you to my wife Rita Hashim, my daughter Aliah Natasha and my son Iqmal Danial and not forgetting my relatives in Malaysia. Last but not least, I would like to dedicate this work to my late father Abdul Hamid Mat Akil and to my late mother Jasminah Asmuni who recently passed away during the writing of the thesis. May God bless their souls.

ABSTRACT

Electrospinning process is a simple and widely used method for producing polymeric nanofibres. However, despite its popularity, significant challenges remain in controlling the fibre deposition due to the complex nature of electrospinning process. The process is renowned for its chaotic motion of fibre deposition, also known as the whipping instability. This instability is caused by electrostatic and fluid dynamics interactions of the charged jet and it is partly responsible for the thinning of the fibres into nanoscale diameters. Due to the instability, an electrospinning process typically deposits random orientated fibres in a circular deposition area. Furthermore, there is no control over the location where the fibres land on the collector electrode except that the fibres always travel through the shortest trajectory between the source and the collector electrodes.

In this study, an alternative controlled deposition technique was proposed based on electric field manipulation (EFM). The main hypothesis of this study is that a consistent and repeatable method of controlled deposition can be achieved by using EFM. EFM was achieved by introducing a pair of charged auxiliary electrodes positioned adjacent and perpendicular to the fibre deposition direction. The applied voltage of either direct current (dc) or time-varying (ac) voltage at the auxiliary electrodes act as control to influence the spatial location and size of the deposition area. Samples were produced on black paper substrates and scanned into greyscale images. An image analysis technique was developed to measure the shift and size of the deposition area. A computer simulation was used to calculate the electric field strength and to simulate the behaviour of fibre response based on the trajectory of a charged particle. An image analysis based on greyscale intensity measurement was also developed to examine the uniformity of the deposition area. Finally, fibre characterisation was carried out to examine the fibre morphology, diameter, and orientation based on scanning electron micrographs.

The results from this study showed that EFM can provide a consistent and repeatable control of the deposition area. When the auxiliary electrodes were independently charged with two dc

voltages, it was observed that the deposition area moved away from the most positive electrode. The magnitude of shift of the deposition area was found to increase linearly with voltage difference between the auxiliary electrodes. Furthermore, the aspect ratio of the deposition area (ratio of width over height) decreased linearly with base voltage *i.e.* lower of the two auxiliary electrode voltages. These two controls were found to act independently from each other and can be described as two separate controls *i.e.* voltage difference for spatial location and base voltage for aspect ratio of the deposition area. A similar response was observed in simulation *i.e.* the particle moved away from the most positive electrode. Simulation results also showed that the x-axis component of the electric field (E_x) was responsible for the shift in location and the reduction of aspect ratio of the deposition area.

When the auxiliary electrodes were charged with two antiphase time-varying voltages, continuous scanning of the electrospinning jet was observed producing a wide electrospun fibre mat. It was first thought the smooth oscillation of a sine wave would produce a more uniform deposition pattern compared to a triangle wave, but the results showed otherwise. The inferior uniformity of the sine wave sample was found due to the variability of the jet scanning speed when compared to the constant speed achieved when using a triangle wave. It was also observed that the deposition pattern can be further improved by using two clipped triangle wave voltages. The results open up the possibility for further exploiting the control voltage to achieve the desired deposition pattern.

Two case studies were presented to demonstrate the applicability of the technique in real electrospinning applications. In the first case study, it was demonstrated that the continuous scanning of electrospinning jet was capable of eliminating the stripe deposition pattern which is commonly associated to a multi-spinneret electrospinning system. In the second case study, it was found that the alignment and distribution of aligned fibres in a gap electrospinning system can be improved by using the EFM technique. A new technique was also introduced to produce a multi-layer orientated fibre construct. These application examples showed that the EFM technique is ready for the production of engineered electrospun fibre constructs. This would extend the use of electrospun fibres to applications which is currently limited by geometrical constraints of the fibre constructs.

TABLE OF CONTENTS

LIST OF TABLES

LIST OF FIGURES

CHAPTER 1

INTRODUCTION

Electrospinning is known as a simple, versatile, and scalable method of producing polymeric nanofibres from a solution or melt using electric charge (Reneker and Chun, 1996). Due to their nanoscale diameters, electrospun fibres have been the subject of much study for applications that require a high surface area to volume ratio (Nayak et al., 2012, Greiner and Wendorff, 2007). A wide variety of applications such as filtration, tissue engineering, wound dressing, drug delivery, composite reinforcement, and electronics, have been proposed (Ramakrishna et al., 2005). However, due to the random nature of the deposition process in electrospinning it is difficult to tailor the deposited fibres for specific needs. Despite a number of potential applications, controlled deposition in electrospinning has not been widely investigated. Thus, it is not surprising that the one application in which electrospun fibres have achieved commercial success so far is filtration (Nurfaizey et al., 2012b).

The objective of this study is to develop, validate, and demonstrate a method of controlled deposition of electrospun fibres based on electric field manipulation (EFM). This study is important as it is the first to quantitatively investigate EFM. In addition, developing a successful EFM method would extend the use of electrospun fibres to applications which is currently limited by geometrical constraints of the fibre constructs. To achieve this objective, a series of experiments were conducted to investigate the practicalities of applying EFM in electrospinning. EFM is achieved by introducing charged auxiliary electrodes that are positioned adjacent and in the plane perpendicular to the direction of electrospinning. The application of an electric field *via* the auxiliary electrodes can be used to manipulate the spatial and areal characteristics of a collection of electrospun fibres.

Controlled deposition in electrospinning is used for two main purposes: (i) control of the location of the deposition area in order to produce uniform coverage of electrospun fibres;

and (ii) production of constructs consisting of aligned fibres. For example, a significant challenge in the synthesis of filtration membranes *via* electrospinning is in achieving a spatially uniform deposition of electrospun fibres. The problem of achieving a uniformly distributed collection of fibres is particularly pronounced in the case of a multi-spinneret system due to electrostatic repulsion between adjacent jets that are like-charged (Theron et al., 2005). Various multi-spinneret setups with mechanically moving collectors or spinning heads have been described with the aim of producing uniform coverage of electrospun fibres (Filatov et al., 2007). Aligned fibres on the other hand are conventionally obtained by mechanical means such as rotating drums (Boland et al., 2001), moving spinning heads or collectors (Sun et al., 2006), or using patterned collectors or gap electrospinning (Li et al., 2003).

The methods based on mechanically moving components are complex which require a higher level of supervision and maintenance of the apparatus (Nurfaizey et al., In press). In terms of mechanically collecting aligned fibres, the inertia of the mechanical system imposes an upper limit to the maximum speed of any electrospinning system. Considerable success has been reported in producing aligned fibres using gap electrospinning (Li et al., 2003); however, a major drawback of the process is that it is highly dependent on the geometry of the collector. In addition, residual charges build up on the suspended fibres across the gap have significant influence on the degree of orientation of the fibres (Liu and Dzenis, 2008).

It was suggested that based on an EFM method, controlled deposition of electrospun fibres can be achieved by manipulating the electric field to some degree (Deitzel et al., 2001). Electrospun fibres carry an amount of electric charge during flight, so it is reasonable to expect that using EFM the trajectory of the fibres can be influenced up to the point of impact of the fibre with the collector. However, concern arises from the need to know the relationship between the control variables and fibre response, namely the applied voltages at the auxiliary electrodes and magnitude of deflection of the fibres. The resulting magnitude of deflection of the fibres must be consistent and repeatable in order for EFM to be a useful control system. To the author's knowledge, there have been no previous studies that have attempted to quantitatively describe the response of the fibres to EFM. Finally, the challenge is to demonstrate how the newly developed technique could address practical issues in a large scale electrospinning environment.

A major advantage of EFM over mechanical techniques is that it would allow for extremely rapid, if not instantaneous, control of the charged jets (Bellan and Craighead, 2006). As no moving parts are involved in EFM, the speed of response of the system is only limited by the speed at which the electrical field can be manipulated rather than the speed at which the mechanical assembly of spinning or collection can be physically moved (Nurfaizey et al., 2012a).

The thesis begins with a literature review (Chapter 2) that covers the historical background of electrospinning, an introduction to the electrospinning process, and previous attempts to control deposition during electrospinning. The basic experimental procedures are then presented in Chapter 3 in order to describe the main experimental apparatus used, materials, sample substrate, and fibre characterization techniques. Specific experimental procedures and results and discussion for each experimental work are presented in Chapter 4, Chapter 5, Chapter 6, and Chapter 7. A general and discussion is presented in Chapter 8 and finally, the conclusions are presented in Chapter 9 along with recommendations for future works.

CHAPTER 2

LITERATURE REVIEW

2.1 Historical background

The history of the scientific developments underpinning electrospinning began more than 400 years ago. The first recorded description of fluid behaviour under an electric field was made in 1600 by William Gilbert. Gilbert (1600) described the disruption of water droplet when a piece of rubbed amber was brought near to the droplet. The droplet changed from semi-spherical to conical shape and smaller droplets were ejected from the tip of the cone. The use of electric charge to produce fibres from fluids was first described in a patent by Cooley (1900) followed by a patent by Morton (1902). Three decades later from 1934 to 1944, a sequence of patents were granted to Formhals (1934) on the process and apparatus of producing artificial threads.

Zeleny (1917) published his works on the behaviour of liquid droplets under an electric field. Droplets protruding at the end of capillary tube were charged using an electrostatic generator. Different materials were used in different conditions to observe the behaviour of resulting jets at the vertex of the cone. Estimation of the diameter and deposition speed of the jets was based on microscopic observations and flow rate of the material, respectively. Taylor (1964) proposed that charged conducting fluid can exist in equilibrium in the form of a cone (which later became known as the Taylor Cone) under an electric field at semi-vertical angle of 49.3°. Later, Taylor (1969) derived a mathematical model to predict the critical electric potential required to transform a droplet of conducting liquid into an equilibrated cone.

Baumgarten (1971) discovered that fibres as fine as 50 nanometres in diameter could be produced from a polymer solution using electric charge. An acrylic polymer in dimethylformamide (DMF) was used at various flow rates, potentials and distances to study

the effects. Baumgarten (1971) observed that at a certain distance the straight jet became chaotic and ‘wave’ of fibres was formed. The region of chaotic flight of the electrospun fibre became known as the whipping instability. A high speed camera equipped with a microsecond flash system was used to capture images of the polymer jet during flight. Based on photographs and electron micrographs, Baumgarten (1971) came to the conclusion that the whipping instability consisted of just a single fibre looping at very high speed.

In the 1990's, electrospinning gained much interest due to global interest in nanotechnology. The process was reintroduced in mid-90's as a method of producing nanoscale fibres and for the first time, the word "electrospinning" was coined by Doshi and Reneker (1995). Doshi and Reneker (1995) demonstrated the effects of processing parameters such as concentration, spinning distance, and voltage to the process and fibre morphologies using aqueous polyethylene oxide (PEO) as model material. The work is often cited as having started the recent wave of interest in the field as evidenced by the rapid increase of publication in the field of electrospinning in the following years (Stanger et al., 2009).

The earliest recorded successful attempt in industrializing electrospun nanofibres took place in the Soviet Union. In 1938 N.D. Rozenblum and I.V. Petryanov-Sokolov, working in Prof. N.A. Fuks’ group at the Aerosol Laboratory of the L.YaKarpov Institute in the USSR, generated electrospun fibres which they developed into non-woven filter materials known as Petryanov Filters®. By 1939, this work had led to the establishment of a factory in Tver for the manufacture of electrospun smoke filter elements for gas masks (Nurfaizey et al., 2012b). At the peak of operation the Soviet Union was producing 21 million m^2 per annum of electrospun filtration material (Filatov et al., 2007).

In the 1980s, electrospun nanofibres have been used to make filter media by companies such as Donaldson Company Incorporation using a trade name Ultra-Web® (Graham et al., 2003) and in 2006, DuPont™ introduced Hybrid Membrane Technology (HMT) which was also targeted for applications such as air filtration, liquid filtration, energy storage, and apparel applications (Anon, 2011). Recently, a new material based on electrospun thermoplastic polyurethane (TPU) nanofibre mats was introduced under the trade name Nanosan® which was marketed for applications that require high surface area to volume ratio as well as good elastic properties (Anon, 2013a).

2.2 The electrospinning process

A basic electrospinning setup consists of two electrodes; a source electrode which is connected to a high voltage power supply (positive or negative polarity); and a grounded conductive electrode or collector which is placed opposite to the source electrode. The collector can also be charged with a potential of different polarity from the source electrode. At the source electrode, a polymer solution is forced to flow through an orifice either by using the constant flow system of a syringe pump (Figure 2-1(a)) or constant pressure system using gravity (Figure 2-1(b)). The component with the orifice is often called the “spinning tip” or “spinneret” (hereinafter called "spinneret"). The spinneret can be a metal syringe needle, plastic pipette tip, or any fitting that has an aperture, normally with an internal diameter in the range of 0.3 to 1.0 mm.

At an appropriate feed rate, a pendant polymer droplet will form at the end of the spinneret. When the droplet is charged, the electrostatic forces between the like charged molecules cause the semi-spherical shape of the droplet to deform, however the surface tension of the droplet prevents it from breaking up. At this moment the shape of the droplet takes on a conical shape (the Taylor cone). When the applied voltage reaches a critical value, the electrostatic forces are higher than the surface tension of the droplet, the surface ruptures and a straight jet of polymer is ejected from the vertex of the Taylor cone accelerating towards the collector. Due to intermolecular bonding, the charged jet does not break up due to the Plateau-Rayleigh instability and thus fibres are formed at the collector instead of droplets (Doshi and Reneker, 1995).

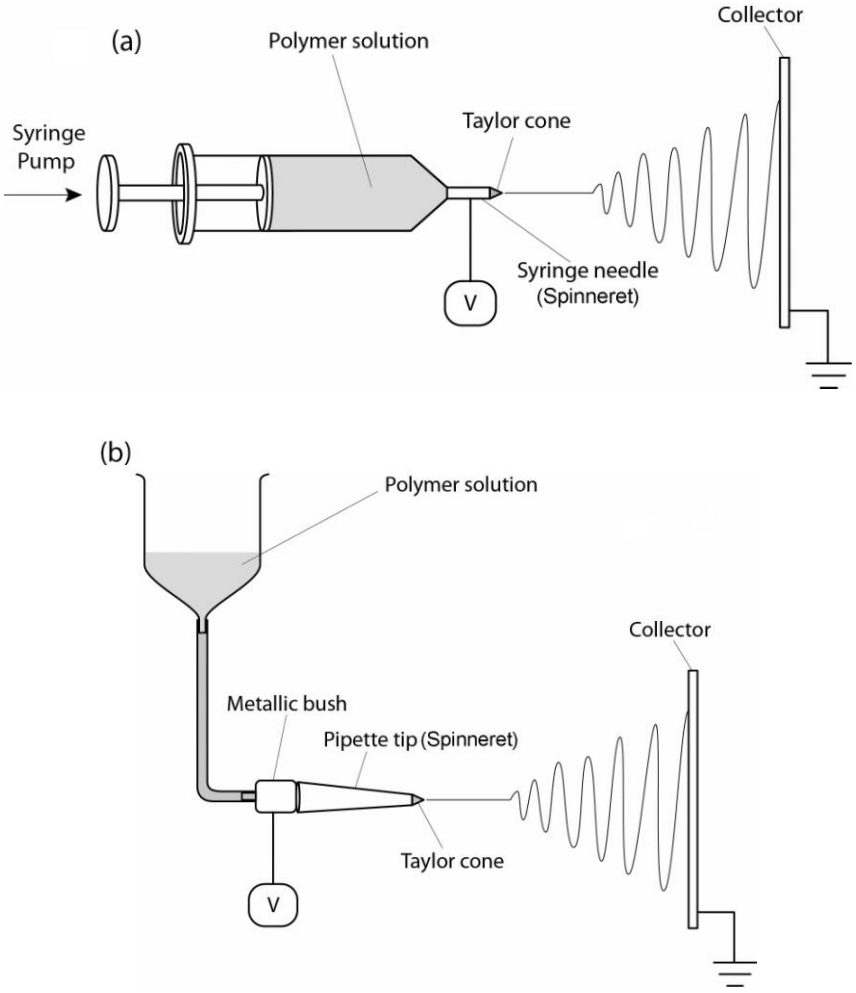

Figure 2-1.Schematics of the electrospinning setup illustrating feed systems based on (a) constant flow rate using a syringe pump and (b) constant pressure using gravity.

The straight path of the jet continues for several millimetres before it becomes unstable (Figure 2-2). Earnshaw's theorem states that a collection of point charges cannot be maintained in a stable stationary equilibrium configuration solely by the electrostatic interaction of the charges; which may explain the instability formation (Earnshaw, 1842). The electrospinning jet is not solely under the influence of electrostatic forces. For example, the drag experienced by the jet is proportional to its surface area, which is continually increasing as the fibre is stretched and solvent evaporates. On the other hand, the driving electrostatic force reduces exponentially as it leaves the spinneret (Wang and Santiago-Aviles, 2007) and as the fibre moves towards terminal velocity it experiences deceleration. Eventually, the drag experienced by the jet matches the driving force and the jet will be subjected to compressive

forces, and will buckle (Reneker et al., 2000). This point is known as the onset of whipping instability (Figure 2-2).

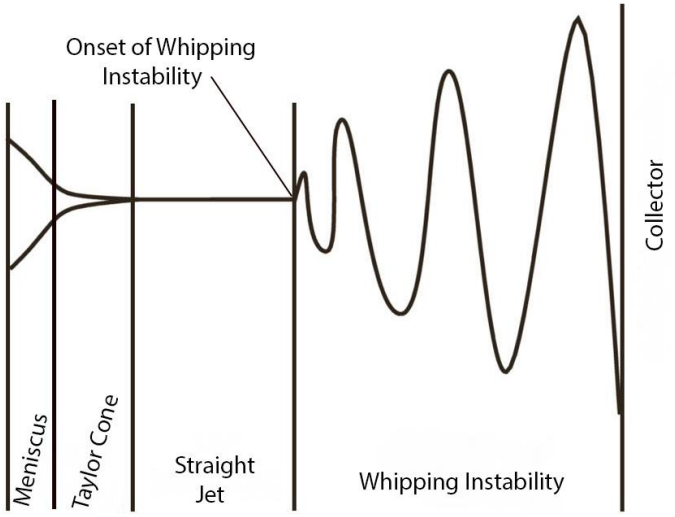

Figure 2-2. The four regions that describe the transport of the polymer between spinneret and collector (Stanger et al. (2009)).

After the onset of whipping instability, the fibre moves spirally as expanding loops of fibre (Figure 2-2). Adjacent loops repel each other due to the charges being carried, thereby increasing the size of the loops prior to reaching the collector. The region of whipping instability typically has the appearance of a cone to the naked eye due to the high velocity of the expanding loops. Further stretching and drying of the fibre continues throughout the region of whipping instability, producing a fibre of sub-micron diameter. Due to the high velocity of the fibre, it was mistakenly thought that the electrospun jet splays or splits into multiple fibres (Doshi and Reneker, 1995). However, high speed photography has confirmed the observation of Baumgarten (1971) that the whipping instability consists of a single fibre looping at very high frequencies (Shin et al., 2001).

Electrospun fibres are collected in the form of random orientated mat due to the whipping instability. The random nature of the spatial deposition of electrospun fibres is due to the formation of loops that are not perfectly symmetrical since each loop will experience some off-axis forces due to electrical repulsion that causes the loop to form a pattern reminiscent of

a hypocycloid. Using a suitable polymer solution at an appropriate applied voltage and spinning distance, dry and straight submicron scale fibres are produced (Figure 2-3(a)). However, if insufficient voltage or distance are used a mix of polymer spits and thick wet fibres are produced (Figure 2-3(b)).

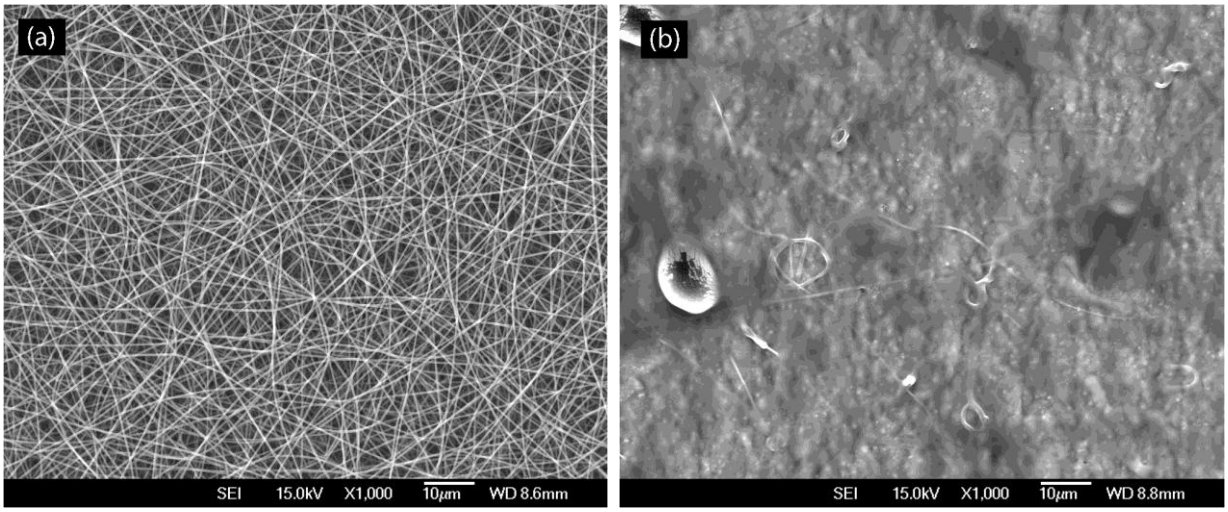

Figure 2-3. Scanning electron micrographs of electrospun fibres based on an 8 wt. %poly(vinyl alcohol) aqueous solution using an applied voltage and spinneret-collector distance of (a)+10 kV and 100 mm, and (b) +3 kV and 50 mm, respectively.

A wide range of polymers have been electrospun to produce fibres including polyvinyl alcohol (PVOH), polyethylene oxide (PEO), polystyrene (PS), polyacrylonitrile (PAN), polycaprolactone (PCL), polylactic acid (PLLA) and cellulose acetate (CA) (Lyons et al., 2005). Often the polymer needs to be dissolved in a solvent at an appropriate concentration prior to electrospinning. A review of polymers and concentrations amenable to electrospinning was provided by Huang et al. (2003).

A number of parameters have been studied in relation to the final properties of the electrospun fibres (Table 2-1). These parameters can be classified into three categories: (i) solution properties, (ii) process variables, and (iii) environmental conditions (Stanger et al., 2009). The effects of solution properties and processing variables in electrospinning such as solution concentration, viscosity, conductivity, applied potential, electric field strength and shape, and working distance have been thoroughly investigated. However, greater attention is

needed in studying the effects and interactions of environmental conditions such as temperature, humidity, and atmospheric pressure on the final properties of the electrospun fibres (Ramakrishna et al., 2005). The lack of studies in relating the environmental conditions to the characteristics of the final fibre is likely to be partially caused by difficulties in setting up electrospinning in a controlled environment.

Table 2-1. Electrospinning process parameters (Stanger et al. (2009)).

Solution properties	Process variables	Environmental conditions
Concentration	Electrostatic Potential	Temperature
Viscosity	Electric Field Strength	Humidity
Surface Tension	Electrostatic Field Shape	Local Atmosphere Flow
Conductivity	Working Distance	Atmospheric Composition
Dielectric Constant	Feed Rate	Pressure
Solvent Volatility	Orifice Diameter	

The main application in which random electrospun fibres have achieved commercial success is filtration. Thin filtration membranes constructed from electrospun fibres have a very high specific surface area coupled with a small pore size due to the presence of fibres with sub-micron or nanoscale dimensions (Nurfaizey et al., 2012b). These features are advantageous for producing filtration media with low pressure drop, but high filtration efficiency. The air flow resistance and filtration efficiency can be controlled by varying the thickness of electrospun fibres (Schreuder-Gibson et al., 2002). Additionally, electrospun fibres have been proposed for various applications such as tissue engineering, wound dressing, drug delivery, composite reinforcement, and electronics (Ramakrishna et al., 2005).

There are a number of variants of the polymer-solvent electrospinning process. One of the earliest modifications was melt electrospinning in which a polymer melt is used as the feed material rather than a polymer dissolved in solution (Norton, 1936). Melt electrospinning is often used for polymers that are difficult to dissolve at room temperature or where a solvent-

free process is desirable so as to avoid the associated accumulation and toxicity of any residual solvent. The use of a heat source to increase the temperature of the polymer into its melting range is the only aspect of the apparatus that differentiates it from a solution-based process (Figure 2-4). The range of temperature required can be as low as 60°C for poly(ε-caprolactone) (PCL) to 410°C for polypropylene (PP) while the melt viscosity typically lies in the range of 40 to 200 Pa.s (Hutmacher and Dalton, 2011). The source of heat used in melt electrospinning has been delivered in a variety of ways including by electric heater (Norton, 1936, Larrondo and Manley, 1981), gas burner (Norton, 1936), circulating hot fluid (Dalton et al., 2008), heated air flow from a heat gun (Dalton et al., 2007), radiant heat source (Reneker et al., 2003), or irradiation using laser beams (Ogata et al., 2007).

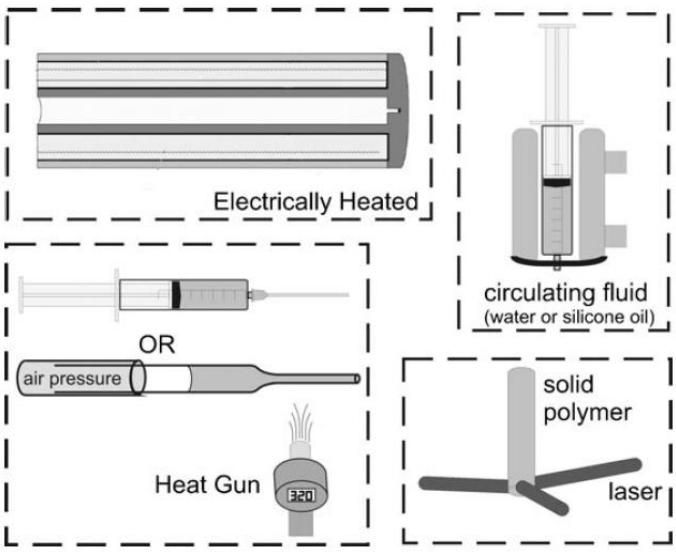

Figure 2-4. Various types of heat sources used in melt electrospinning (Hutmacher and Dalton, 2011).

Cooling leads to the solidification of the polymer in the form of fibres during melt electrospinning. Melt electrospun fibres are commonly produced without the occurrence of whipping instability due to rapid solidification of the jet, particularly with high molecular weight polymers (Hutmacher and Dalton, 2011). The whipping instability can also appear when the electrospinning is carried out above the glass transition temperature of the polymer (Zhmayev et al., 2008). The absence of whipping instability results in less fibre stretching,

and thus less thinning of the fibre diameter. Hence, melt electrospinning can be less attractive than solution electrospinning for certain applications as the diameter of melt electrospun fibres are generally in the range of microns rather than nanometres (Hutmacher and Dalton, 2011).

2.3 Controlled deposition of electrospun fibres

2.3.1 Controlled deposition for achieving uniform coverage of electrospun fibres

One of the main goals of controlled deposition in electrospinning is to produce uniform coverage of the collector substrate by the electrospun fibre mat. A low production rate remains one of the major obstacles for the industrial application of electrospinning (Niu and Lin, 2012). Depending on the process parameters such as solution flow rate and concentration, typical single spinneret electrospinning will only produce a few tenths of a gram per hour (Ramakrishna et al., 2005).

A commonly used technique for increasing the output of electrospinning process is to increase the number of spinneret by using a multi-spinneret spinning head (Tomaszewski and Szadkowski, 2005). However, it is known that a multi-spinneret setup suffers from mutual Coulombic interactions between the like-charged jets (Theron et al., 2005). Thus, a multi-spinneret electrospinning setup will produce multiple deposition areas that do not freely overlay each other due to this mutual repulsion between jets (Figure 2-5(a)). Likewise, a horizontally mounted multi-spinneret head will produce a mat with a striped appearance on a moving collector due to this mutual repulsion between adjacent jets (Figure 2-5(b)).

Therefore, significant industrial challenges remain in obtaining uniform deposition of fibres from multi-spinneret electrospinning (Heikkila et al., 2007). Several mechanical setups have been described to address the issue including the setups used in the production of filter materials known as “Petryanov filters” (Filatov et al., 2007). These consist of either spinnerets that scan to-and-fro perpendicular to the direction of a moving conveyor (Figure 2-6(a)), a rotating spinneret assembly and a moving conveyor (Figure 2-6(b)), and rotating drums that move around on a rail track (Figure 2-6(c)). However in such setups, the cost of scaling up the process is high due to complexity of the mechanical designs.

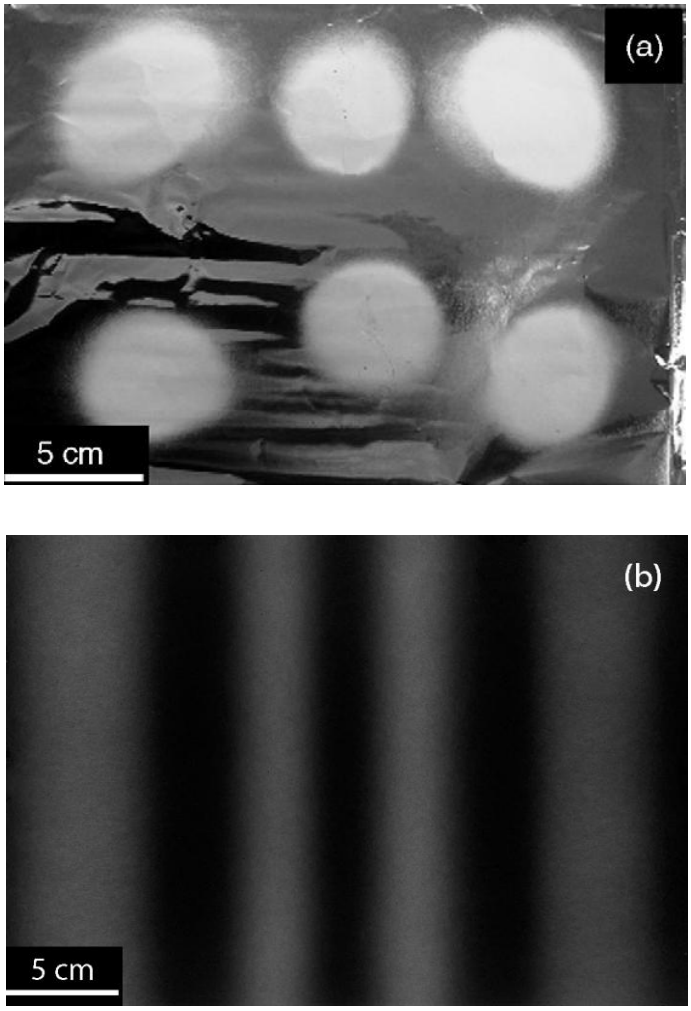

Figure 2-5. Photographs of the (a) spatial arrangement of the deposition areas resulting from a six-spinneret setup mounted in 2×3 array collected on a stationary collector (Varesano et al., 2009), and (b) typical stripe-patterned deposition created by an "in-line" four-spinneret setup collected on a rotating collector.

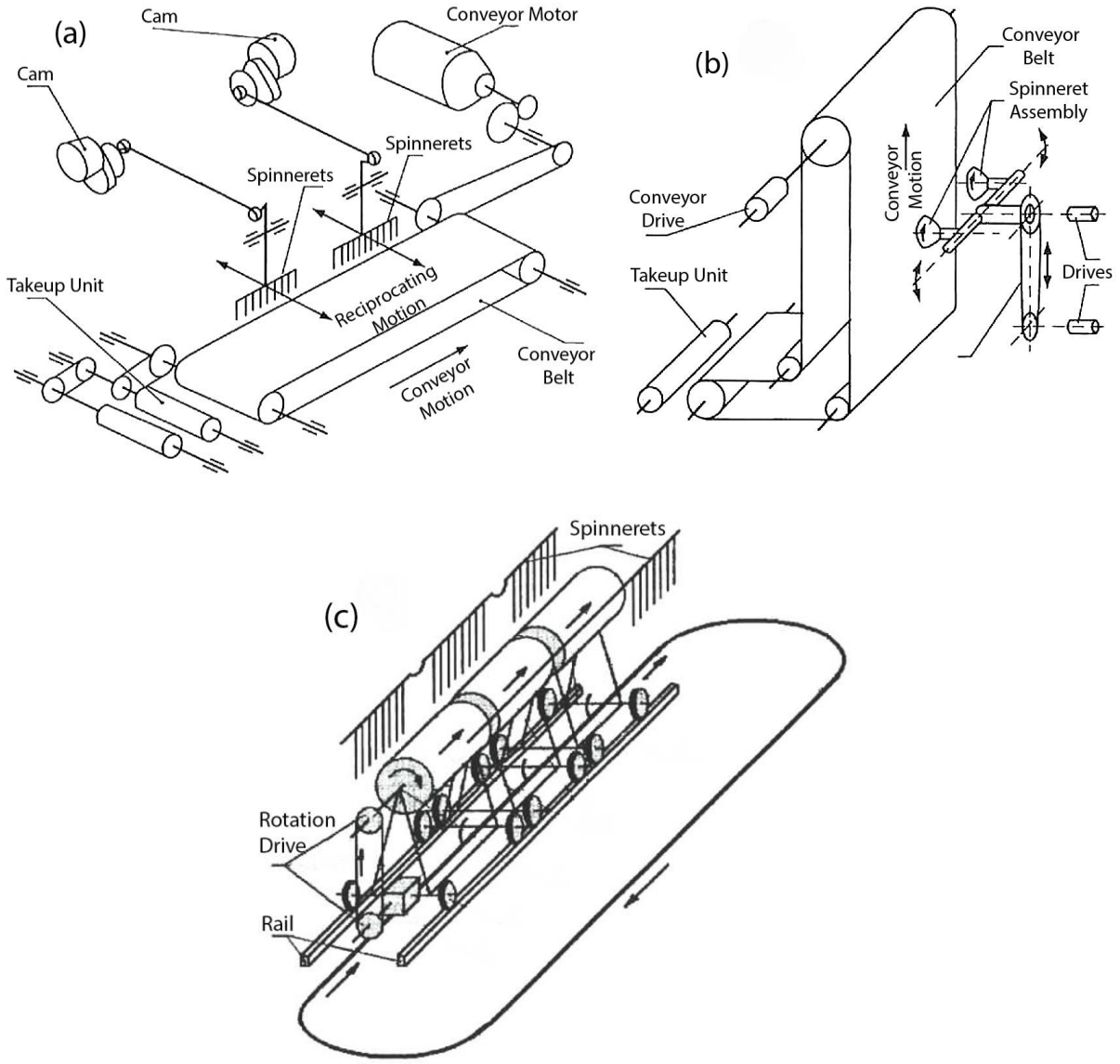

Figure 2-6. Various setups described in the production of Petryanov filters to produce uniform coverage of electrospun fibres (Filatov et al. (2007)).

Currently, a commercial electrospinning machine which is based on collectors that move in two dimensions relative to a multi-spinneret head is available under a trade name Nanospinner24 (Anon, 2013b). The machine has a multi-spinneret head pointing upwards to a rotating drum which is capable to move horizontally to the direction of deposition (Figure 2-7). Other than producing uniform coverage of electrospun fibres, a multi-spinneret setups with a moving collector or spinnerets are also capable of producing a uniform blend of different electrospun fibres (Ding et al., 2004). Ding et al. (2004) used a laterally moving

multi-spinneret head using a motorised track to produce a uniform blend of poly(vinyl alcohol) (PVOH) and cellulose acetate (CA) fibres.

Figure 2-7. Nanospinner24 electrospinning machine consists of a multi-spinneret head (bottom) and a rotating collector (top assembly) with horizontal stroke (Anon, 2013b).

In contrast, spinneret-less electrospinning or free liquid surface electrospinning offers high productivity and mechanical simplicity (Petrík, 2011). In the pioneering study by Yarin and Zussman (2004), a two layer system was used containing a magnetic fluid under a layer of poly(ethylene oxide) (PEO) solution. A permanent magnet or electromagnet was used to invoke instability in the magnetic fluid causing "spikes" to emerge on the upper surface of the fluid. Multiple jets emerge from the upper polymer surface accelerating towards a grounded collector under the influence of an electric field. Spinneret-less electrospinning has attracted considerable attention, resulting in a number of patents that were granted aiming at increasing the productivity (Jirsak et al., 2005, Petras et al., 2008, Petras et al., 2010). A typical spinneret-less spinning head consists of a rotating cylinder partially immersed in a polymer solution (Figure 2-8). Multiple polymer jets emerge from the exposed surface of the rotating cylinder and move toward a collector under a high electric field. As the jets emerge randomly from the cylinder surface, there is no fixed position of the deposited fibres on the

collector resulting in uniform coverage of electrospun fibres on the collector. Currently, production-scale machines based on this principle are commercially available by Elmarcos.r.o. under the trade name Nanospider^{TM}(Petrík, 2011).

Figure 2-8. Photograph of a typical spinneret-less electrospinning setup that consists of a rotating cylinder partially immersed in a polymer solution (Petrík, 2011).

At any voltage the concentration of charge on a cylindrical surface is always lower than that at a spinneret tip (Halliday et al., 2001). Thus, spinneret-less electrospinning requires a higher voltage compared to conventional spinneret electrospinning (Niu et al., 2009). Moreover, spinneret-less electrospinning may produce thicker fibres compared to conventional electrospinning (Niu and Lin, 2012). Furthermore, the polymer-solvent solution is exposed to the open environment during spinneret-less electrospinning for which solvent evaporation, and thus solvent selection, is a potentially limiting and problematic factor in the process (Niu et al., 2011).

2.3.2 Controlled deposition for achieving aligned fibres

Moving targets have also been used to produce aligned fibres during electrospinning. One of the simplest methods for obtaining aligned electrospun fibres is to use a rotating drum (Boland et al., 2001) (Figure 2-9(a)). The drum is typically constructed from an electrically conductive material such as stainless steel or aluminium. In a typical setup, the rotating cylinder is grounded while the spinneret is charged at a suitable voltage. Depending on the geometries of the setup, the rotation of the drum may be set at an appropriate speed to match with the speed of fibre deposition. Boland et al. (2001) successfully aligned polyglycolic acid (PGA) electrospun fibres using a rotational speed of 1000 rev/min. Alternatively, Theron et al. (2001) used a rotating disk to collect aligned fibres based on the notion that the sharp edge of the disc would concentrate the electric field, enhancing fibre alignment (Figure 2-9(b)).

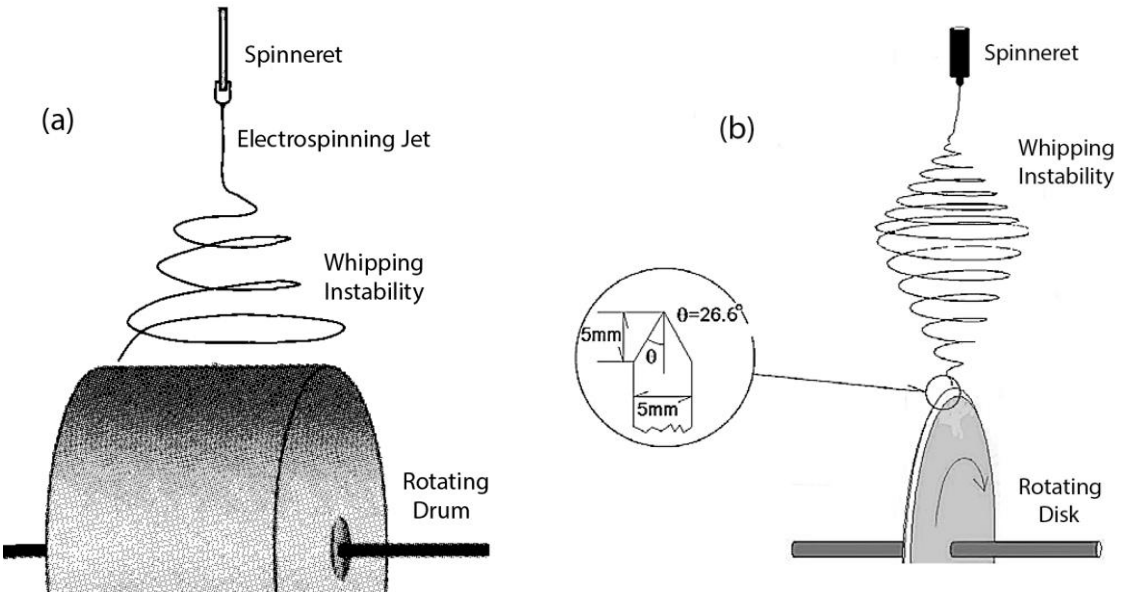

Figure 2-9. Method of collecting aligned electrospun fibres using a (a) rotating drum (Ramakrishna et al. (2005)), and (b) rotating disk (Theron et al. (2001)).

Combinations of rotating drum and counter-electrodes have also been used to improve fibre alignment. Teo et al. (2005) used oppositely charged parallel conducting strips and sharp-edged bars to produce aligned polycaprolactone (PCL) electrospun fibres (Figure 2-10(a) and

(b)). Another method was introduced by Sundaray et al. (2004) using an oppositely charged steel pin to encourage fibre alignment (Figure 2-10(c)). The steel pin was put inside an insulating rotating drum opposite to the spinneret. The rotational speed of the drum is controlled by a dc motor (M2) to match that of the velocity of fibre deposition. A stepper motor (M1) was used to move the drum assembly in lateral direction to encourage uniform deposition across the drum.

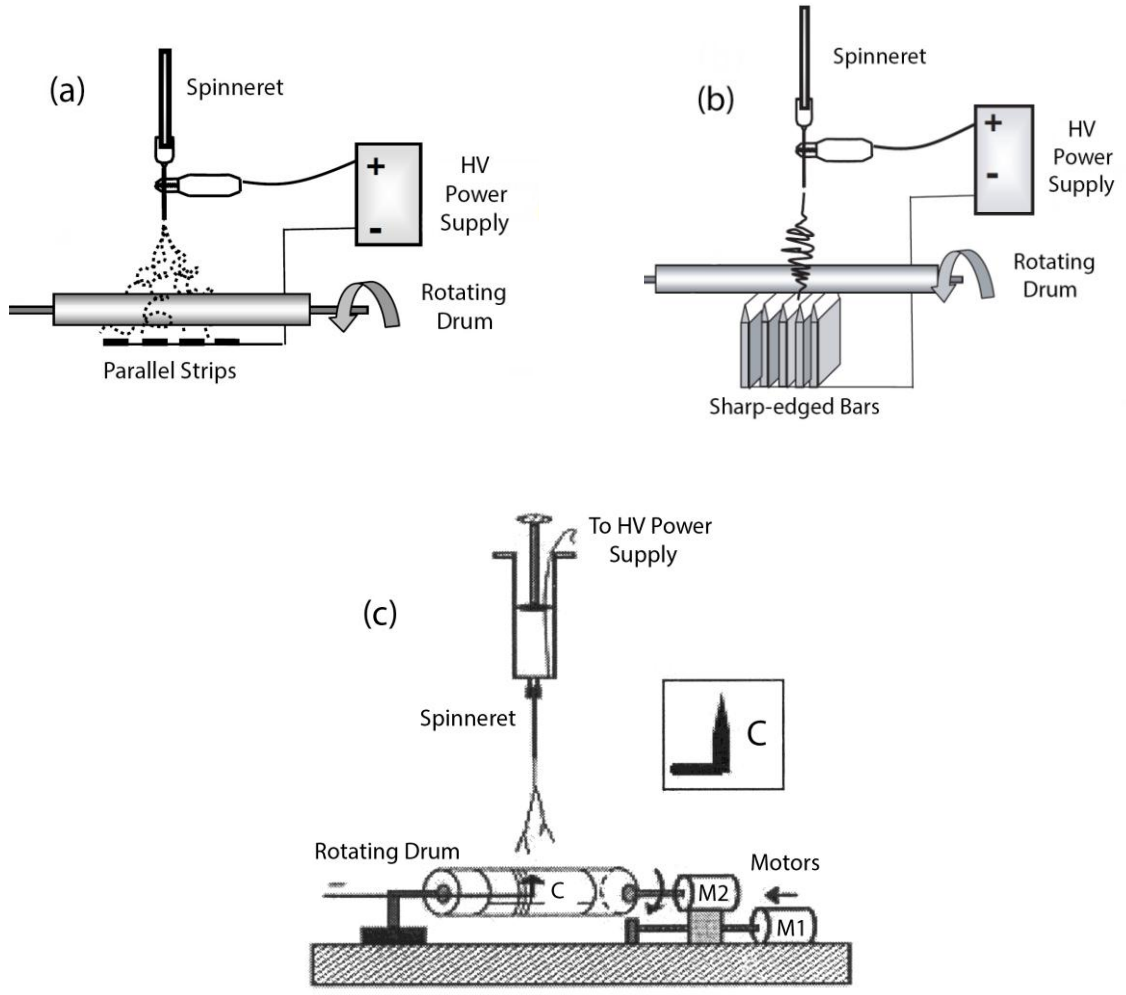

Figure 2-10. Various combinations of rotating drum and counter-electrodes: (a) parallel conducting strips (Teo et al. (2005)); (b) sharp-edged bars counter-electrodes (Teo et al. (2005)); and (c) oppositely charged steel pin to encourage fibre alignment (Sundaray et al. (2004)).

Carnell et al. (2008) further developed the technique by using an oppositely charged electrode placed behind a rotating drum (Figure 2-11(a)). It was observed that the whipping instability was suppressed when the voltage was set at an appropriate value to produce highly aligned fibres. The process was capable of producing mats with alternating 0° and 90° layers, achieved by repositioning the spun mat at 90° to the previous orientation (Figure 2-11(b)). However, the produced fibres were notably in the range of micrometres rather than nanometres and this is likely due to the absence of the whipping instability.

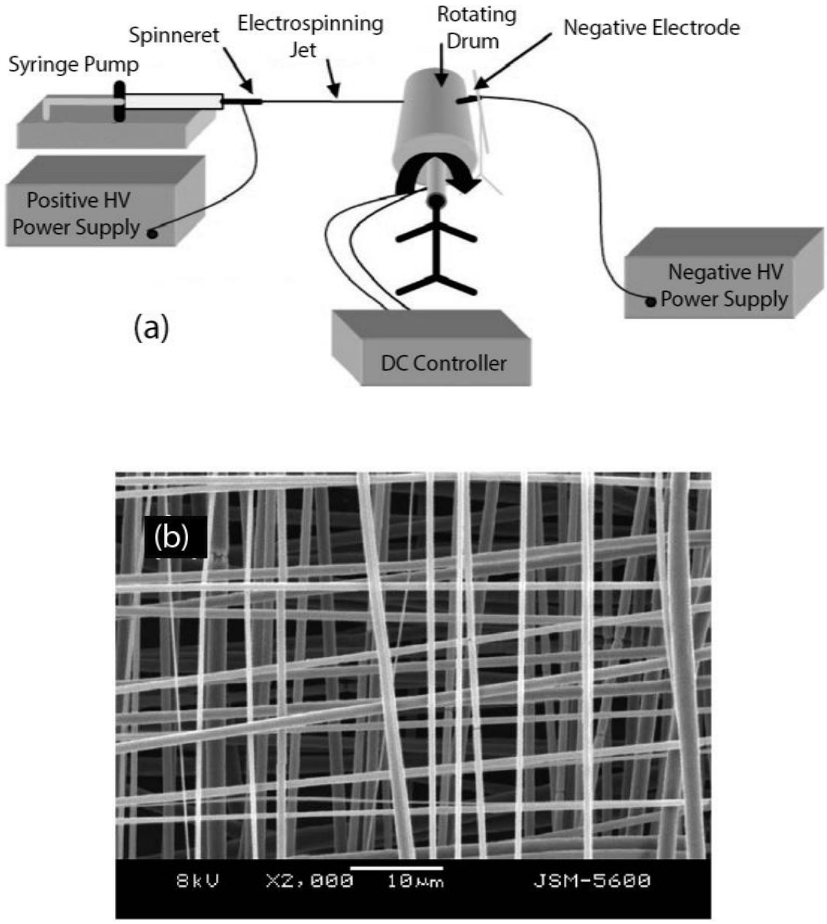

Figure 2-11. A schematic illustrating (a) electrospinning with oppositely charged counter-electrode placed at the back of a rotating cylinder, and (b) scanning electron micrograph of the resulting pseudo 0°/90° woven polyglycolic (PGA) electrospun fibres (Carnell et al. (2008)).

Near-field electrospinning (NFES) is another technique for producing aligned fibres. Although NFES has been popularized quite recently, it is worth noting that one of the earliest

attempts at short distance electrospinning was demonstrated by Huebner (1948). The main feature of this technique is the short distance between the spinneret and collector that is typically in the millimetre range (Huebner, 1948). Consequently, the applied voltage required in NFES is significantly lower than for conventional electrospinning. In a patent, Huebner (1948) described a technique for producing threads or filaments electrically using spinneret-to-collector distances on the order of several millimetres and an applied voltage as low as 3 kV. Drozin (1954) noted that when a fluid droplet was placed 15 mm from a high electric charge source, it required a lower voltage to form a 'cloud' of fine threads compared with a distance of 40 mm.

Kameoka et al. (2003) described a method of short distance electrospinning called "Scanning Tip Electrospinning Deposition" (STED) (Figure 2-12). A solid silicon tip was dipped into polyethylene (PEO) solution to form a droplet which was then charged at 4.5 kV. A rotating surface perpendicular to deposition axis was used as collector and maintained at distances between 5 to 15 mm from the silicon tip. Aligned fibres were collected at a matching speed between fibre deposition and rotation speed of the collector. It was also noted that a minimum spinneret-to-collector distance of between 5 and 10 mm was required to produce dry fibres (Kameoka et al., 2003).

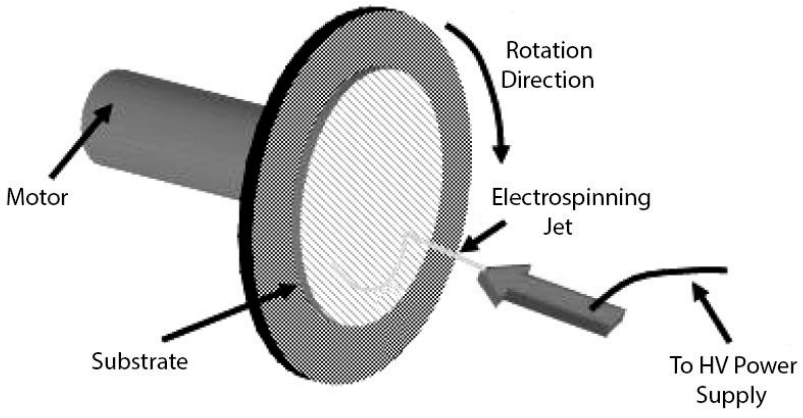

Figure 2-12. Scanning tip electrospinning deposition (STED) (Kameoka et al. (2003)).

Sun et al. (2006) further developed the method used by Kameoka et al. (2003) by using a similar dip method with a solid tungsten tip of 25 µm diameter. A shorter spinneret-to-collector distance of 0.5 to 3 mm and 0.6 to 1 kV applied voltage were used. The comparatively short spinning distance allows aligned fibres to be collected in a direct-write manner since the whipping instability does not develop. The collector is mounted on an X-Y table that moves at a matched speed to the fibre deposition to collect the aligned fibres. It was demonstrated that aligned polyethylene oxide (PEO) fibres could be produced at a collector speed of 200 mm/s (Sun et al., 2006). The method was further developed by Zheng et al. (2010) to include a microscope and video capture device with an improved accuracy of fibre positioning to within 1μm (Figure 2-13).

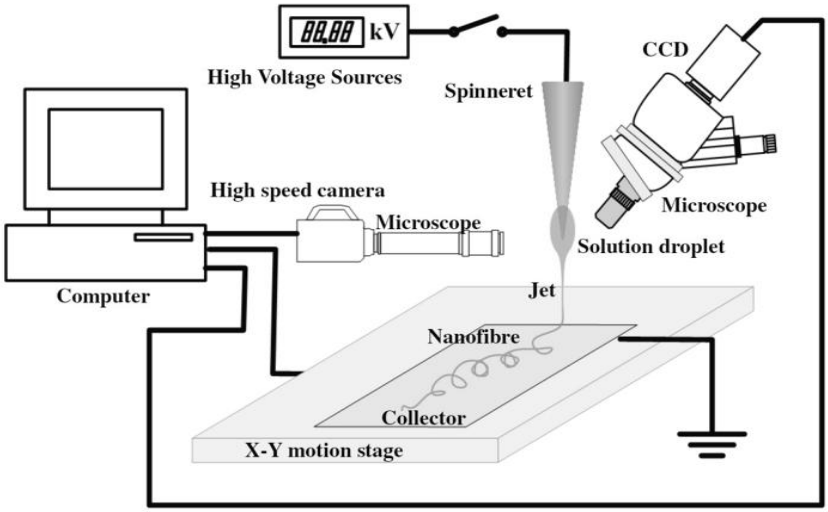

Figure 2-13. Schematic of NFES setup (Zheng et al., 2010).

There is less time available for solvent evaporation and fibre thinning due to the short spinning distances used in NFES. Consequently, NFES yields electrospun fibres that are relatively thick (up to several millimetres) (Hellmann et al., 2009). A dipping method using very fine tips similar to that of Kameoka et al. (2003) and Sun et al. (2006) is required to produce smaller polymer droplets and hence finer jets. This is important to allow the fibres to dry and still be drawn to nanoscale diameters before arriving at the collector. The major drawbacks of this dipping method are (a) limits on the total length of fibre and (b) variation

in fibre diameter due to a decrease in the volume of the polymer droplet as it is consumed during the process. Alternatively, a continuous supply of polymer can be achieved using a fine syringe needle of 0.1 mm inner diameter (Chang et al., 2008). The control capability of the setup was demonstrated by drawing the word "Cal" on a substrate (Figure 2-14). However, coiled fibres are still produced when the x-y table moves at a reduced speed, particularly during directional changes. Jet formation was initiated below the critical potential for normal jet initiation by "poking" the droplet with a 1 μm tungsten tip in order to produce fibres in the nanoscale range (Chang et al., 2008).

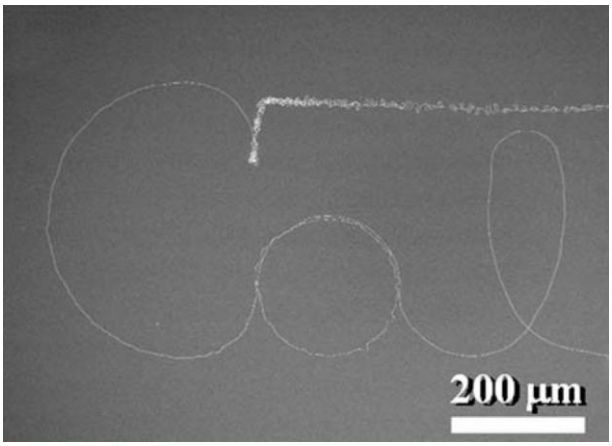

Figure 2-14. Scanning electron micrograph showing the word "Cal" written on a substrate by NFES (Chang et al., 2008).

Similarly, the absence of the whipping instability during melt electrospinning has been recognized as an advantage for controlled fibre collection (Larrondo and Manley, 1981). Another niche advantage is the ability to produce solvent-free fibres which makes melt electrospinning a preferable process for making electrospun tissue scaffolds (Dalton et al., 2008). The capability of the process to direct-write a fairly complex 3D structure has been demonstrated by Brown et al. (2011) (Figure 2-15). However, as mentioned earlier the produced fibres are significantly inferior in terms of final fibre diameters (up to several hundred microns) due to less thinning of the fibre diameter during the process (Hutmacher and Dalton, 2011).

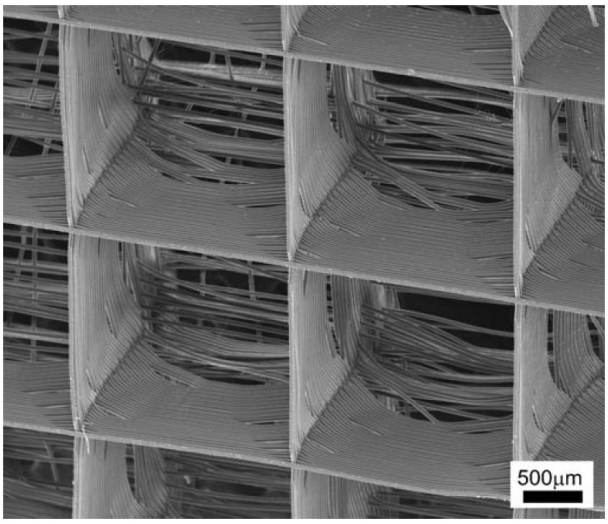

Figure 2-15. Scanning electron micrograph showing a 3D structure constructed *via* melt electrospinning (Brown et al., 2011).

In contrast to the previously mentioned methods, gap electrospinning uses non-mechanical systems to achieved fibre alignment. A clear advantage of gap electrospinning is that the efficiency is not limited by the movement of mechanical components. Typical gap electrospinning uses two parallel conducting collectors placed at a distance of several centimetres (Li et al., 2003) (Figure 2-16(a)). Due to the fact that fibres in flight are carrying electric charges, fibre alignment in this method is achieved by shaping of the electric field near the collector (Dersch et al., 2003) (Figure 2-16(b)). When a fibre reaches the collector, one part of the fibre which is closest to one of the collectors will get attracted to the edge of the collector by electrostatic force (Figure 2-16(c)). Subsequently, another part of the fibre which is closest to the other collector will also get attracted. As the process continues, eventually uniaxial aligned fibres are formed across the gap. Electrostatic repulsion between the deposited fibres are also believed to assist the alignment of the fibre (Li et al., 2004).

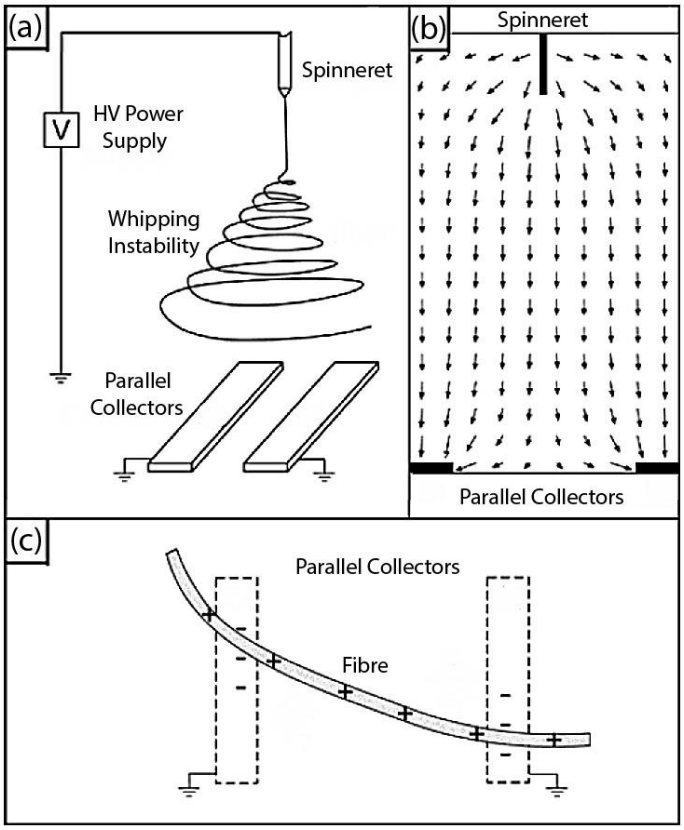

Figure 2-16. Schematics showing the (a)typical setup using two parallel collectors, (b) associated electric field distribution, and (c) mechanism of fibre alignment in gap electrospinning (Li et al. (2003)).

Li et al. (2004) further developed the method to produce multi-axial orientated fibres. A dedicated four-electrode and six-electrode gold patterns were deposited on a quartz wafer (Figure 2-17(a) and (c)). Each opposite pair of electrodes were alternately grounded for 5 seconds to produce biaxial and triaxial aligned fibres as in Figure 2-17(b) and (d).

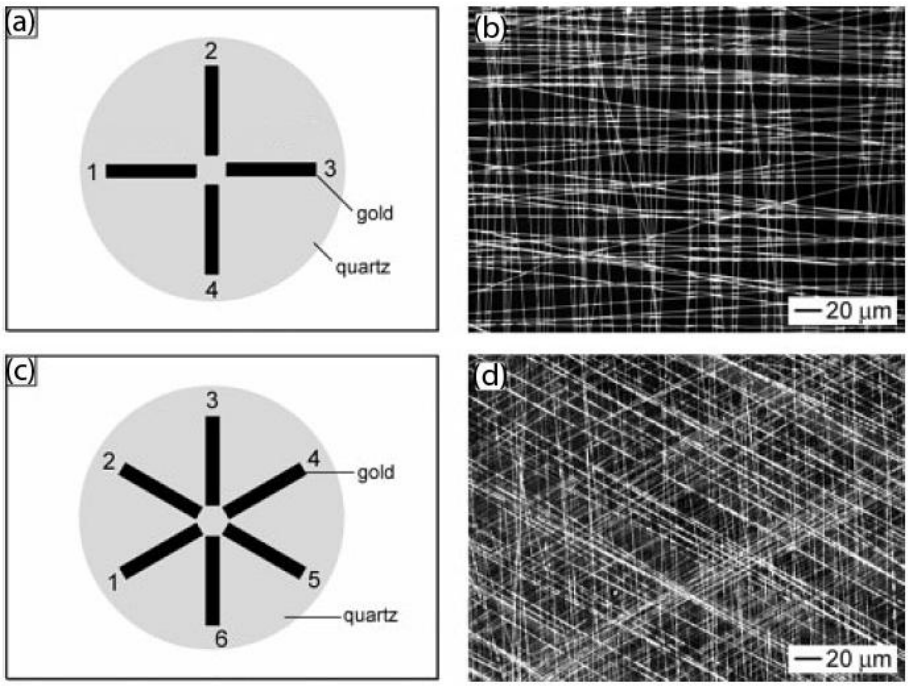

Figure 2-17. (a) The electrode pairs of 1-3 and 2-4 were alternately grounded to produce biaxial aligned fibres at 90° orientation as in (b). (c) The electrode pairs of 1-4, 2-5 and 3-6 were alternately grounded to produce triaxial aligned fibres at 60° orientation as in (d) (Li et al. (2004)).

2.4 Controlled deposition using electric field manipulation

Another method of achieving controlled deposition in electrospinning is through electric field manipulation (EFM) using one or more charged auxiliary electrodes. Several attempts at using EFM have been reported claiming considerable success with objectives of either controlling the deposition areas of a single or multi-spinneret system, or producing aligned fibres (Bellan and Craighead, 2011). This method takes the advantage of mutually repulsive or attractive forces between the electrospinning jet and the charge on the auxiliary electrodes. The auxiliary electric field deflects the trajectory of the jet from its default location and the applied voltages at the auxiliary electrodes are used as control variables. The main advantage of using EFM is that no moving component is required and hence theoretically the efficiency of the method is not limited by the inertia intrinsic to any mechanical system.

Jaeger et al. (1998) devised a secondary ring electrode in an arrangement to spin fibre vertically downwards. The secondary electrode was held at a similar voltage to the spinneret,

and the formation of a fibre was initiated by gravity. It was noted that moving the secondary electrode relative to the spinneret shifted the onset of whipping instability.

Deitzel et al. (2001) further developed the technique by Jaeger et al. (1998) by basing the equipment on that used by Melcher and Warren (1971) in an attempt to control the electrospinning process by influencing the shape and strength of the electrostatic field. A vertical electrospinning experimental set up was used with up to eight ring electrodes and the ability to charge the collector electrode (Figure 2-18). The charged collector electrode was used to increase the driving force exerted on the fibre, and the secondary electrode array was used as an "electrostatic lens". This constrained the path of the fibre to the extent that the change of flight pattern associated with the onset of instability was suppressed. Consequently, the area over which the fibre was deposited was also decreased.

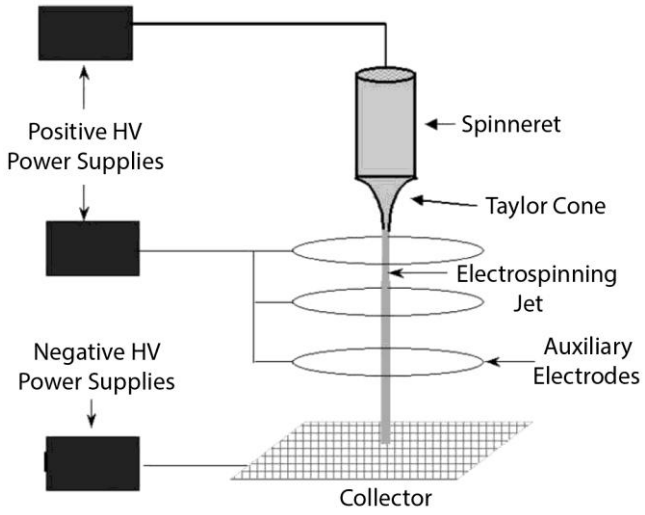

Figure 2-18. A vertical electrospinning experimental set up with three ring electrodes (Deitzel et al. (2001)).

Electric field manipulation has also been used in multi-spinneret systems. To compensate for the repulsion effect in a five-spinneret system, a cylindrical coaxial secondary electrode surrounding the spinnerets was used by Kim et al. (2006) (Figure 2-19). It was reported that the auxiliary electrode confined the jets to some extent and a stable electrospinning process was maintained (Figure 2-19(d)). Unfortunately, the final shape of the deposition areas was

not reported. However, presumably the system still produced non-uniform coverage of electrospun fibres based on the photographs of the jets in Figure 2-19(d).

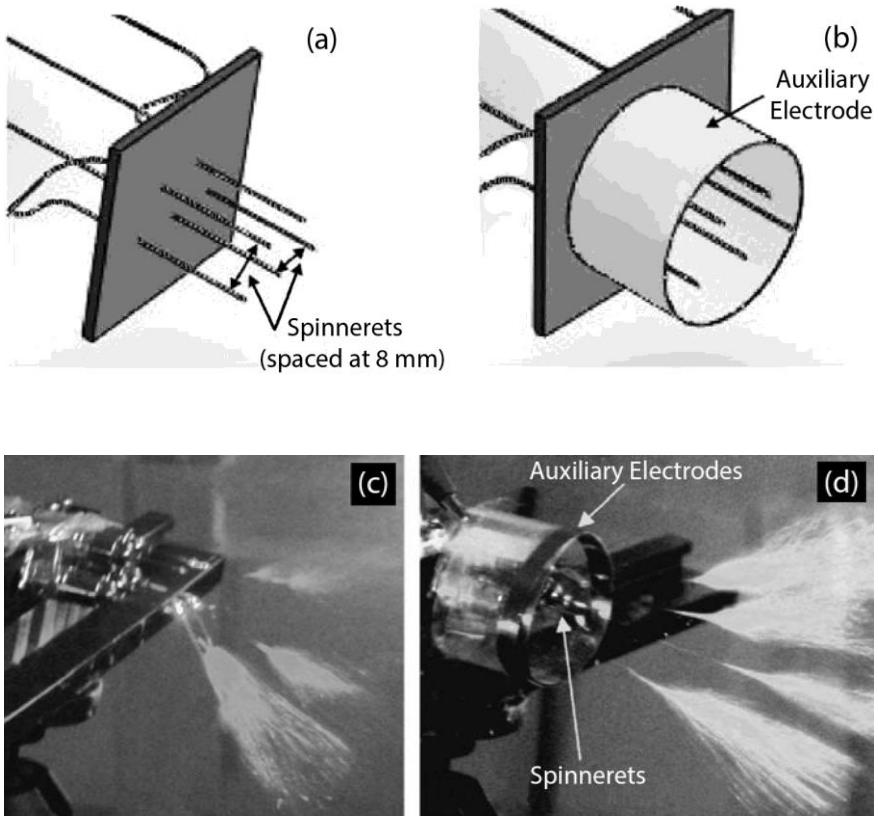

Figure 2-19. Schematics of a five-spinneret set-up (a) without and (b) with an auxiliary electrode. Photographic evidence of (c) repelling electrospinning jets due to like-charges between adjacent jets, and (d) increased spatial confinement of adjacent jets due to the presence of the auxiliary electrode (Kim et al. (2006)).

Varesano et al. (2009) used setups consisting of 2 to 16 spinnerets arranged in a number of configurations surrounded by a round auxiliary electrode (Figure 2-20(a)). Based on final deposition areas and photographic images, it was concluded that the addition of auxiliary electrode reduced the divergence angles between the jets from 43˚ to 27˚ (Figure 2-20(b) and (d)) thus reducing the separation of deposition areas from adjacent spinnerets (Varesano et al., 2009) (Figure 2-20(c) and (e)). Recently, Xie and Zeng (2012) claimed that uniform coverage of electrospun fibres can be achieved from a three-spinneret system. The spinnerets were arranged linearly with their ends protruding through a flat auxiliary electrode (Figure

2-21(a)). Although the addition of an auxiliary electrode reduces the distance between the areas of fibre deposition from each spinneret, gaps between the deposition areas still remain visible (Figure 2-21(b)), yielding a non-uniform deposition of fibres on the collector.

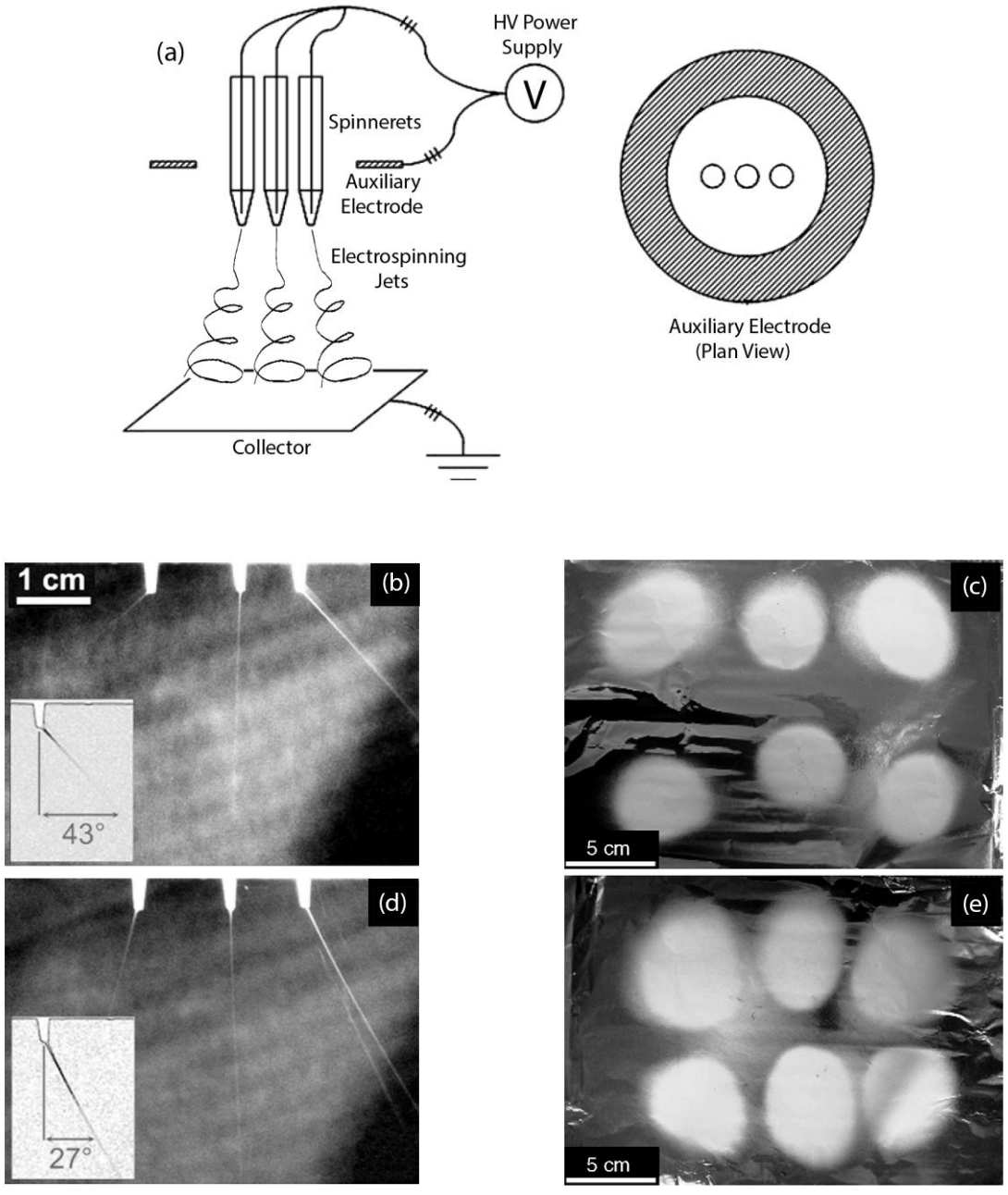

Figure 2-20. (a) A multi-spinneret setup with a circular auxiliary electrode. Photographs showing the resulting divergence angles of the jets and deposition patterns (b, c) without and (d, e) with the use of the circular auxiliary electrode shown in (a) (Varesano et al. (2009)).

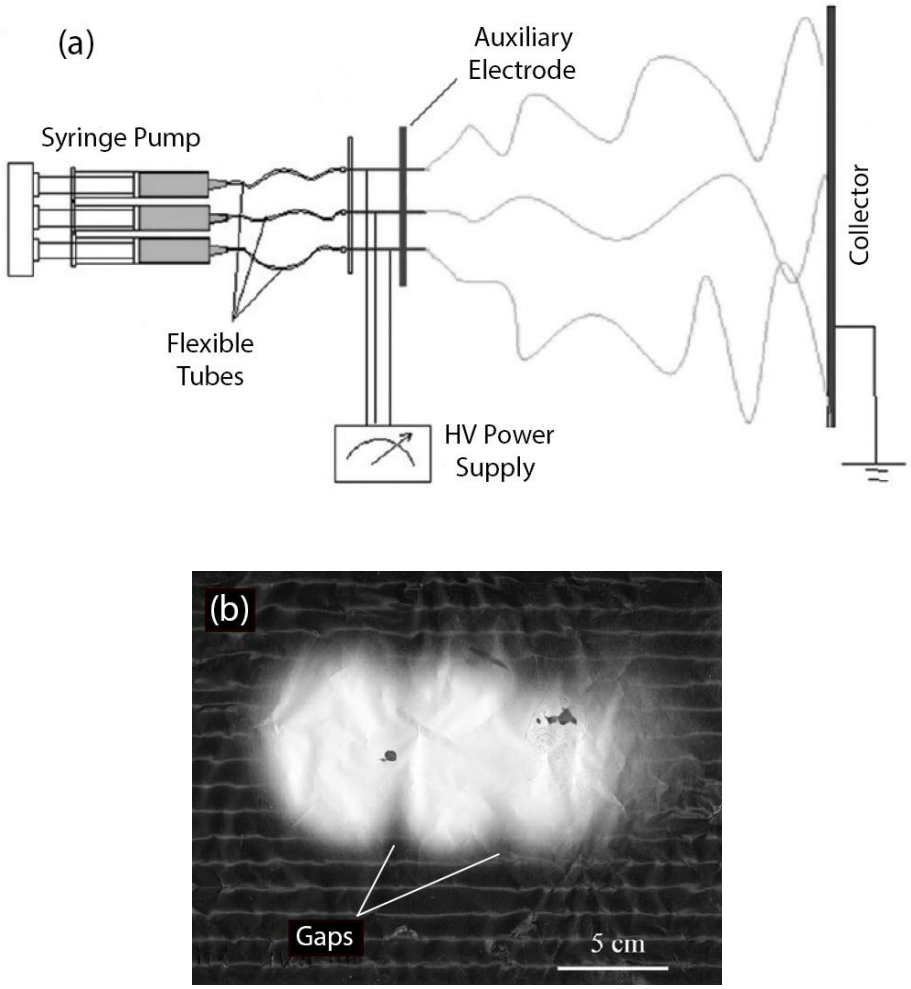

Figure 2-21. (a) A schematic of a three-spinneret setup with a flat auxiliary electrode and (b) photograph of the resulting electrospun mat that shows evidence of gaps in the deposition area (Xie and Zeng (2012)).

Bellan and Craighead (2006) extended the notion of using an auxiliary electrode to produce aligned fibres by devising a split ring electrode system with the intention of first constraining the beam, and cyclically varying the potential difference to cause the fibre flight path to scan to-and-fro on the collector electrode (Figure 2-22). High voltage relays were first used to give a step variation in the voltage, and then a proportional system to allow faster variation of electrode voltage was used to investigate the system response up to 1 kHz, finally allowing the production of aligned fibres.

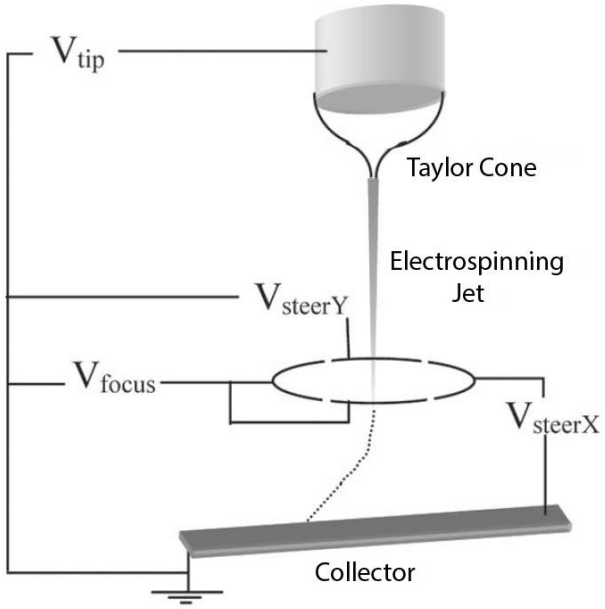

Figure 2-22. Vertical electrospinning setup with a split ring electrode system. Fibre scanning movement is achieved by switching V_{steerX} and V_{steerY} relative to V_{focus} at high speeds (Bellan and Craighead (2006)).

Arras et al. (2012) combined the use of a rotating drum with a pair of auxiliary electrodes with the aim to improve fibre alignment. Identical plate-like electrodes were placed between the spinneret and drum, and the auxiliary electrodes were both charged at an adjustable voltage of the same polarity as the spinneret. It was noted that the whipping instability could be spatially constrained for a given applied voltage thereby improving the angular deviation of the collected fibres from 70˚ to only 2˚ (Arras et al., 2012).

Recently, Grasl et al. (2013) further improved the process by Arras et al. (2012) by using time-varying (ac) voltages to charge the auxiliary electrodes (Figure 2-23(a)). The mechanism involved in EFM using an ac voltage is similar to the one using a dc voltage except that in the case of ac voltage, the auxiliary electric field changes with time and therefore the electric field also changes with time. The electrodes were connected independently to two high voltage power supplies. The applied voltages at the electrodes were in the form of a direct current (dc) biased square wave which were antiphase to each other. A square waveform was chosen to enable rapid switching of maximum and minimum voltages between the electrodes thus forcing the fibres to flick to-and-fro. Aligned fibres were produced when the frequency of the waveforms were in the range of 30-60 Hz depending on

the geometry and applied voltages (Grasl et al., 2013). The capability of the setup to produce aligned fibres of different orientation angles (-10˚/+10˚) was also demonstrated by rotating the electrodes to the desired angles (Figure 2-23(b)).

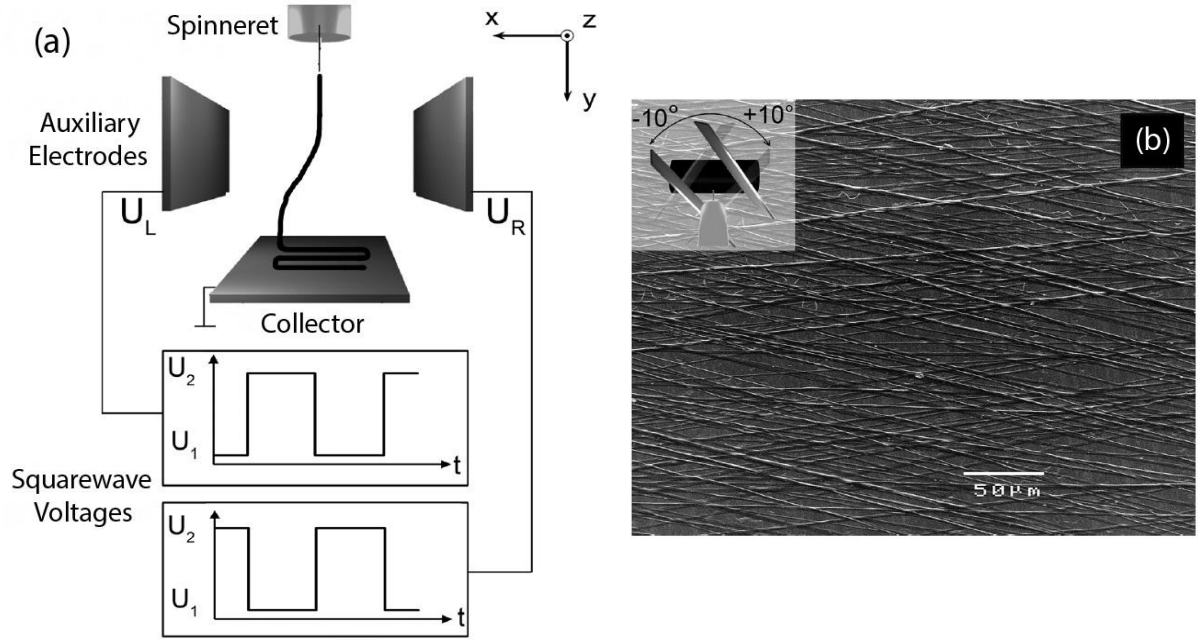

Figure 2-23. (a) Electrospinning setup with a pair of auxiliary electrodes charged with time-varying voltages (square waveforms). (b) Two layers of aligned fibres orientated -10˚ and +10˚ from the default horizontal orientation (Grasl et al. (2013)).

Acharya et al. (2008) and Jafari et al. (2011) studied the applicability of introducing auxiliary electrodes to improve fibre alignment in gap electrospinning. A pair of auxiliary electrodes were placed midway between the spinneret and a gap collector. Both studies concluded that the degree of fibre alignment was significantly improved when the electrodes were charged at an appropriate voltage of the same polarity with the spinneret.

2.5 Project scope

Several attempts on using electric field manipulation (EFM) for controlled deposition of electrospun fibre have been reported with a considerable success (Deitzel et al., 2001, Bellan and Craighead, 2006, Kim et al., 2006, Varesano et al., 2009). However, most attempts have

been about demonstrating a reduction in the resulting deposition area when the auxiliary electrodes were charged at a certain applied voltage. There have been no studies on validating EFM as a control method. A main concern arises if EFM would provide a consistent and repeatable result due to the complex nature of electrospinning process. In other words, would the same effect on the deposition area occur every time the auxiliary electrodes are charged at the same applied voltage, and if the applied voltage is changed would the change of deposition area will be predictable?

Apparently, there is a significant gap in the knowledge of EFM for use in controlling the deposition of electrospun fibres. It is the interest of this study to fill this gap by developing and investigating the validity of using EFM as control method. The main hypothesis of this study is that a consistent and repeatable method of controlling the deposition area of electrospun fibre can be achieved by using a pair of charged auxiliary electrodes. A preliminary test was conducted by using a pair of direct current (dc) charged auxiliary electrodes positioned adjacent to the spinneret. The results showed that the deposition area on the collector electrode can be shifted if there was a voltage difference between the electrodes. In addition, visual observations suggest the magnitude of shift of the deposition area correlates with voltage difference between the electrodes.

To test the main hypothesis, an experimental study will be carried out to measure the effect of changing the applied voltage at the auxiliary electrodes on the magnitude of shift of the deposition area. A new method for collecting and measuring the shift of the deposition area is required to obtain reliable data. To the author's knowledge, there have been no quantitative studies carried out on measuring the response of fibres when subjected to auxiliary electric field. When the fibre is subjected to an auxiliary electric field, the electrostatic force that responsible for the deflection of the fibre trajectory is proportional to the electric field strength. Therefore it is reasonable to hypothesize that the magnitude of shift of the deposition area would be proportional to the voltage difference at the auxiliary electrodes. A computer simulation can be used to calculate the electric field strength when the auxiliary electrodes are charged at a certain voltage combination. The experimental and simulation results can be compared in order to understand the relationship between the applied voltage and the shift of the deposition area.

Deitzel et al. (2001) and Bellan and Craighead (2006) demonstrated that the size of a single jet deposition area can be reduced from several centimetres to less than a centimetre by constraining the whipping instability using charged ring electrodes. Such investigations demonstrate the ability to deposit fibre within a targeted area, although it is not clear why a smaller deposition area was an objective of these studies. From the perspective of mass production, this would be an inefficient way of collecting electrospun fibre due to a reduction in the collected area. Furthermore, the use of EFM in order to eliminate the whipping instability leads to an increase in the fibre diameter (Shin et al., 2001). Interestingly, there was no discussion made on the effect of using EFM on fibre diameter in the studies carried out by Deitzel et al. (2001) and Bellan and Craighead (2006). However, it was reported by Kim et al. (2006) that thicker fibres (more than 50% increase) were produced when a charged cylindrical auxiliary electrodes was used in a five spinneret electrospinning system.

In this study, an EFM technique will be used to increase the size of the deposition area rather than confining the deposition area. This can be done by continuously moving the deposition area by applying time-varying voltage at the auxiliary electrodes. In previous studies, time-varying voltage in the form of two antiphase square waves have been used by Bellan and Craighead (2006) and Grasl et al. (2013) to produce aligned fibres. The square wave voltage enables instantaneous change between maximum and minimum applied voltage at the auxiliary electrodes. At an appropriate frequency, the two antiphase voltages generate cyclical attractive and repulsive forces that cause the fibre to flick to-and-fro between the electrodes before it reaches the collector as aligned fibres.

In this study, it is hypothesized that the application of time-varying voltage at the auxiliary electrodes would provide a continuous scanning of the jet producing a wide and uniformly distributed electrospun fibre mat. The technique differs from the previous studies in the sense that a smooth change of voltage at the auxiliary electrodes is preferable. This can be achieved for example, by using a low frequency sine wave voltage at each electrode. The waveforms will be antiphase to each other so that the voltage difference between the electrodes changes over time thus shifting the deposition area accordingly. The use of antiphase waveforms also means that when one electrode is at a maximum the other will be at a minimum – this minimises the constraining of the whipping instability, which is important for maintaining the submicron diameter of the electrospun fibres.

Finally, two case studies will be presented to demonstrate the applicability of the EFM technique to overcome real issues in electrospinning. Studies have shown that using a conventional dc EFM technique, the divergence angles between the jets in a multi-spinneret electrospinning system can be reduced but the technique was still unable to eliminate the gaps between the deposition areas (Xie and Zeng, 2012, Kim et al., 2006, Varesano et al., 2009). In the first case study, the EFM technique will be used to resolve the issue by using time-varying voltage. The hypothesis is that the continuous scanning of electrospinning jets using time-varying EFM could eliminate the stripe deposition pattern in a multi-spinneret electrospinning system.

In the second case study, the applicability of the time-varying EFM technique will be demonstrated in a gap electrospinning system. Previously, a pair of dc charged auxiliary electrodes have been used to constrain the whipping instability to improve fibre alignment in a gap electrospinning system (Acharya et al., 2008, Jafari et al., 2011, Arras et al., 2012). By combining the constraining and continuous scanning of an electrospinning jet, it is hypothesized that the application of time-varying EFM could improve the alignment and distribution of the aligned fibres in a gap electrospinning system.

CHAPTER 3

EXPERIMENTAL PROCEDURES

3.1 Electrospinning apparatus

A laboratory scale electrospinning machine (Model ES4), courtesy of Electrospinz Ltd., New Zealand was used throughout this study (Figure 3-1). Further details of Model ES4 can be found in Appendix 1. The machine is a twin head bench top electrospinning machine using two EMCO 4330 high voltage power supplies (EMCO High Voltage Corporation, USA). The driving voltage at each spinning head can be independently controlled from zero to 33 kV DC, positive or negative depending on the polarity of the power supplies. Polymer solution is supplied through a silicone hose to a spinneret (Axygen T-200-Y pipette tip) from a glass header tank. A constant pressure polymer supply is maintained by adjusting the height of the header tank to an appropriate level. Electrospun fibres are collected on a grounded collector mounted on the polyethylene target plane. A number of modifications were made to the machine as described in detail in Chapter 4, Chapter 5, Chapter 6, and Chapter 7.

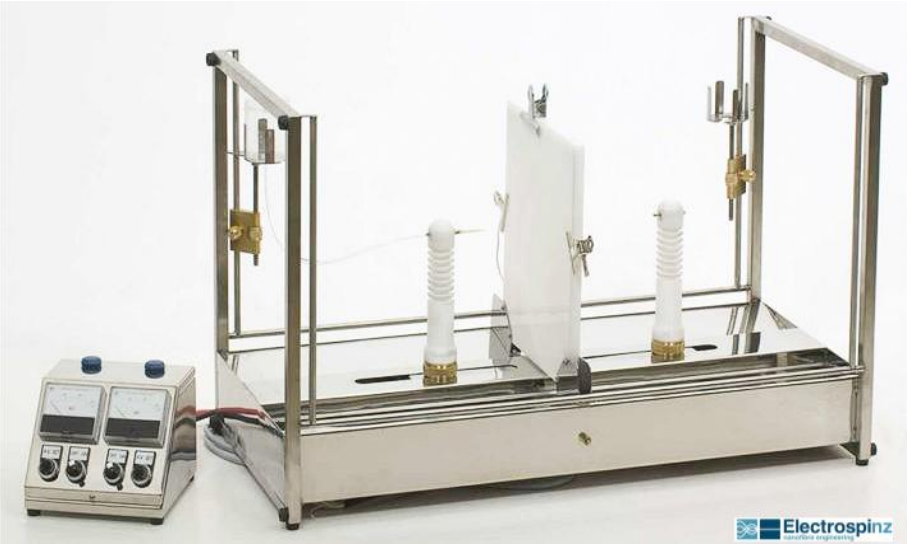

Figure 3-1. Model ES4 electrospinning machine (photo courtesy of Electrospinz Ltd., New Zealand).

3.2 Experimental material

Electrospinning was carried out using an aqueous solution of poly(vinyl alcohol) (PVOH) (Chemiplas NZ limited, Wellington, NZ). The PVOH had an average molecular weight of 118,000-124,000 g/mol and degree of hydrolysis (DH) in the range of 86–89% according to the manufacturer. An aqueous polymer solution was prepared by dissolving PVOH in distilled water for approximately 2 h at 60 °C, stirring at 500 rev/min using an overhead stirrer with an impeller blade. The polymer concentration was verified by drying a small sample in a convection oven at 80 °C to determine the total solvent content. Any loss of solvent during the mixing process was then adjusted with distilled water to give a final concentration of 8 wt.%. All weights were measured using a four figure balance (Mettler AE200). Further details of the material can be found in Appendix 2.

3.3 Sample substrate

Unless otherwise specified, a sheet of A4 80 g/m^{2}Kaskad Raven Black paper (no. 1516RB) was used as a substrate to aid visualisation of the deposited fibre. The paper is mounted in a registered position onto the grounded collector. The paper type was chosen based on prior observations that suggest the inclusion of the paper did not change the typical shape and size

of the deposition area. The collection of electrospun fibres on a sheet of paper also ease the handling of the samples for image analysis as described in detail in Chapter 4, Chapter 5, and Chapter 6.

3.4 Electrospun fibre characterisation

Scanning electron microscopy (SEM) images were taken using a JEOL Neoscope JCM-5000 SEM machine (JEOL Ltd., Japan). Scanning electron micrographs were taken under high vacuum at 10 kV accelerating voltage with a magnification ranging between 150 to 5000 times. The as-spun fibres were cut into 1 × 1 cm^2 samples and mounted onto an aluminium stub. The samples were sputtered with gold (Au) for 120 seconds using Quorum Q150R sputter coating machine (Quorum Technologies Ltd., United Kingdom).

The mean fibre diameter and orientation were measured using Electrospinz SEM Analyser software from triplicates of scanning electron micrographs (Electrospinz Ltd., New Zealand) (Figure 3-2). Electrospinz SEM Analyser is a Net-based software designed to analyse scanning electron micrographs of fibre products. The measuring process was carried out using the same setting for each set of sample to maintain consistency of the data. The default histograms generated by the software were used to represent the distribution of fibre diameter and orientation. The raw data was exported to Microsoft Excel® for error analysis. The mean fibre diameter is presented with a standard deviation to represent the error.

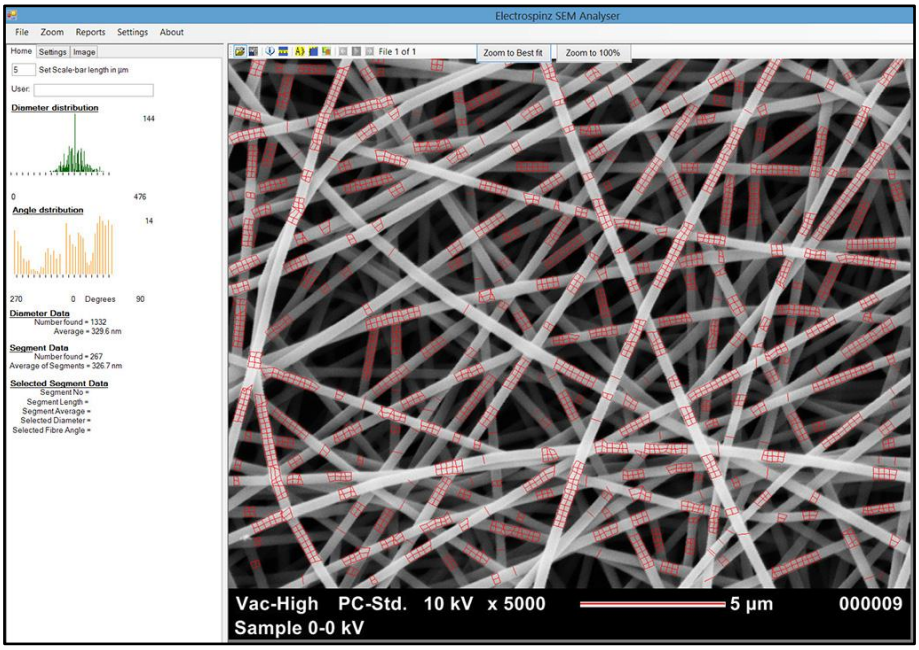

Figure 3-2. Screenshot of fibre diameter measurement using SEM Analyser software (courtesy of Electrospinz Ltd., NZ).

CHAPTER 4

CONTROL OF SPATIAL LOCATION AND SIZE OF THE DEPOSITION AREA USING AUXILIARY ELECTRODES CHARGED WITH DIRECT CURRENT ELECTRIC VOLTAGE

4.1 Introduction

Controlled deposition of electrospun fibres has gained a lot of attention since the first patenting of electrospinning (Cooley, 1900). The development is driven by the fact that the unique properties of electrospun fibres are only beneficial if the fibres can be produced in a suitable form that suits the intended application. Various methods of controlled deposition have been reported in literature mainly by means of mechanical methods such as rotating collectors or by shaping the collector electrodes (Ramakrishna et al., 2005). Controlled deposition methods based on electric field manipulation (EFM) have also been introduced but this method is still comparatively understudied (Deitzel et al., 2001, Bellan and Craighead, 2006, Kim et al., 2006). One of the reasons probably due to difficulties of dealing with the complexity of the electrostatic field (Tomaszewski and Szadkowski, 2005).

Even though EFM has been used to achieve some degree of controlled deposition in electrospinning, apparently there have been no studies validating the use of EFM as a control method. Most of the previous studies have been about concentrating the deposition area by damping the whipping instability using a confining auxiliary electric field (Deitzel et al., 2001, Kim et al., 2006, Varesano et al., 2009) or producing aligned fibres by forcing the fibres to flick to-and-fro using high speed voltage switching between the auxiliary electrodes (Bellan and Craighead, 2006, Grasl et al., 2013). To the author's knowledge, there have been no reports on quantifying the nature and magnitude of the fibre response.

The strength of the electric force exerted on the fibre during electrospinning at any point can be determined by using the Lorentz electrical force expression:

$$F = qE \qquad \textbf{Equation 4-1}$$

and the acceleration imparted by the field to the particle is determined by the equation

$$a = \frac{qE}{m} \qquad \textbf{Equation 4-2}$$

where, F is the electric force, q is the charge carried by the particle, E is the electric field, a is the acceleration, and m is the mass of the particle.

The objective of this study was to validate the use of electric field manipulation to control the spatial location and size of the deposition area. From Equation 4-1, the electrostatic force that responsible for the deflection of the fibre's trajectory is proportional to the electric field strength. Therefore it is reasonable to hypothesize that when the fibre is subjected to an auxiliary electric field, the magnitude of shift of the deposition area would be proportional to the applied voltage at the auxiliary electrodes.

Manipulation of the electric field is achieved by introducing a pair of charged auxiliary electrodes adjacent and parallel to the line of deposition of the electrospinning jet. A special technique was established to measure the magnitude of shift of the deposition area and subsequently its relationship with the applied voltage at the auxiliary electrodes. Finite element analysis (FEA) has been used to demonstrate the effects of modified spinning heads (Xie and Zeng, 2012, Angammana and Jayaram, 2011), or auxiliary electrodes (Cui et al., 2011), or patterned collectors (Wang et al., 2010) on the electric field distribution. In this study, FEA was used to calculate the electric field strength when the auxiliary electrodes were charged and its effects to the behaviour of electrospun fibre based on the trajectory of a charged particle. The relevance of FEA for prediction of the trajectory of electrospun fibre was also explored by comparing results from experiment and simulation

4.2 Experimental procedures

4.2.1 Experimental apparatus

The ES4 electrospinning machine was modified to include a pair of auxiliary electrodes in the form of two sets of parallel rods (6061 aluminium, CAMS Ltd., NZ) measuring 6.3 mm in diameter (Figure 4-1). The electrodes were fixed in position at a distance of 100 mm either side of the spinneret and 75 mm to the collector. Each electrode was connected to an EMCO 4330 high voltage power supplies (EMCO High Voltage Corporation, USA) with their applied voltages V_2 and V_3 controlled independently of each other. A 300 × 300 mm sheet of 316 stainless steel was attached to the high density polyethylene backplane of the ES4 electrospinning machine to be used as the grounded collector electrode. A constant voltage difference of +10 kV (V_1) and distance of 100 mm was used between the spinneret and a grounded collector throughout the experiment.

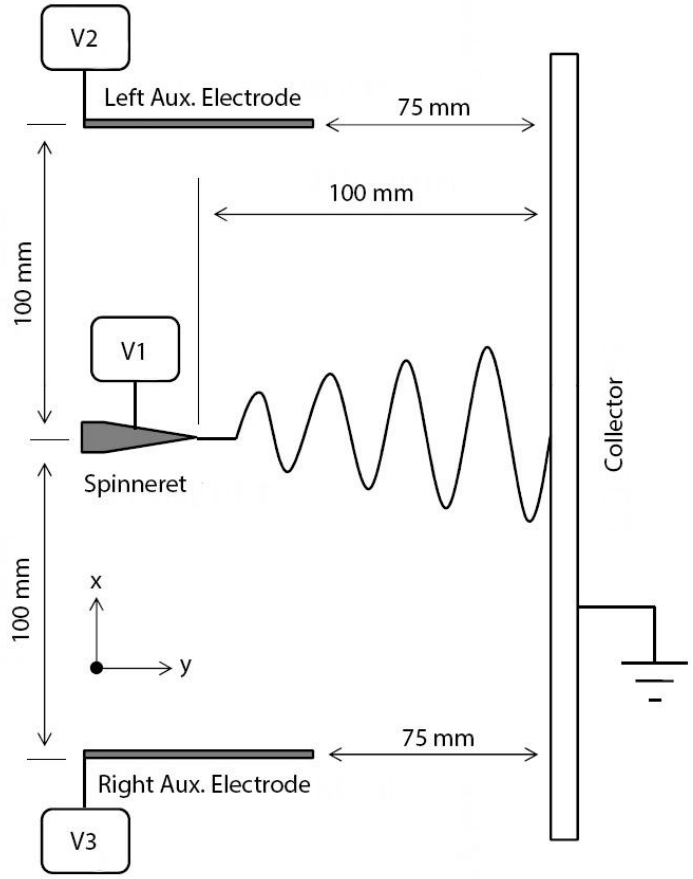

Figure 4-1. The plan view of the experimental setup.

4.2.2 Sample preparation

Two different sets of electrospun PVOH samples were prepared by use of (i) a single auxiliary electrode that was charged while the other was held at zero voltage (E1); and (ii) both auxiliary electrodes charged with voltage combinations between +2 to +10 kV (E2) (Table 4-1). A reversed order of voltage combination was also used for E1 and E2 to demonstrate that the arrangement was acceptably symmetrical. E1 was conducted to ascertain the maximum possible shift of the deposition area (L_{exp}) that could be obtained using the described apparatus and voltage difference. Voltage difference (V_d) is defined as the voltage difference between the two auxiliary electrodes. Meanwhile E2 was conducted to determine if the base voltage (V_b) (*i.e.* lower of the two auxiliary electrode voltages) influences the magnitude of shift of the deposition area.

A naming convention is adopted here to describe the applied voltages and the manner in which they were applied. For example, 8-2 kV indicates that a voltage of +8 kV and +2 kV was applied to the left (V_2) and right (V_3) electrodes, respectively, giving a voltage difference (V_d) of +6 kV and base voltage (V_b) of +2 kV. Changes in shift of the deposition area were measured relative to default conditions* (Table 4-1). Samples of the electrospun mat were produced in triplicate.

Table 4-1. The various voltage combinations V_2 and V_3 used to charge the auxiliary electrodes in E1 and E2. N.B. * indicates the default condition used for comparisons.

Experiment	V_2-V_3 (in kV)	Total samples
E1	0-0* 2-0, 4-0, 6-0, 8-0, 10-0, 12-0 0-2, 0-4, 0-6, 0-8, 0-10, 0-12	39
E2	2-2*, 4-4*, 6-6*, 8-8* 2-4, 2-6, 2-8, 4-6, 4-8, 4-10, 6-8, 6-10, 8-10 4-2, 6-2, 8-2, 6-4, 8-4, 10-4, 8-6, 10-6, 10-8	66

4.2.3 Measurement of spatial location and size of the deposition area

The as-deposited electrospun fibre mats were scanned at a resolution of 300 dpi and converted to 2481×3509 pixel JPEG images. Image analysis software (UTHSCSA

ImageTool, Version 3.0) (Dove, 2002) was used to measure the spatial location and size of the deposition area. Four measurements positioned relative to a predefined origin were made for each sample (Figure 4-2). These were the distance to the centre of the deposition area in the x and y direction and the width and height of the deposition area in the x and y direction. The ratio of the width of deposition area to its height is later referred to as the aspect ratio. Initially, the centre of the A4 size paper was used as the origin of the x-y co-ordinates. Three measurements were taken during image analysis to get an average. The scanning and measuring process were carried out using the same setting to maintain consistency of the data. The data collected from this analysis produced a set of x-y coordinate positions in millimetres as a function of the applied voltages in kV.

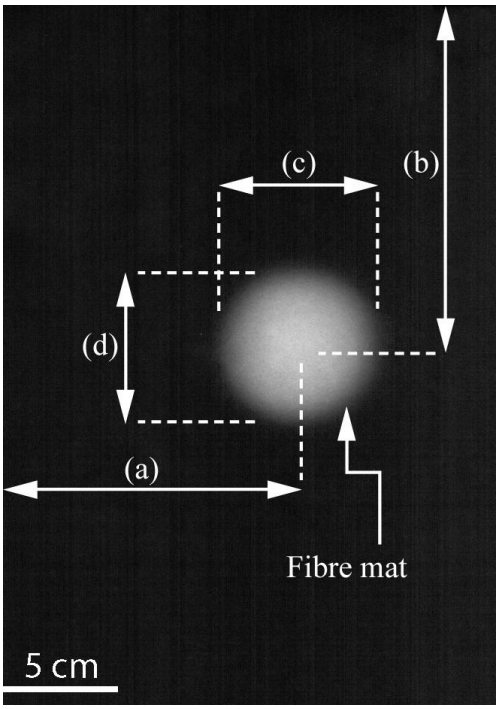

Figure 4-2. Measurement positions of the samples: (a)-(b) are the distances to the centre of the deposition area in the x and y direction, and (c)-(d) are the width and height of the deposition area in the x and y direction, respectively.

4.2.4 Simulation of the electric field

The simulation of the electric field was carried out using COMSOL microelectromechanical systems (MEMS) module version 3.5a (COMSOL Inc., USA). The 3D model of the

electrospinning apparatus in Figure 4-1 was drawn within a cubic boundary measuring 2×2×2 m. The alignment of the auxiliary electrodes and spinneret were made parallel with the x axis, while the deposition direction of fibre was parallel with the z axis. The calculation of the electric field was restricted to the region of interest between the spinneret, auxiliary electrodes and collector. The spinneret was charged at +10 kV whilst the collector and outer boundary were grounded. The voltages at the auxiliary electrodes were varied to replicate the experimental values used in Table 4-1.

The effect of V_d on the magnitude of shift of the deposition area was quantified by simulating the magnitude and direction of electric field component E_x as a function of position along the z direction (Figure 4-3). Additionally, the components of the electric field as a function of position in the x and y directions (E_x and E_y) were also calculated on an imaginary plane that is equidistant to the spinneret tip and collector, and normal to the z axis (Figure 4-3). E_x and E_y represent components of the electric field along two orthogonal axes labelled as x'-x" and y'-y" (Figure 4-3). 2D plots of each E_x and E_y as a function of position were produced over a distance of 200 mm.

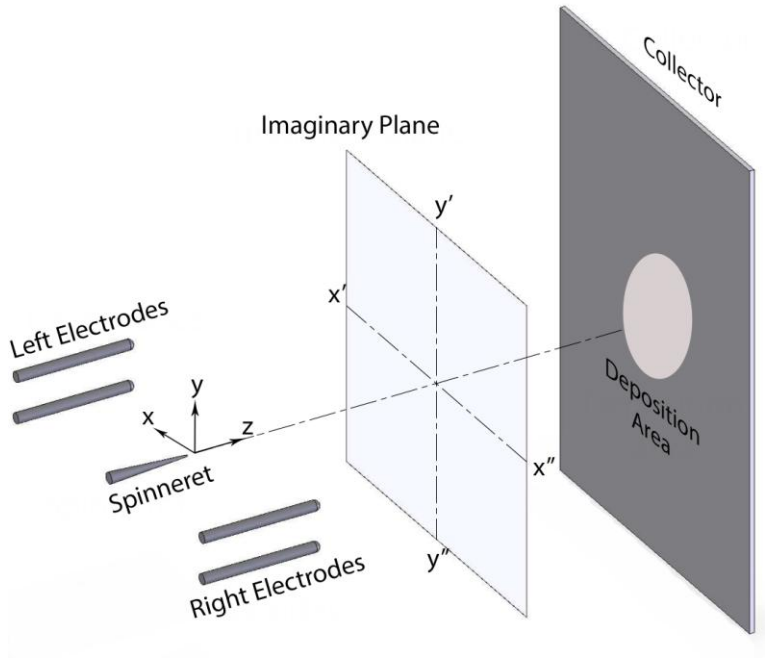

Figure 4-3. A schematic illustrating the 3-D model used in simulation.

4.2.5 Simulation of a charged particle trajectory

In post-processing mode, the particle tracing option was used to trace the path of a charged particle in the simulated electric field. The paths of charged particles with and without mass were calculated. The massless particle is defined as a particle with an invariant mass of zero and carrying an elementary charge of $1.60217646 \times 10^{-19}$ C. For a particle with mass, the actual mass was calculated based on the ratio of charge per unit mass and by assuming an elementary charge of $1.60217646 \times 10^{-19}$ C, giving a calculated particle mass of 1.67×10^{-21} kg. The ratio of charge per unit mass for the same poly(vinyl alcohol) used in this work was estimated previously as 96.1 C/kg by Stanger et al. (2012) based on the gradient of the plot of mass deposition rate and current at the spinneret. The calculated values were validated by experimenting at different applied voltages and electrospinning distances. The starting point of the particle was set at the tip of the spinneret which was taken to be the origin (0, 0, 0). The x-y coordinates of the point of "impact" of the particle at the collector (L_{model}) were then plotted as a function of V_d. Comparisons were made between L_{exp} and L_{model} to evaluate the relevance of this approach to simulate the electrospinning process.

4.2.6 Regression analysis

Regression analysis was used to study the relationships between V_d, V_b, L_{exp}, L_{model} and the aspect ratio. Scatter plots of dependent variables, L_{exp}, L_{model} and aspect ratio as a function of independent variables V_d and V_b were made for both E1 and E2. First-order probabilistic models based on best fit lines to the data were used to describe the relationships. The coefficient of determination, R^2 was used to measure the goodness of fit in explaining the variation of the data. The p-values were used to determine the significance of the relationships found between the variables.

4.3 Results and discussion

4.3.1 General observations

The electrospinning process produces a typical circular deposition area with a diameter of several centimetres (Figure 4-4(a) and (b)). The visibility of the deposition area was aided by the contrast between the white of the deposited fibres and the black of the A4 paper substrate. Without the influence of the auxiliary electric field, the location of the deposition area on the collector corresponds approximately to the closest distance between the spinneret and the collector. When the auxiliary electrodes were charged, it was observed that the deposition area was shifted parallel to the x axis in a direction opposite to the most positive auxiliary electrode. For example, if the left electrode was charged at +12 kV and the right electrode was kept at 0 kV, the deposition area moved to the right as the result of repulsive forces imposed by the left auxiliary electrode (Figure 4-4(a)). Similarly, the deposition area moved to the left when the auxiliary electrodes were charged in an opposite manner (Figure 4-4(b)). However, the fibres were deposited at the middle of the axis if both electrodes were charged at the same voltage.

Stable electrospinning was observed throughout the experiment suggesting that the introduction of the auxiliary electrodes affect neither the nature nor formation of the Taylor cone nor the onset of the whipping instability of the electrospinning process. The stable electrospinning process and the formation of a typical PVOH deposition area also suggest that the placement of the black paper in front of the grounded collector had no noticeable effect on the process.

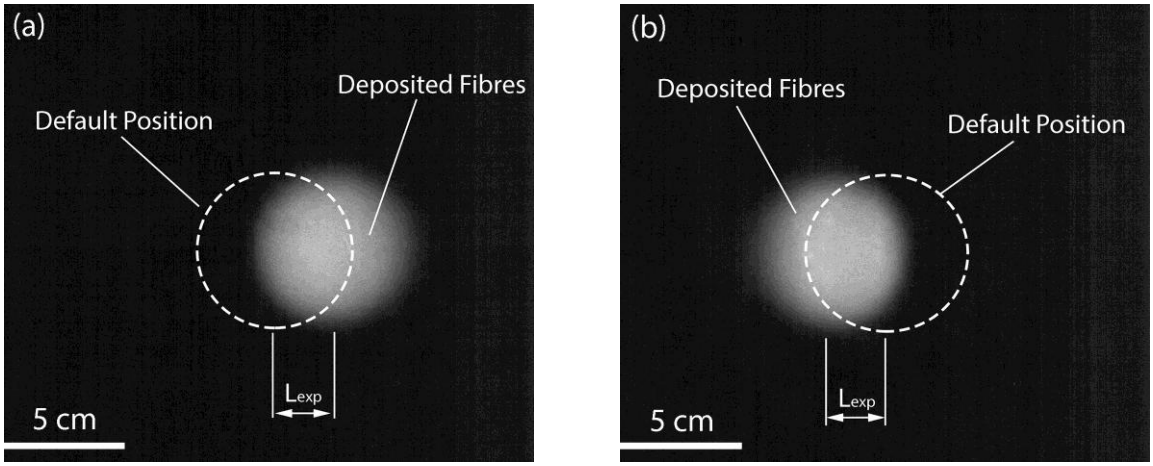

Figure 4-4. Scanned images showing the shift of the deposition area (L_{exp}) with the left and right auxiliary electrodes charged at (a) +12 and 0 kV, respectively, or (b) 0 and +12 kV, respectively.

4.3.2 Effect of voltage difference on magnitude of shift of deposition area

The magnitude of shift of the deposition area (L_{exp}) increases linearly with voltage difference between the auxiliary electrodes (V_d) for both E1 and E2 (Figure 4-5). The average maximum L_{exp} was approximately 23.4 mm from its default position, at a V_d of +12 kV. It should be noted that this limit is expected to be strongly dependent on the electrode geometry and applied electrospinning voltage. The gradients suggest that every 1 kV of voltage difference will shift the deposition area about 2 mm from the origin in a direction away from the most positive electrode (*i.e.* ~2 mm/kV). The magnitude of L_{exp} was found by regression analysis to vary linearly as a function of V_d for both experiments, E1 and E2. A statistically significant linear relationship ($p < 0.05$) between V_d and L_{exp} was observed. The R^2 values of 97% and 90% suggest that the linear regression lines and data are a good fit.

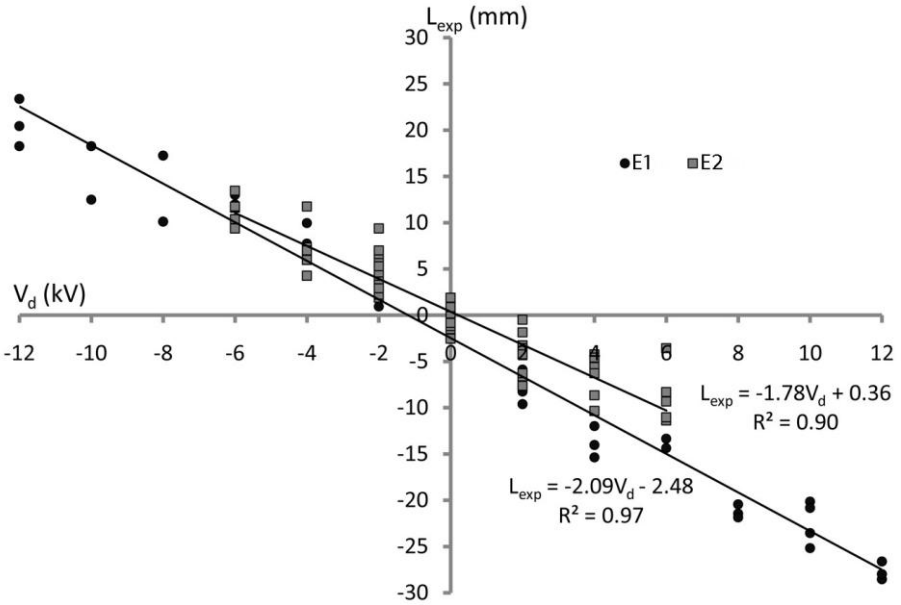

Figure 4-5. The magnitude of shift of the deposition area (L_{exp}) as a function of V_d for E1 and E2. Solid lines indicate lines of best fit from regression analysis.

4.3.3 Effect of base voltage on aspect ratio

E2 offered the opportunity to examine the effect of having both auxiliary electrodes charged. The aspect ratio of the deposition area decreases as the base voltage (V_b) increases, changing the shape of the deposition area from a primarily circular to elliptical shape (Figure 4-6). An inverse linear relationship ($p < 0.05$) was observed between aspect ratio and V_b (Figure 4-7). The observed decrease in the aspect ratio of the deposition area can be described as a "squeezing" effect whereby the lateral electric field constrains the whipping instability region resulting in a narrower deposition area.

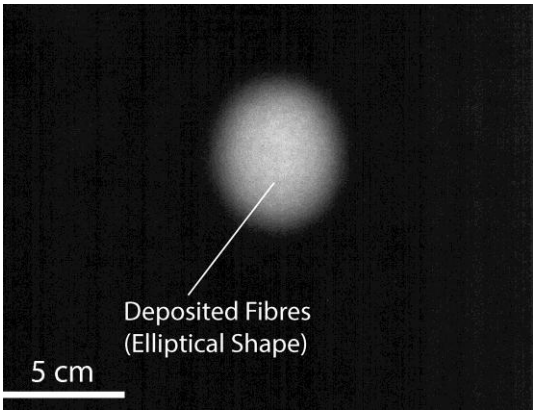

Figure 4-6. The reduction of the aspect ratio of the deposition area when both auxiliary electrodes were charged in E2. The aspect ratio is the ratio of the width of the deposition area to its height.

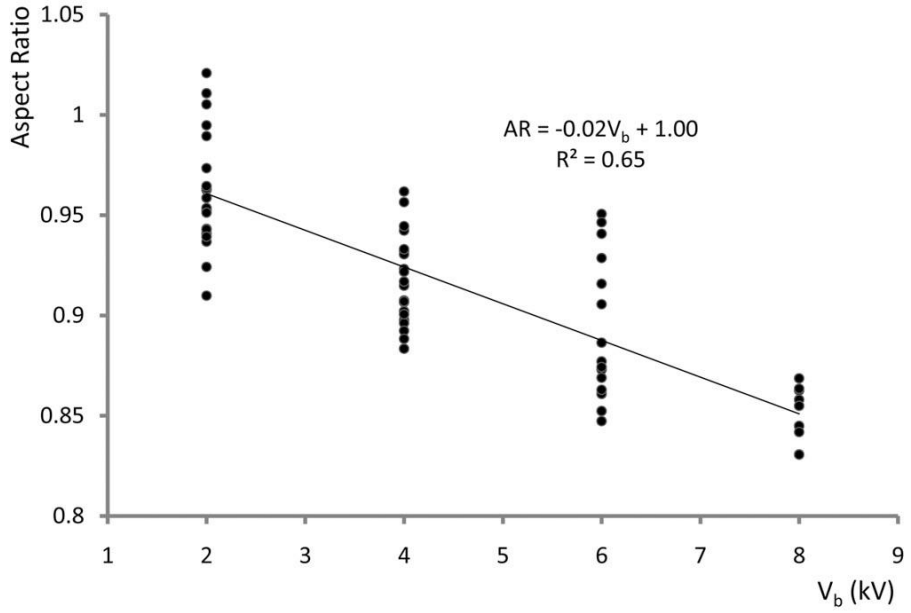

Figure 4-7. The aspect ratio of the deposition area as a function of the base voltage (V_b). Each dot represents the recorded aspect ratio of individual deposition area in E2. Solid line indicates line of best fit from regression analysis.

4.3.4 Voltage difference and base voltage as two independent controls

E2 also offered the opportunity to test if the two control fields, i.e. the V_d for shift and the V_b for changing the aspect ratio of the deposited fibre mat, are independent of each other. Performing a linear regression on L_{exp} as a function of V_b found no significant relationship (p

> 0.05) (Figure 4-8(a)). Further, performing a linear regression on the aspect ratio as a response to V_d shows no significant relationship ($p > 0.05$) (Figure 4-8(b)). Interestingly, it is observed that the variability in L_{exp} or aspect ratio decreases as V_b or V_d increases. However, this may be due to fewer samples taken at the extremes of measurement.

The results demonstrate that not only does V_b not interfere with the shift but that V_d does not interfere with the aspect ratio. The two control fields are therefore independent in their action on the electrospun fibre in flight. In considering the control of the fibre in flight one can simply sum the effects of the different applied electric fields to reach the desired response within the limits of control. A final linear regression was performed on the off-axis deflections (y axis) as a response to the V_d and no significant relationship ($p > 0.05$) was found. Therefore, the deflection field only causes a response along the axis intended.

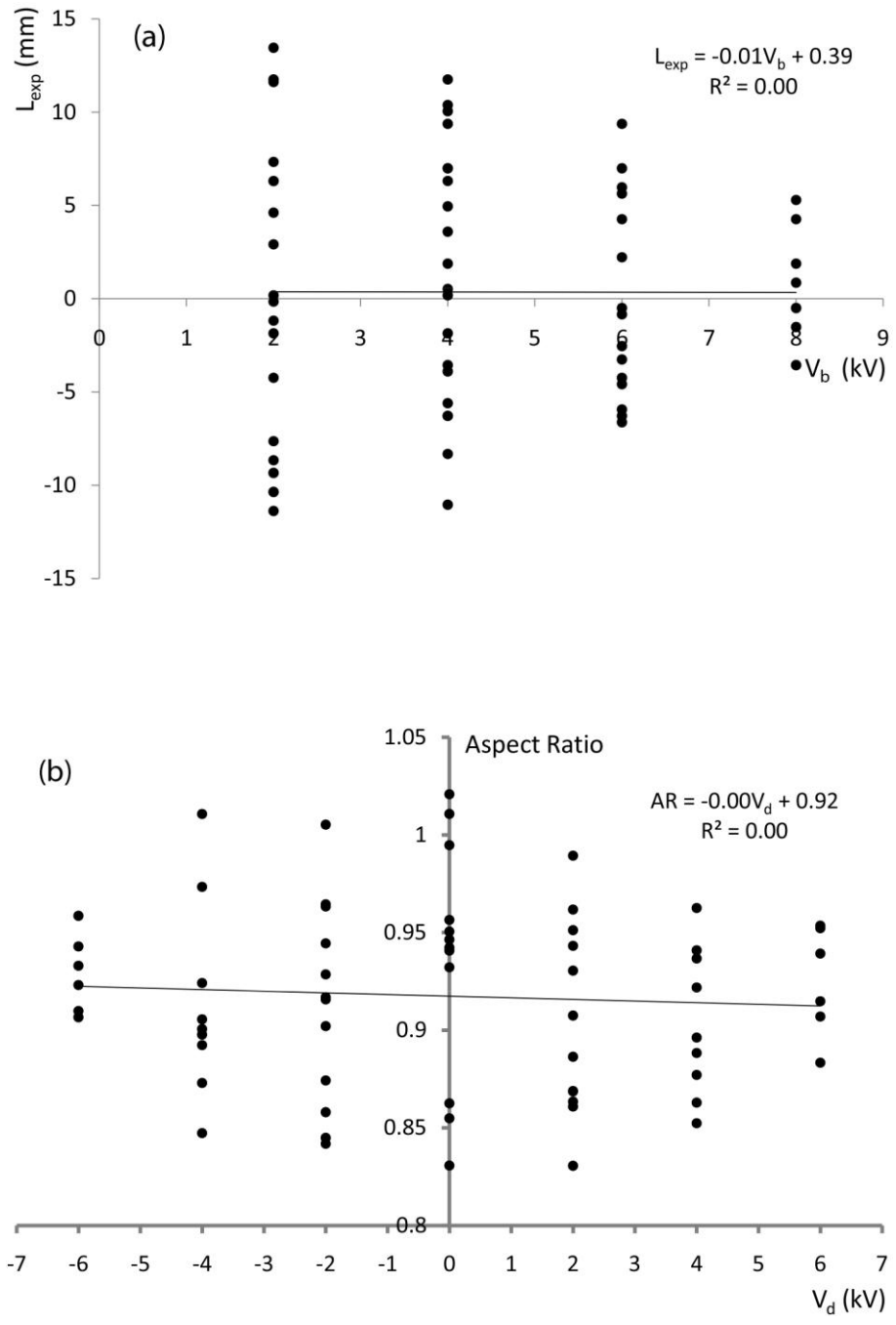

Figure 4-8. (a) The magnitude of shift of the deposition area (L_{exp}) as a function of the base voltage (V_b). (b) The aspect ratio of the deposition area as a function of voltage difference (V_d).

4.3.5 Fibre morphology

Direct observation of the fibres was carried out on scanning electron micrographs of samples produced under the most extreme conditions (*i.e.* 8-8 kV, 12-0 kV, 0-12 kV) and comparisons were made with a control sample (*i.e.* 0-0 kV). The extreme conditions were chosen because at these voltage combinations, the deposition process was subjected to a maximum electrostatic force imposed by the auxiliary electrodes resulting in either maximum shift of deposition area or minimum aspect ratio (Figure 4-5 and Figure 4-7). Randomly deposited PVOH fibres were observed with no sign of morphological abnormalities such as beading or ribbon formation (Figure 4-9(a)-(d)).

When both electrodes were kept at zero, the mean diameter of the control fibres was 325.1 nm (± 46.5 SD) (Figure 4-9(a)). Regardless of direction, the mean fibre diameter was barely changed at 338.8 nm (± 43.9 SD) and 344.9 nm (± 40.8 SD) if one of the electrodes was at +12 kV and the other at 0 kV (Figure 4-9(c) and (d)). However, thicker fibres with a mean diameter of 383.2 nm (± 43.6 SD) were produced when both electrodes were held at +8 kV (Figure 4-9(b)). This is an increase in the fibre diameter by 17.8%, with an actual difference of 58.1 nm.

One of the likely reasons is that when both auxiliary electrodes were charged the electric field along the deposition axis was "squeezed" by the auxiliary electric fields. This confined the area where the whipping instability took place resulting in less thinning of the fibres (Shin et al., 2001). Although the fibre diameters (383.2 nm± 43.6 SD) were still within the expected range of the material and parameters used in this study (300-400 nm), the increase in fibre diameter was outside the standard deviation value of the control sample. In addition, the actual difference of 58.1 nm was more than double of the pixel size (18.3 nm) used in SEM Analyser software. Therefore, the measured difference was significant and the results suggest that thicker fibres will be produced when both auxiliary electrodes are charged at an appropriate voltage.

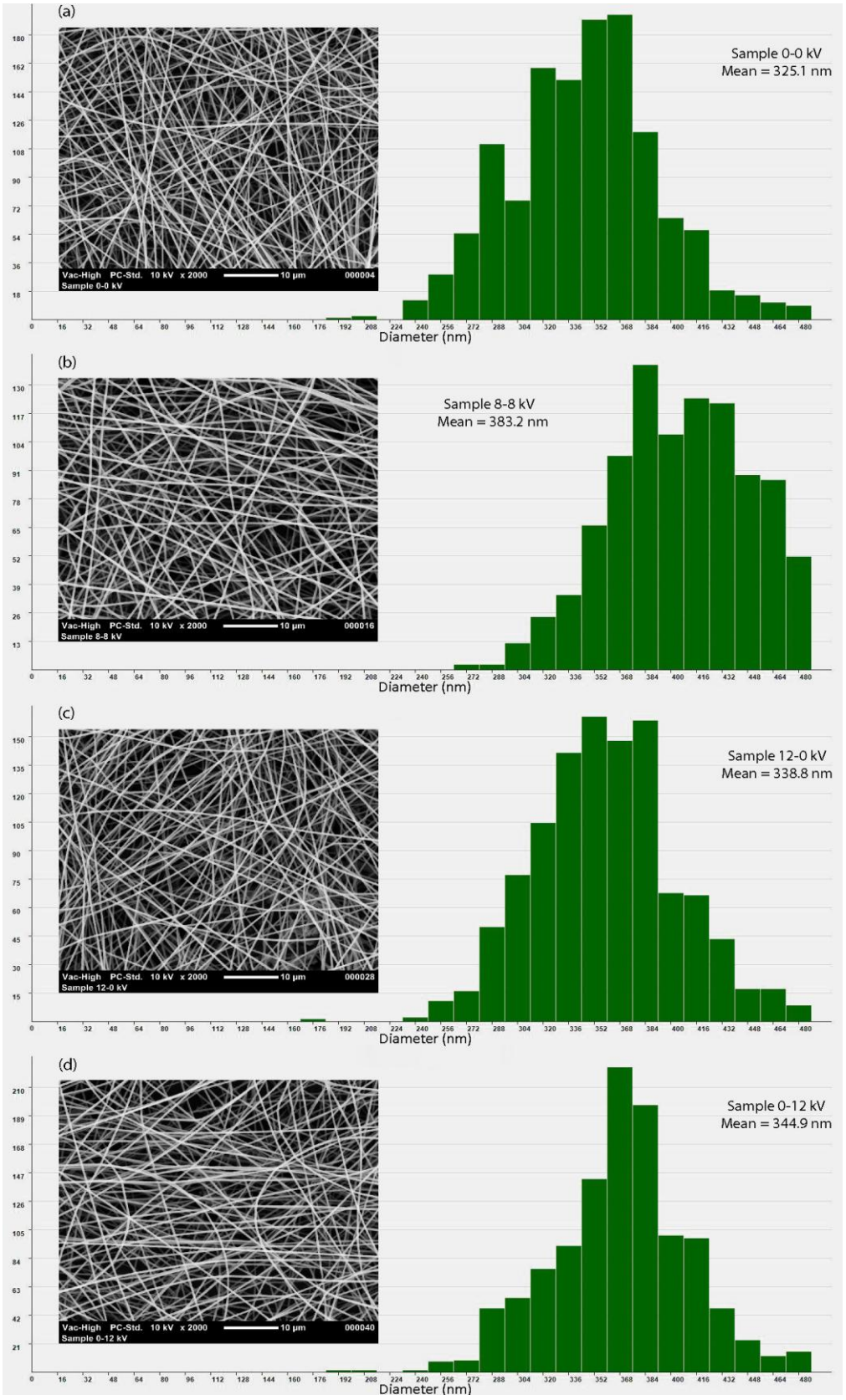

Figure 4-9. Scanning electron micrographs of fibre and distribution of fibre diameter when the auxiliary electrodes were at (a) 0-0 kV (control) (b) 8-8 kV (c) 12-0 kV (d) 0-12 kV.

4.3.6 Simulated electric field strength and the magnitude of shift of the deposition area

The deflection response of the particle to the applied electric field (*i.e.* the particle moved away from the most positive electrode) as calculated in the simulations was similar in nature to that observed experimentally (Figure 4-5). The FEA model depicts the field arrows dispersing evenly from the spinneret towards the collector when both auxiliary electrodes are kept at 0 kV (default condition), causing no deflection in the trajectory of the particle (Figure 4-10(a)). However, the directions of the arrows are deflected to the right from the centre position if a higher voltage is applied to the left electrode (+12 kV) compared to right electrode (0 kV), causing a deflection in the particle trajectory that is influenced by the electric field (Figure 4-10(b)).

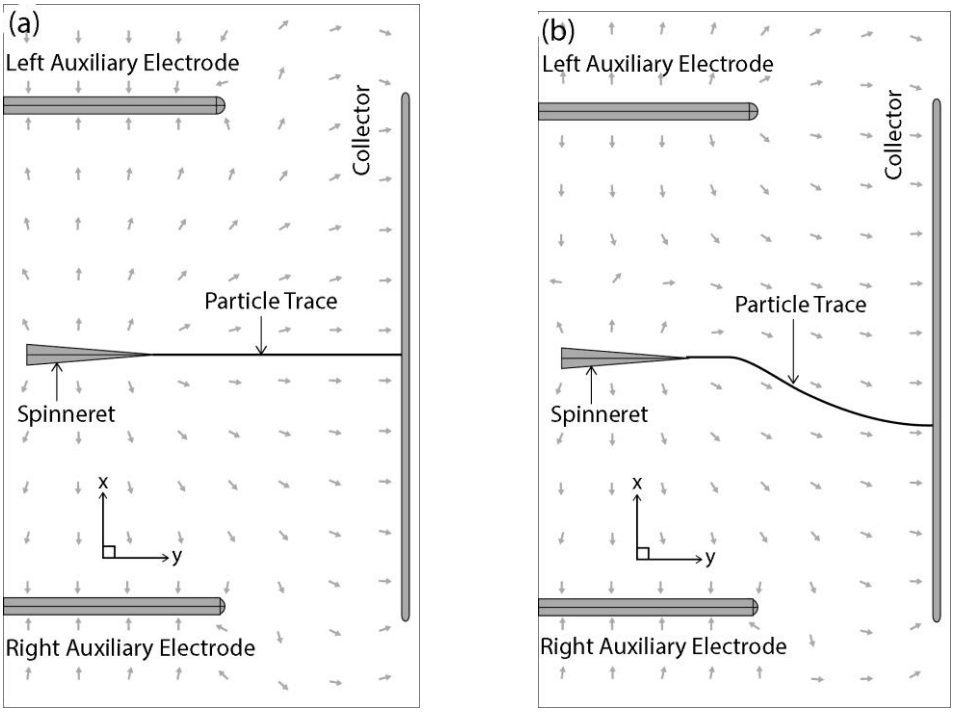

Figure 4-10. The simulated trajectory (solid line) of a charged massless particle (plan view) with voltages of (a) 0-0 kV and (b) +12-0 kV. The electric field direction is represented by the arrows originating from the higher positive potentials (spinneret or charged electrodes) toward the lower potentials.

Due to the alignment of the electrodes only in the x axis (Figure 4-1), only the x axis component of the electric field (E_x) was reported in examining the effect of V_d on the magnitude of shift of the deposition area. The x axis component of electric force F_x is directly proportional to the x axis component of electric field E_x (Equation 4-1). Therefore, plotting the strength of E_x under different applied voltage conditions at the auxiliary electrodes would approximately represent the change of electric force experienced by the electrospinning jet. The magnitude of E_x along the z axis at 10 mm intervals between the spinneret and collector is shown in Figure 4-11. A positive E_x value indicates that the field is acting in the positive x axis direction (or to the left of the experimental setup) and *vice versa* for a negative E_x.

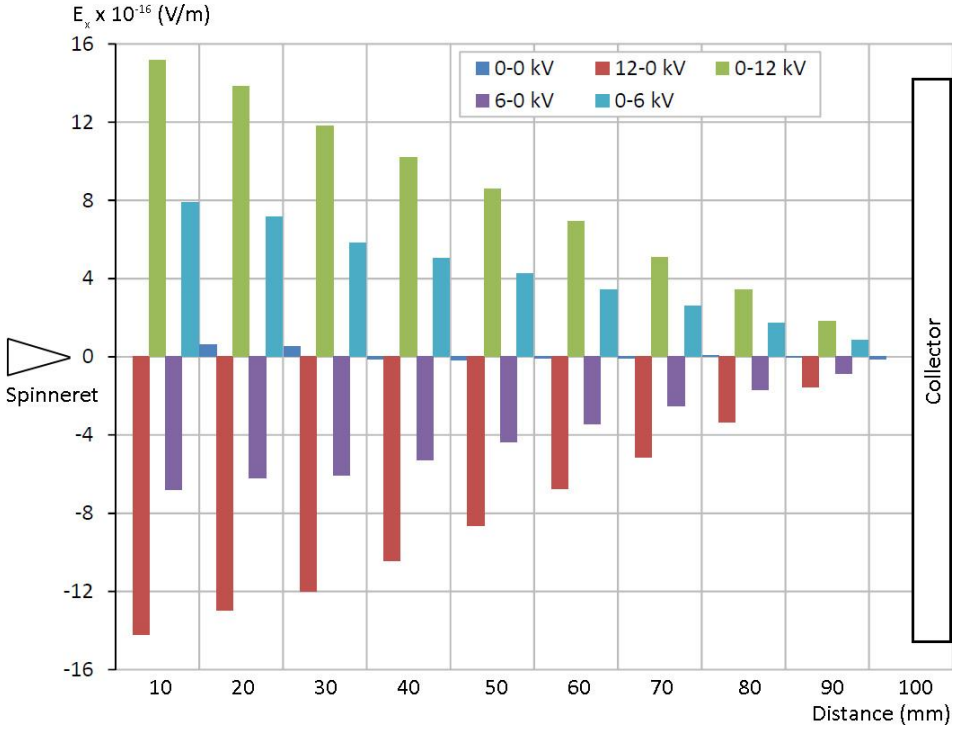

Figure 4-11. The magnitude and direction of electric field component (E_x) along the z axis at 10 mm intervals from the spinneret to collector as a function of V_d.

The magnitude of E_x was negligible along the z axis in the default condition (*i.e.* 0-0 kV), causing no deflection of the particle trajectory (Figure 4-11). However, it is noted that the values of E_x are not zero as expected and this could be due to computational errors resulting from rounding. Using the voltage combinations as in Table 3-1, the simulations show that the

magnitude of E_x increased as V_d increased. For example, the magnitude of E_x at a given position along the z axis when V_d= +12 kV (*i.e.* 12-0 or 0-12) is approximately double that of V_d= 6 kV (*i.e.* 6-0 or 0-6) (Figure 4-11). The simulation results are consistent with the experimentally observed linear relationships in E1 and E2 (Figure 4-5) where L_{exp} increased when V_d increased (*i.e.* ~ 2 mm/kV).

The magnitude of E_x is at a maximum near the spinneret and then reduces to a minimum at the collector due to the auxiliary electrodes' location in relation to the spinneret (Figure 4-11). Thus, the influence of the auxiliary electric field on fibre direction is greater during the earlier rather than later stages of flight between spinneret and collector. The use of longer auxiliary electrodes would increase the magnitude of transverse electric field at the later stages which in turn would prolong its influence on the fibre flight direction.

4.3.7 Simulated electric field strength and the aspect ratio of the deposition area

The FEA model is capable of explaining the "squeezing" effect as evidenced experimentally in E2 (Figure 4-6) by a reduction of the aspect ratio of the deposition area. The deposition process takes place along the z axis (Figure 4-3) which is coincide with the centre of Figure 4-12(a) and (b). The change of electric field components E_x and E_y (Figure 4-12(a) and (b)) correspond to the change of electric forces F_x and F_y that were acting along two orthogonal axes x'-x" and y'-y" (Figure 4-3). The shape of plots is symmetrical with respect to the origin denoting the contrary direction of the forces along the axes - illustrated by the arrows in Figure 4-12(a) and (b). A positive value of E_x or E_y means that the direction of F_x or F_y is to the right and vice versa. Note that the resultant E_x and E_y are zero at the centre due to symmetrical alignment of the setup.

At a low V_b for example 2-2 kV, the auxiliary electric field is less influential than the driving electric field between the spinneret and the collector. The direction of E_x near the centre is pointing outward but changes to the opposite direction (inward) only at a closer distance to the auxiliary electrodes (~ ±65 mm) (Figure 4-12(a)). Therefore at low V_b, there is no constraining of the whipping instability caused by the electric field near the deposition axis. At a higher V_b, the auxiliary electric field has more influence on the deposition process. The

direction of E_x is pointing inward at any position along the x'-x" axis as denoted by the 6-6 and 8-8 kV curves (Figure 4-12(a)). A higher E_x peak which corresponds to a higher electric force (F_x) is produced with a higher V_b at the auxiliary electrodes. The force acts to constrain the whipping instability and reduce the size of the deposition area in the x direction.

The E_y component along y'-y" also increased with V_b but the direction of E_y is always pointing outward suggesting no constraining of the whipping instability in the y axis. Note the magnitude and change in E_y is less than for E_x for a given V_b (Figure 4-12(b)). This is solely due to the alignment of the auxiliary electrodes in the x axis but not the y axis. This examination of E_x and E_y corresponds to the reduction of the aspect ratio of the deposition area which occurs in the x axis rather than the y axis.

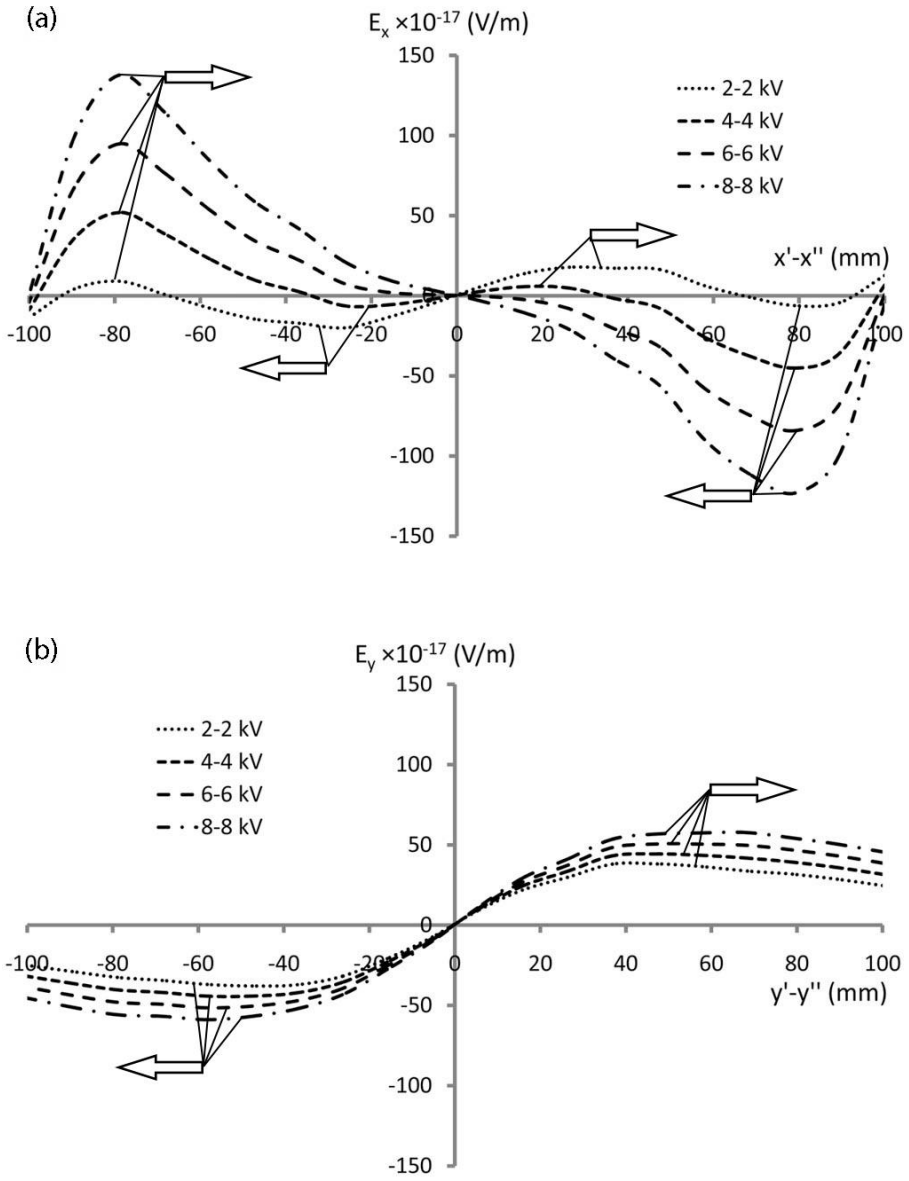

Figure 4-12. The electric field components shown as a function of distance in an x-y plane that is normal to the z axis and equidistant from the spinneret and collector for (a) E_x along x'-x'' and (b) E_y along y'-y''.

4.3.8 Comparison between experiment and simulation

Comparisons are made between the shift of deposition area from experiments (L_{exp}) and simulations (L_{model}) in evaluating the relationships between experiments and simulations (Figure 4-13(a) and Figure 4-13(b)). As expected, the deflection of the particle without mass was greater than the particle assigned a mass. The gradient of the best fit line for the massless particle was 2.64 compared with 0.41 for the particle with mass for E1 (Figure 4-13(a)).

Similarly, the gradient for the massless particle was 2.13 compared with 0.43 for the particle with mass for E2 (Figure 4-13(b)). Clearly, a charged particle with mass has an inertia that decreases its deflection in a given electric field although it does spend more time in the region of transverse electric field compared to a massless particle. A particle without mass will experience infinite acceleration (Equation 4-2) so that the trajectory of the particle is simply guided by the direction of the electric field lines.

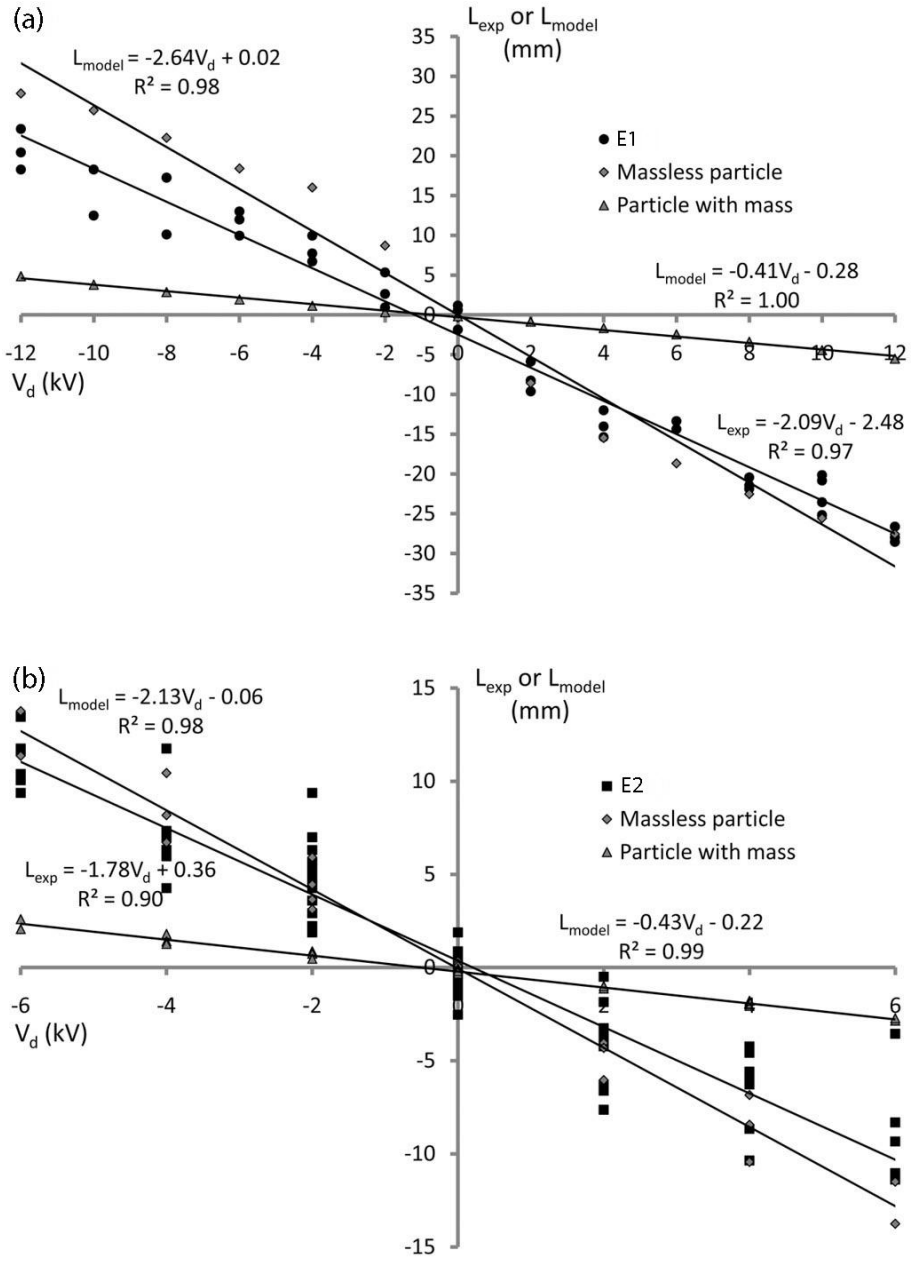

Figure 4-13. L_{exp} and L_{model} as functions of V_d for (a) E1 and (b) E2. Solid lines indicate lines of best fit from regression analysis.

Interestingly, the value of L_{exp} from electrospinning of PVOH correlates more closely with that of a charged particle without mass rather than a charged particle with mass. This would indicate that the direction of the electrospun fibres should follow the electric field lines. However, this conclusion would be contrary to some preliminary experimental observations (Figure 4-5). Further experiments and simulations were performed using an electrospinning distance of 130 mm to eliminate the possibility of a coincidental correlation due to the specifics of the experimental setup. Additionally, the auxiliary electrodes were shifted 30 mm further away from the spinneret. The spinning voltage was also increased from +10 kV to +12 kV to achieve stable electrospinning. The gradients from the linear fits were determined to be 1.53 and 3.15 for the experimental and simulated (massless particle) results, respectively (Figure 4-14).

These results confirmed that the correlation found earlier between L_{exp} and a charged particle without mass was coincidental. In the simulation, the extra distance between the spinneret and collector allows more time for the massless particle to travel further before reaching the collector. However, increasing the distances in an experiment would only lead to less influence from the control field on the electrospun fibre.

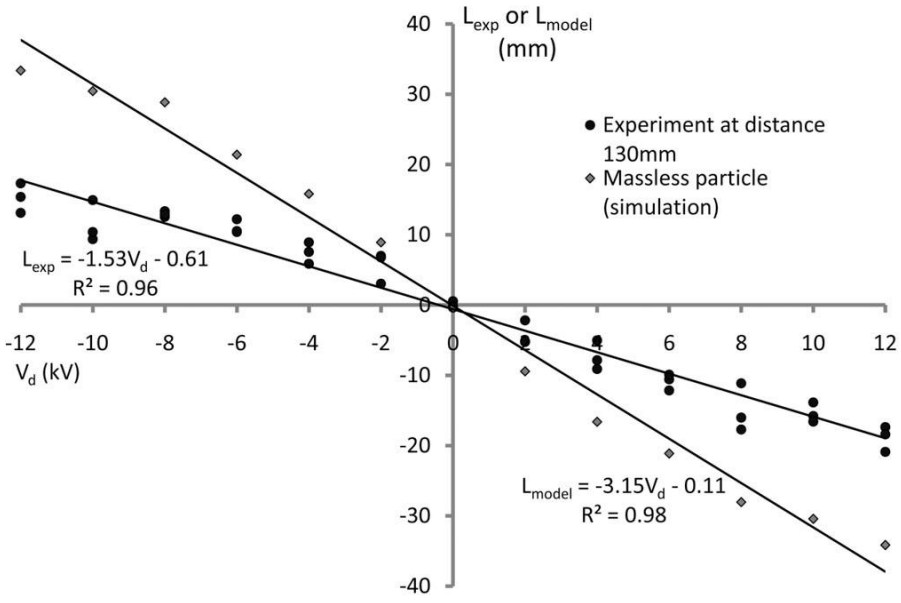

Figure 4-14. L_{exp} and L_{model} as functions of V_d and using a spinneret-collector distance of 130 mm. Solid lines indicate lines of best fit from regression analysis.

CHAPTER 5

CONTINUOUS SCANNING OF A SINGLE ELECTROSPINNING JET USING AUXILIARY ELECTRODES CHARGED WITH TIME-VARYING ELECTRIC VOLTAGE

5.1 Introduction

The knowledge gained in Chapter 4 was further developed by using time-varying electric (alternating current, ac) voltage. As opposed to direct current (dc) where the electric charges flow in only one direction, the flow of charges periodically reverses direction in a time-varying voltage. A typical form of a time-varying voltage is a sine wave voltage in which the amplitude of the voltage falls and rises within a period in accordance to a sine waveform (Boylestad, 2000).

One of the earliest applications of time-varying voltage in electrospinning was described in a patent by Norton (1936). Time-varying voltage was applied at a pair of auxiliary electrodes as a method to introduce alternating lateral forces on the fibres in flight to produce crimped fibres. Time-varying voltage has also been proposed as the driving voltage in electrospinning for achieving better fibre alignment due to reduced whipping instability (Kessick et al., 2004, Sarkar et al., 2007). Reduced whipping instability was achieved because the alternating polarity of the applied voltage lowered the net charge of the fibres and therefore the electric forces which responsible for producing the instability also reduced (Kessick et al., 2004). However, it was noted that the reduced whipping instability caused less thinning and drying of the fibres producing thicker and beaded fibres (Kessick et al., 2004).

Recently, the use of time-varying voltage in the form of a square wave was described for producing aligned electrospun fibres (Grasl et al., 2013). A pair of dc biased antiphase square wave voltages were used to charge a pair of auxiliary electrodes. Compared to a conventional

sine wave voltage, a square wave voltage in practise provides an instantaneous change of voltage at the electrodes. It was found that at a high switching frequency (f = 30-60 Hz) the varying electric field influenced the whipping instability causing the fibres to flick between the electrodes (Grasl et al., 2013). As a result, horizontally aligned fibres were collected on the collector.

In this study, the intention was to produce a wider deposition area rather than producing aligned fibres. It is hypothesized that the application of two antiphase time-varying voltages at the auxiliary electrodes would provide a continuous scanning of the jet producing a wide and uniform electrospun fibre mat. Therefore instead of square waves as used by Grasl et al. (2013), two low frequency (f = 0.1 Hz) sine or triangle wave voltages were used. The uniformity of the samples was examined using an image analysis technique as described in detail in later section.

5.2 Experimental procedures

5.2.1 Experimental apparatus

The Model ES4 electrospinning machine (Electrospinz Ltd., New Zealand) was modified to include a pair of auxiliary electrodes and a rotating drum as the collector (Figure 5-1). The electrodes were stainless steel plates (T430, CAMS Ltd., NZ) measuring 100 × 100 × 0.7 mm placed to the sides of the spinneret at a distance of 100 mm. The drum was a stainless steel cylinder measuring 300 mm wide with a circumference of 1 m and was grounded through its electrical connection. The distance between the drum and the spinneret was 100 mm. The drum was connected to a three phase motor and the rotational speed was set at 25 rev/min.

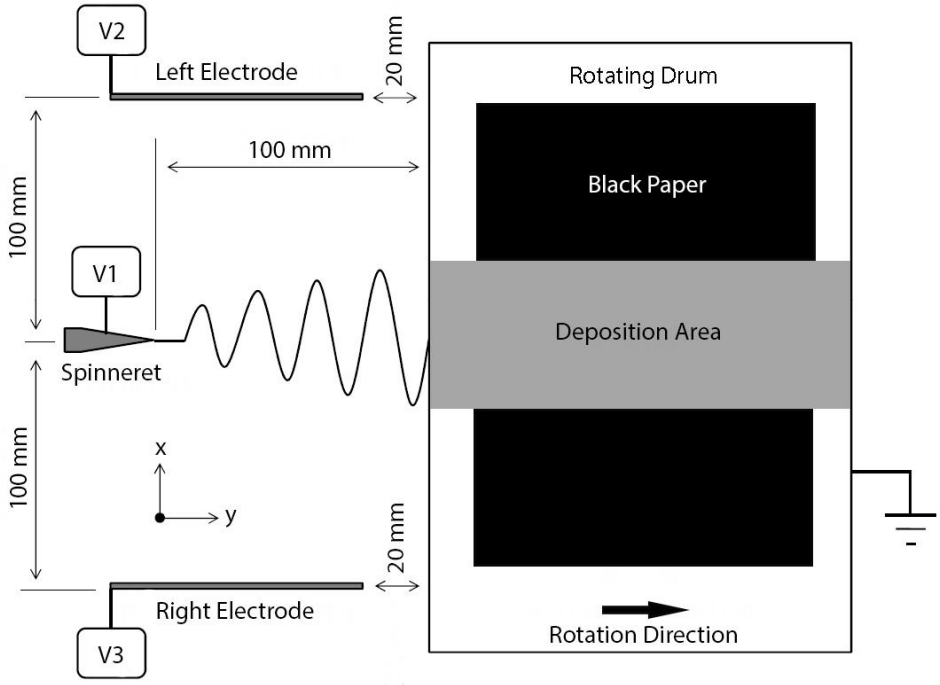

Figure 5-1. The plan view of the experimental setup.

The applied voltage at the spinneret V_1 was +16 kV dc (Glassman High Voltage, Inc.) throughout the experiment. A higher driving voltage compared to the one used in Chapter 4 was applied due to different geometry *i.e*. longer auxiliary electrodes for achieving maximum deflection of the deposition area. The auxiliary electrodes were independently connected to two high voltage power supplies V_2 and V_3 (Model 4330, EMCO High Voltage, Corp.). The applied voltages at the spinneret V_1 and at the auxiliary electrodes V_2 and V_3 were controlled using a LabVIEW^{TM} program (Version 10.0, National Instruments) (Appendix 3) and a compactDAQ data acquisition platform (NI cDAQ-9174 with NI9263 module).

5.2.2 Samples preparation

Similar to Chapter 4, a sheet of A4 black paper (80 g/m^{2}Kaskad Raven Black 1516RB) was used as the substrate and mounted in a registered position on the surface of the drum (Figure 5-1). Two different experiments were conducted in which the auxiliary electrodes were charged (i) by time-varying voltages and (ii) using a combination of dc voltages.

In the first experiment, a LabVIEW^{TM} program (Appendix 3) was used to generate two antiphase time-varying waveforms of either sine or triangle waves as input signals to the power supplies (Figure 5-2(a) and (b)). The output voltages V_2 and V_3 at the auxiliary electrodes were two time-varying voltages with a dc offset of +9 kV, amplitude of +9 kV, and period (*T*) of 10 seconds (Figure 5-2(a) and (b)).

The two waveforms were antiphase to each other and a suitable dc offset component was applied (+9 kV) to make sure the applied voltages V_2 and V_3 were always in the positive range (Figure 5-2(a) and(b)). This was done to avoid fibres from being attracted to the auxiliary electrodes if V_2 and V_3 are in the negative range (reverse polarity). The application of two antiphase time-varying voltages at the auxiliary electrodes can be described by applying a series of voltage combinations within a cyclical time frame. As the magnitude of shift of the deposition area relates to voltage difference between the electrodes (Figure 4-5) therefore the application of time-varying voltages will cause the electrospinning jet to move periodically according to the voltage change.

Samples were collected in triplicate for a period of 500 s which was equivalent to 50 cycles of the waveforms. Triplicates of control samples were also collected for 120 s with both auxiliary electrodes at an applied voltage of 0 kV. Note that a shorter deposition time of 120 s was used because the jet was in stationary mode, hence less time required to accumulate a decent amount of fibres for image analysis. The uniformity of the samples was examined using an image analysis technique based on greyscale profiles which will be described in detail in the next section.

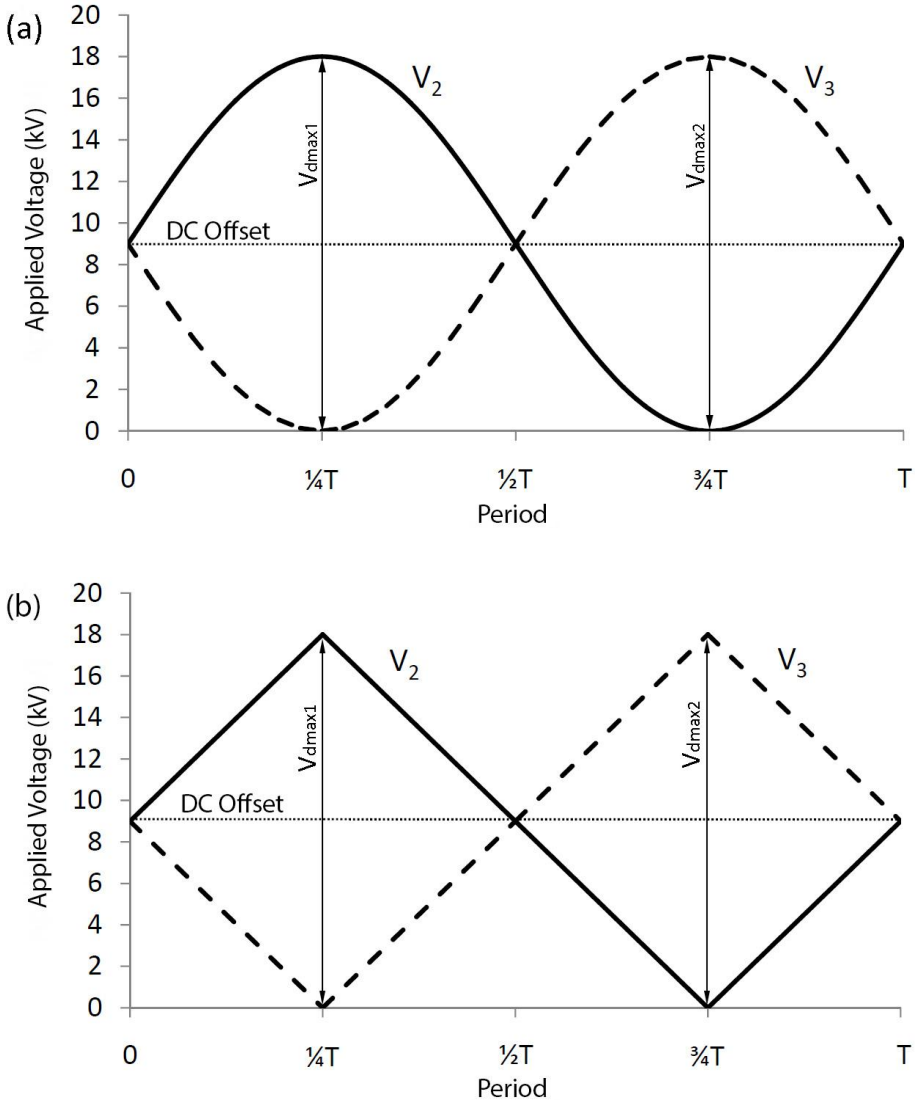

Figure 5-2. Applied voltages V_2 and V_3 at the auxiliary electrodes as a function of time using (a) sine waveforms (b) triangle waveforms.

In the second experiment, the auxiliary electrodes were charged with combinations of dc voltages V_2 and V_3 as shown in Table 5-1. The voltage combinations were chosen to represent the change of V_2 and V_3 at 3 kV intervals, as it goes along the waveforms (Figure 5-2(a) and (b)). Triplicate samples were collected for 120 s for each combination.

The formation of the greyscale profiles when using sine and triangle wave voltage were simulated using Matlab. The applied voltages at the auxiliary electrodes are a combination of voltages V_2 and V_3 that are changing with time as controlled by the type of waveform being applied. There is a correlation between voltage combination (V_2 and V_3) and spatial location

of the deposition area according to Figure 4-5. Therefore, superimposing all the greyscale profiles obtained from each voltage combination should give a prediction of the final greyscale profile by considering the dV/dt.

Table 5-1. The various dc voltage combinations and the times required for the voltage to fall or rise in the 3 kV range (t_1-t_7.).

Samples (kV)	18-0	15-3	12-6	9-9	6-12	3-15	0-18
V Range (kV)	16.5-16.5	16.5-13.5	13.5-10.5	10.5-7.5	7.5-4.5	4.5-1.5	1.5-1.5
Time	t_1	t_2	t_3	t_4	t_5	t_6	t_7
Sine Wave (s)	1.89	0.72	0.56	0.56	0.56	0.72	1.89
Triangle Wave (s)	0.83	0.83	0.83	0.83	0.83	0.83	0.83

The times required for the voltage to fall or rise in the 3 kV range (t_1-t_7) were calculated using a graphical method so as to simulate the effect of different voltage change rates (Table 5-1, Figure 5-3(a) and Figure 5-3(b)). The calculated times were then used as weightages when superimposing the greyscale profiles so as to mimic the speed of the passes of the jet with varying dV/dt.

The rate of voltage change is not consistent when using a sine wave voltage (Figure 5-3(a)). As expected, the longest time occurs during the voltage rise and fall around V_{dmax1} and V_{dmax2} ($t_1 = t_7 = 1.89$ seconds) when the electrospinning jet is at the maximum deflection point. Meanwhile, the shortest time occurs when the electrospinning jet passes the default position ($t_3 = t_4 = t_5 = 0.56$ seconds). However, the rise and fall times at all time points are equivalent (*i.e.* $t_1 = t_2 = t_3 = t_4 = t_5 = t_6 = t_7 = 0.83$ seconds) when applying the voltage with a triangle wave (Figure 5-3(b)).

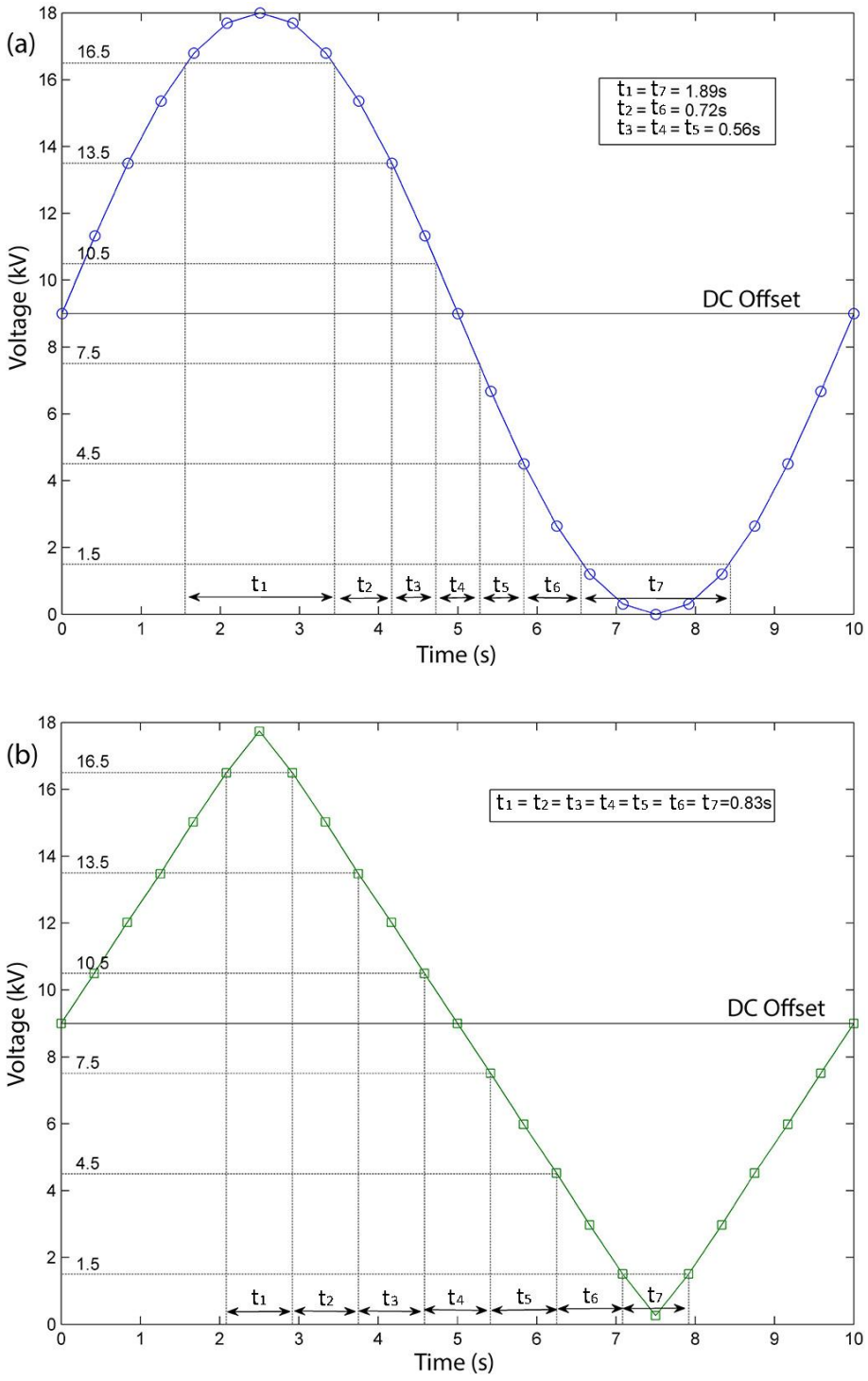

Figure 5-3. The plot of voltage as a function of time when using (a) sine and (b) triangle waveform.

5.2.3 Image analysis technique for examining the uniformity of the deposition area

Image analyses were carried out using Adobe® Photoshop® version CS6 (San Jose, United States) and ImageJ version 1.46r (National Institutes of Health, USA). Samples were scanned at 300 dpi (MICROTEK ArtixScan 1800f) and saved as 8-bit greyscale TIFF images. The brightness level of the scanned image was calibrated within Photoshop® using a photographer's standard grey card (Agfa-Gevaert N.V., Belgium) to maintain consistency between the images.

In an 8-bit greyscale image, the greyscale value of each pixel ranges from 0 to 255 which represented black and white respectively (Burg, 2008). ImageJ was used to measure the greyscale value of a line of pixels along the long side of the scanned images (1 × 3481 pixels) (Figure 5-4). A total of 1000 measurements were done simultaneously to give an average value (hereinafter called greyscale average). The total measured area of 1000×3481 pixels is marked (yellow) in Figure 5-4. The data was exported to Microsoft Excel® for analysis. The profiles of greyscale average as a function of the position on the substrate were plotted. The uniformity of the deposition area was examined by observing the variation of the greyscale average.

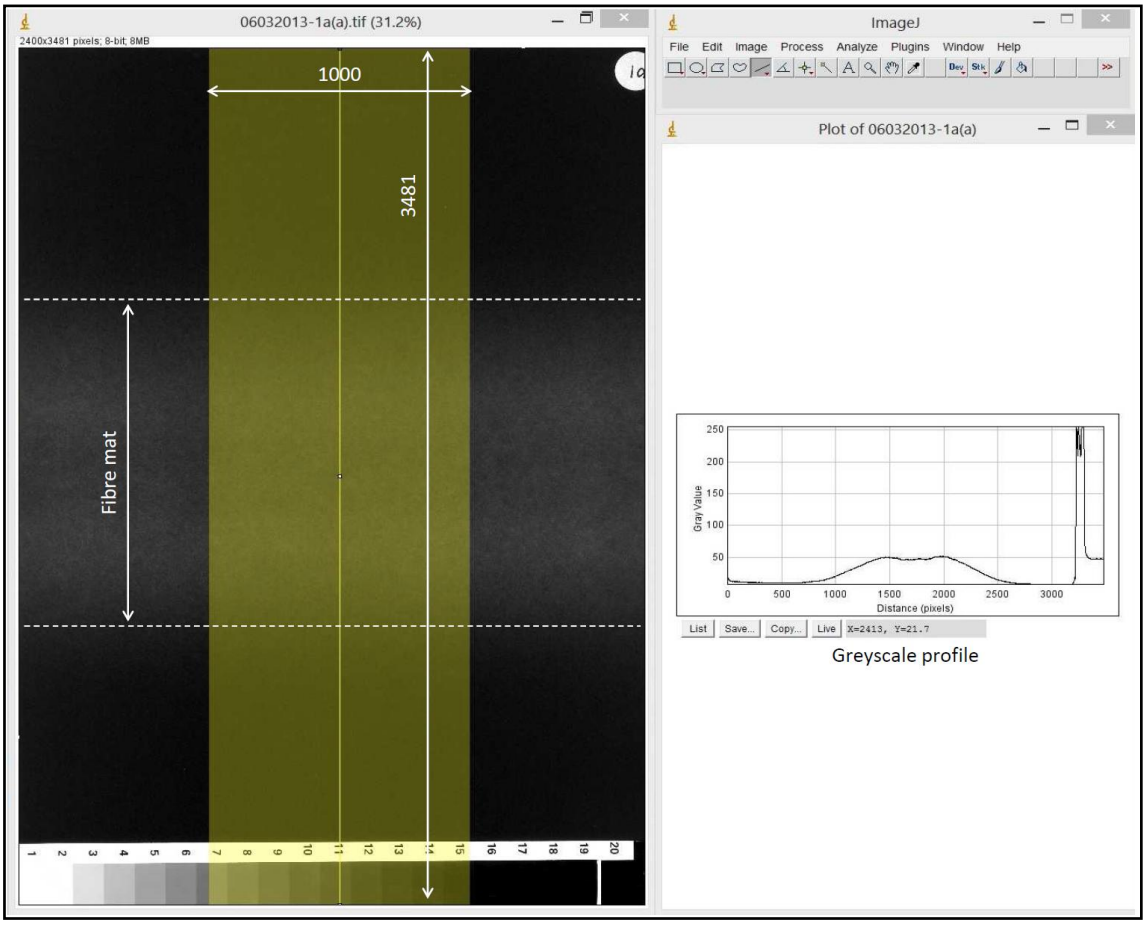

Figure 5-4. Screenshot of the measurement method used to determine greyscale averag eusing ImageJ. The measured area (yellow) of 1000×3481 pixels is shown on the left and the corresponding profile of greyscale values across the substrate is shown on the right.

5.3 Results and discussion

5.3.1 General Observations

In the absence of the auxiliary electrodes or when the auxiliary electrodes were both kept at 0 kV, a typical electrospinning jet was observed with a straight part of several millimetres before the onset of the whipping instability. When the auxiliary electrodes were charged with time-varying voltages, the electrospinning jet was observed to periodically deflect to-and-fro in accordance with the changing electric field. The scanning speed of the jet is dependent on the switching frequency of the waveform used. When the frequency of the waveform increased, the scanning speed increased. At a period (T) of 10 s or f = 0.1 Hz, the scanning movement of the jet was sufficiently slow to be observed by naked eye.

The magnitude of deflection of the jet depends on the voltage difference between the auxiliary electrodes (*i.e.* $V_d = |V_2-V_3|$) (Figure 5-2). The jet started as a straight jet at a default position at t = 0 when both V_2 and V_3 = +9 kV (V_d= 0 kV). After that as V_2 increases and V_3 decreases, the jet moved to the right with its magnitude of deflection increasing over time. The deflection of the jet continues until reaching the first maximum deflection point at ¼*T*. At this point, the voltage difference is at a maximum when V_2 = +18 kV and V_3 = 0 kV giving V_d = 18 kV (V_{dmax1}). After ¼*T*, the deflection magnitude of the jet decreases when V_2 decreases and V_3 increases until reaching the default position again at ½*T* when V_d = 0kV. From the default position, the jet moved to the other direction (left) as V_2 continue to decrease and V_3 increases. The deflection continues until reaching the second maximum deflection point at ¾*T* when voltage difference is at another maximum V_d = 18 kV (V_{dmax2}). After ¾*T*, V_2 increases and V_3 decreases reducing the jet deflection until it reaches the default position at *T* and subsequently the cycle continues.

5.3.2 Uniformity of the deposition area

5.3.2.1 Uniformity of deposition area without an auxiliary electric field

The deposited fibres on a black paper substrate formed a white stripe parallel to the direction of rotation of the drum collector. When both of the auxiliary electrodes were held at 0 kV, there was no shift of deposition area observed and the stripe was located around the centre of the drum which coincides with the position of the spinneret (Figure 5-5(a)). A greyscale plot of the sample showed a symmetrical single peak close to a normal distribution (Figure 5-5(b)). The peak of the curve was located just over the 14 cm position and the overall width of deposition was about 8 cm wide. Based on prior tests, it was observed that the greyscale value increased with deposition time. The greyscale value peaked at nearly 25 after a deposition time of 120 s. The shape and location of the greyscale profile suggest that there was no influence imposed by the auxiliary electrodes when both are held at 0 kV.

It is noted that the greyscale profile in Figure 5-5(b) appears to be wider compared to the original scanned image in Figure 5-5(a). This is thought due to the inferiority of human eyes in distinguishing grey levels compared to a computer (Russ, 2007). The greyscale profile also

suggests that the highest density is around the centre and minimum at the edges. The difference in density is thought to be due to the random nature of depositing a long fibre in the form of coils caused by the whipping instability. Repulsive forces exist due to the same charge between the coils and these forces are balanced by the viscoelasticity of the fibre preventing it from strayed away. Considering a typical round deposition on a stationary collector, it can be visualized as depositing a huge number of small coils within a bigger circle similar to a hypocycloid-like pattern but in a random manner. This would create a deposition profile as depicted in Figure 5-5(b).

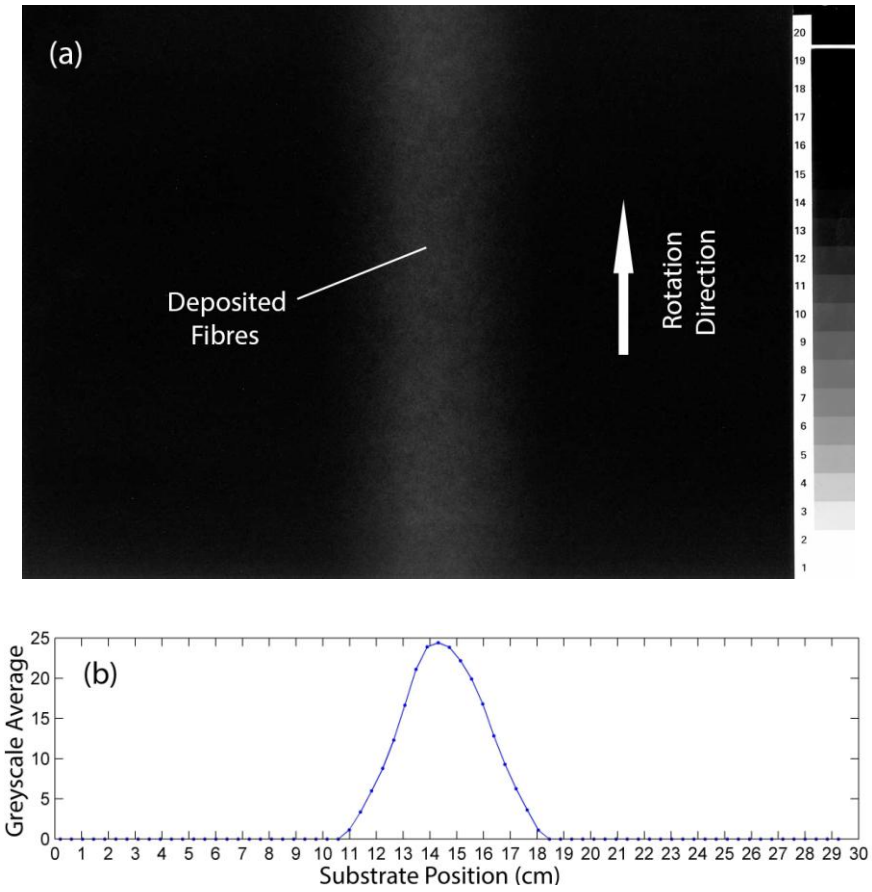

Figure 5-5. (a) A scanned image depicting the deposition pattern of electrospun PVOH fibres after 120 seconds on a piece of A4 black paper substrate with auxiliary electrodes at 0 kV. The scale on the right shows the grey card used to calibrate the scanned images. (b) The corresponding greyscale average as a function of position on the substrate.

5.3.2.2 Effect of sine and triangle wave voltages on deposition area

When the auxiliary electrodes were charged with time-varying voltages, the electrospinning jet was observed to periodically deflect in accordance to the changing electric field. Therefore, the deposition area was observed to have widened compared to the one obtained without the auxiliary electric field (Figure 5-5(a)). Interestingly, the deposition pattern produced was distinctly different when using a sine and triangle wave voltage. The deposition pattern consisted of a two distinct white stripes with a slightly thinner area in the middle when using the sine wave voltage (Figure 5-6(a)). However, the deposition pattern produced a single white stripe when using the triangle wave voltage (Figure 5-6(b)). The density of both samples also appeared to be thicker as the result of a longer deposition time (500 seconds) compared to the control sample (120 seconds).

The greyscale profile of the sine wave voltage sample exhibits twin peaks with a valley at the centre that is close to a bimodal distribution. In contrast, the greyscale profile of the triangle wave voltage sample appeared to have the usual normal distribution (Figure 5-6(c)). The two peaks of the sine wave voltage sample represent the dense area whilst the valley represents the thinner area in the middle (Figure 5-6(c)). The peaks of the greyscale profile when using sine wave voltage are slightly lower (~40) compared to the peak when using triangle wave voltage (~50). However, the width of the deposition area of the sine wave voltage sample is wider (~16 cm) compared to triangle wave voltage sample (~13.5 cm) (Figure 5-6(c)).

Interestingly, the area under each of the greyscale profile was found to be almost the same for these waveforms. By summing the numbers of greyscale average, the total numbers are 379.9 and 345.8 for the sine and triangle waveforms, respectively – a percentage difference of ~9.4%. As the time of deposition is the same, this suggests that to a limit the total greyscale intensity (area under the greyscale profile) correlates with the total fibre deposited.

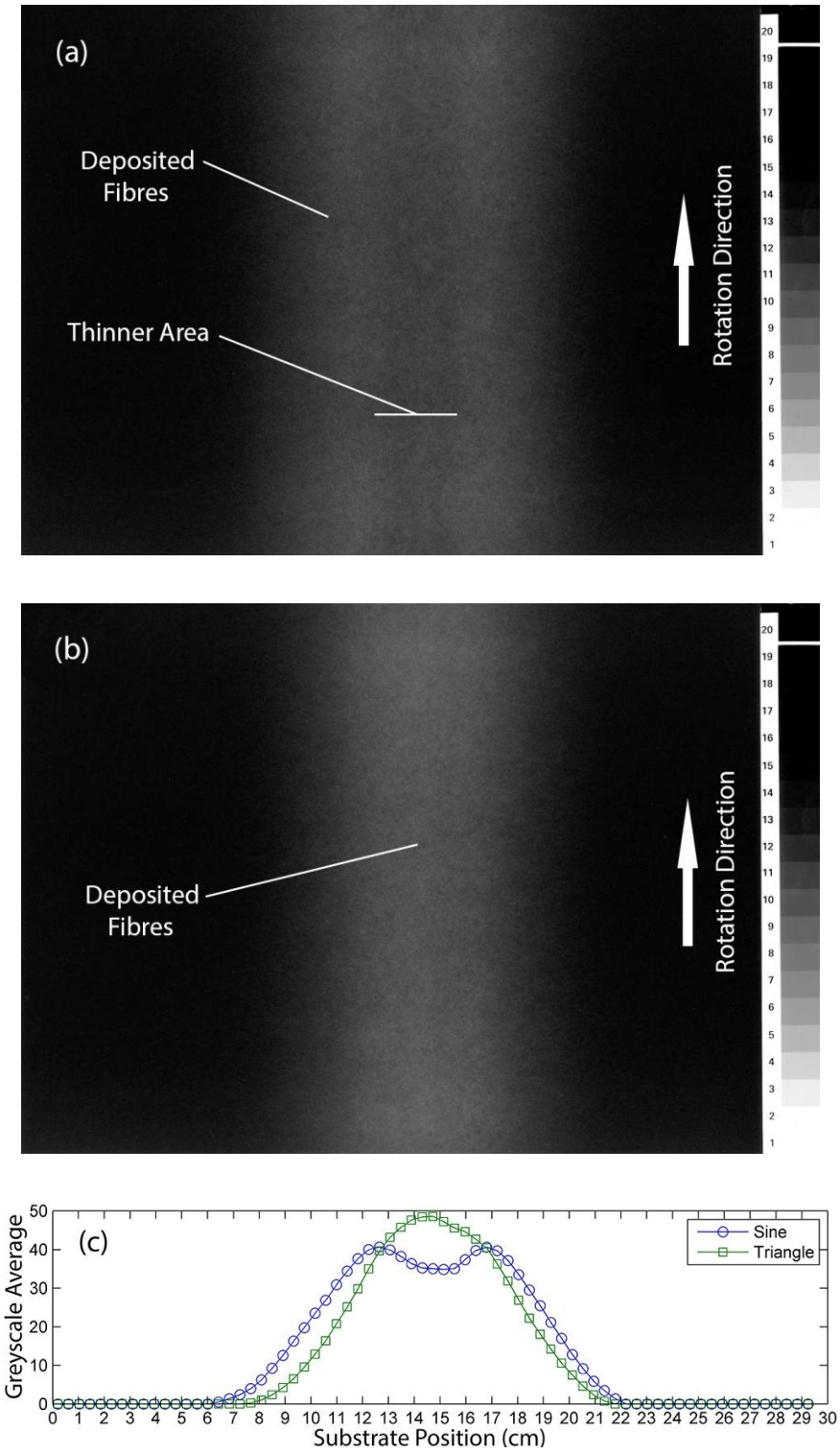

Figure 5-6. A scanned image of the deposited fibres when the auxiliary electrodes were charged with time-varying voltages using the (a) sine wave or (b) triangle wave voltage, and the (c) corresponding profile plots of the greyscale average as a function of position on the substrate.

5.3.3 Scanning speed of the jet when using sine and triangle wave voltages

The difference between the deposition patterns when using sine and triangle wave voltages can be explained by understanding the waveform characteristics. As observed in Figure 4-5, the magnitude of shift of the deposition area is related to voltage difference between the auxiliary electrodes. When using time-varying voltages, the applied voltage at each auxiliary electrode will change periodically, hence changing the deposition direction accordingly. The only differentiating feature of the two waveforms is the rate of voltage change (dV/dt) since the amplitude and frequency are the same.

Only half of the electrode set up needs to be considered since the applied voltages V_2 and V_3 are identical and antiphased. The output voltage (V_2) at the left auxiliary electrode is expressed by Equation 5-1 when using a sine wave voltage.

$$V = f(t) = 9 + 9\sin(\omega t) \qquad \textbf{Equation 5-1}$$

The output voltage (V_2) at the left auxiliary electrode is expressed by Equation 5-2 by using the Fourier series when using a triangle wave voltage.

$$V = f(t) = 9 + \frac{72}{\pi^2}(\sin\omega t - \frac{1}{9}\sin 3\omega t + \frac{1}{25}\sin 5\omega t - ...) \qquad \textbf{Equation 5-2}$$

Graphic representations of the output voltage (V_2) of Equation 5-1 and Equation 5-2 are shown in Figure 5-7(a). The rate of voltage change (dV/dt) would give an approximation of the scanning speed of the electrospinning jet and it is determined by the gradient of Equation 5-1 and Equation 5-2. The dV/dt is plotted in Figure 5-7(b) by differentiating Equation 5-1 and Equation 5-2 to give Equation 5-3 and Equation 5-4, respectively.

$$\frac{dV}{dt} = \frac{df(t)}{dt} = 9\omega\cos(\omega t)$$ **Equation 5-3**

$$\frac{dV}{dt} = \frac{df(t)}{dt} = \frac{72}{\pi^2}(\omega\cos\omega t - \frac{\omega}{3}\cos 3\omega t + \frac{\omega}{5}\cos 5\omega t - ...)$$ **Equation 5-4**

The differentiation of the sine function produced a cosine function however the differentiation of the triangle function produced a square wave function when the Fourier series is summed to infinity (Figure 5-7(b)). Both functions have the same period as the original functions. The y axis values represent dV/dt with positive or negative values representing the direction of change.

When using sine wave voltage, the dV/dt varied with time; with a maximum dV/dt (5.65 kV/s) peaked at t = 0 and t = 0.5*T*; and a minimum (zero) at t = 0.25*T* and 0.75*T* (Figure 5-7(b)). As might expected, the scanning jet moves with varying speeds over the period *T*. Both of the auxiliary electrodes were at +9 kV at t = 0, and the jet started at its default position (centre). Immediately after t = 0, the jet moves rapidly to the right as V_2 increased and V_3 (not shown in Figure 5-7(a)) decreased at their highest voltage change rate. As V_2 increased towards its maximum at t = 0.25*T*, the dV/dt reduced significantly until reaching its minimum rate (zero) at t = 0.25*T*. At this point, V_2 = +18 kV and V_3 = 0 kV giving the maximum voltage difference between the auxiliary electrodes (*i.e.*V_{dmax1} = 18 kV). At this stage, the jet stops momentarily at its maximum deflection magnitude in the right direction. After t = 0.25*T*, the jet moved towards its default position again as V_2 decreased and V_3 increased. At this stage, the voltage change rate increased rapidly until reaching its highest rate at t = 0.5*T*. This causes the jet to spend less time when the jet passed through its default position compared to the time spend when the jet at its maximum deflection. After the jet crossing the default position, the jet continues to move to the left towards another maximum deflection position at t = 0.75*T* where the maximum voltage difference (V_{dmax2}) is experienced. When the jet reaches its maximum deflection magnitude in the left direction, the scanning speed of the jet reduces significantly and again stops momentarily when the voltage change rate tends to zero. Consequently, the combination of slow passes at the edges and fast passes through the centre leads to a deposition area with two stripes pattern (Figure 5-6(a)).

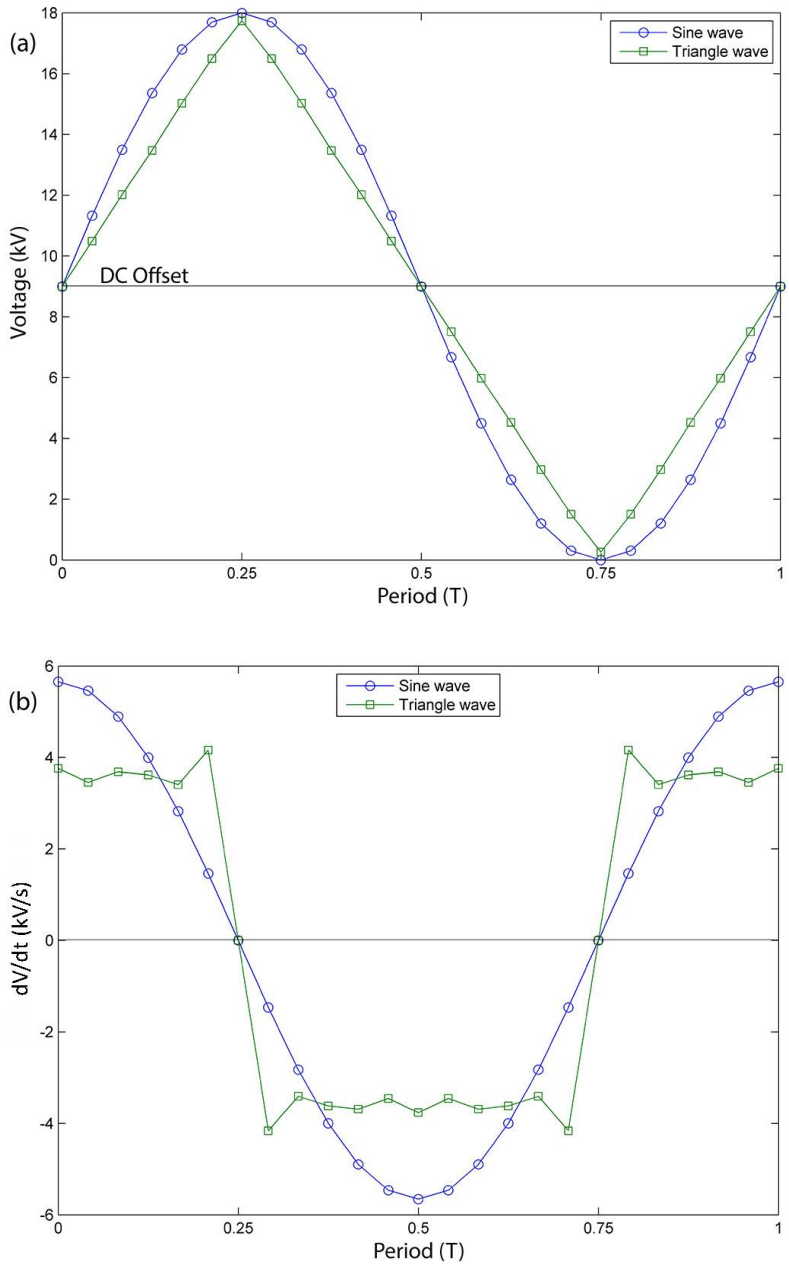

Figure 5-7. (a) Output voltage (V_2) at the left auxiliary electrode when using sine and triangle wave voltages and (b) the dV/dt at the auxiliary electrode when using sine and triangle wave voltages.

In contrast, the dV/dt followed a square wave function when using a triangle wave voltage. Thus, the scanning speed of the jet did not vary at any time point and was found to be a constant rate of ~4 kV/s (Figure 5-7(b)). Moreover, the jet does not pause at the maximum deflection points of t = 0.25*T* and 0.75*T*, so the change of direction of the jet occurs

instantaneously (Figure 5-7(b)). Hence, the use of triangle wave voltage results in a constant jet speed, producing a more uniform deposition pattern compared to that from a sine wave voltage (Figure 5-6(b)).

5.3.4 The simulated greyscale profiles

The greyscale profiles of the samples in Table 5-1 indicate that the magnitude of shift of the deposition area increases as V_d increases (Figure 5-8). The narrowest deposition area was observed when V_b is a maximum (*i.e.* 9-9 kV). It is also noted that the greyscale profiles of the samples that have the same voltage combination but in reverse order are almost symmetrical. These findings are also in agreement with the results from Chapter 4 (Figure 4-5).

Although the greyscale profile for 9-9 kV was found to be the narrowest, it is noted that the height of the peak (*i.e.* density of fibres) is slightly lower than 6-12 kV or 12-6 kV. Thus, the auxiliary electric field may be influencing the deposition rate of the process where both auxiliary electrodes are at +9 kV. Angammana*et al*. (2011) also reported that in a system with multiple sources of electric charge (*i.e.* multiple spinnerets), the local electric field at the spinnerets will deteriorate due to mutual influence between the electric fields.

The simulated greyscale profiles (Figure 5-8) from a sine or triangle waveform were similar to the experimental results (Figure 5-6). A two peaks and a valley profile is produced when using a sine wave voltage as a result of the variability in voltage change rate. In contrast, a profile with a single peak that is slightly narrower than that due to a sine wave is produced when using a triangle wave voltage. It is noted that the simulated profiles were not perfectly smooth, although this would be improved if more dc voltage combinations are used.

The simulation results provide useful information for understanding how the deposition patterns observed in experiment (Figure 5-6) were produced. The results showed that the variation of the deposition patterns was due to dV/dt which coincides with the claim made in the previous section (Figure 5-7(b)). Furthermore, the simulation technique could be a useful tool to predict the deposition pattern by knowing the type of the waveform prior to electrospinning process.

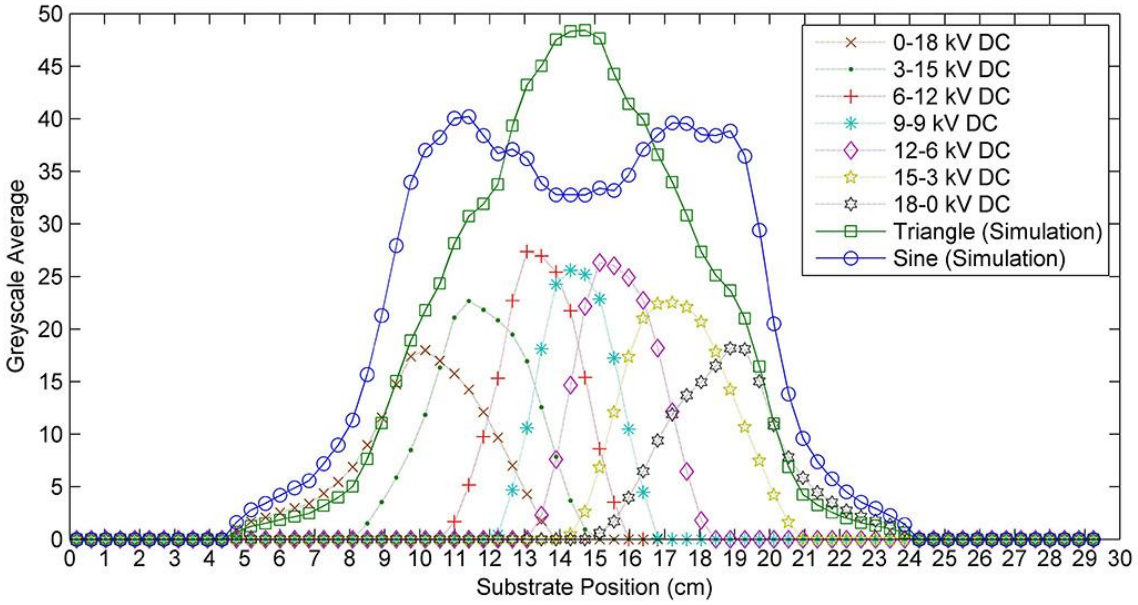

Figure 5-8. A profile plot of greyscale average of various dc voltage combinations and simulated profiles when using sine and triangle waveforms as a function of position on the substrate.

5.3.5 Optimization of the deposition area uniformity using clipped triangle wave voltage

The use of a triangle wave voltage at the auxiliary electrodes produces a more consistent deposition pattern compared to that from a sine waveform. However, the deposited pattern from a triangle waveform still has a relatively narrow peak at the centre. It would be desirable to achieve a deposition pattern that has a flat peak and a wide coverage in order to maximise the usable area from a deposited mat.

The possibility of optimizing the results was studied by combining the two characteristics of both waveforms; a constant scanning speed of the triangle wave voltage for achieving uniform distribution and a temporary stop time of the sine wave voltage for maximising the width of the deposition area. To achieve this goal, the triangle waveforms were altered to produce two antiphase clipped triangle waveforms (Figure 5-9) (Appendix 3). By using this approach, the output voltage at either side of the electrodes will stay at a constant value when it reaches the maximum or minimum value (plateau). The duration of the plateau is called the stop time (t_s).

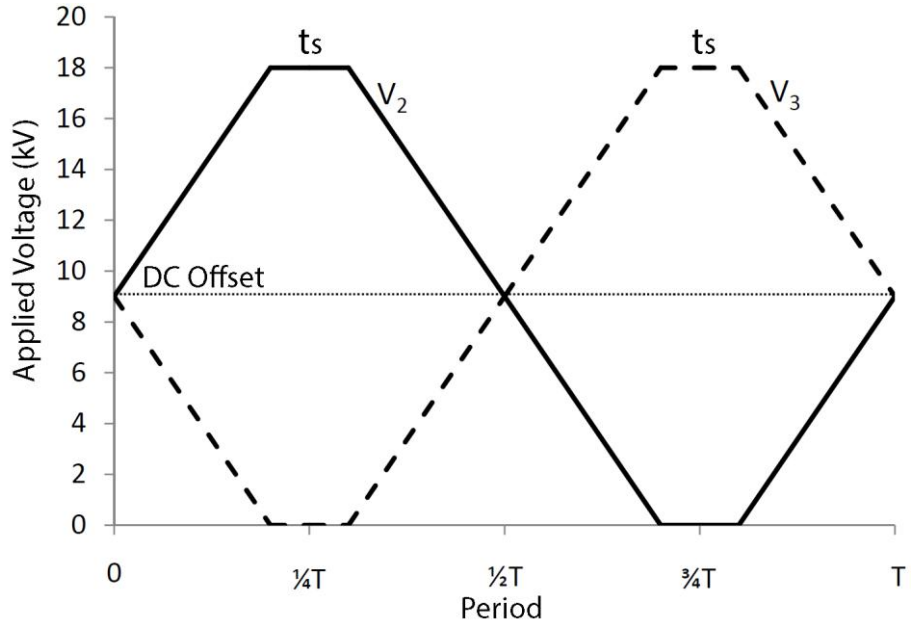

Figure 5-9. Clipped triangle wave voltages V_2 and V_3 with a stop time of t_s.

It was observed in experiments that continuous scanning of the electrospinning jet can be achieved with a controlled stop time at the edges by using a clipped triangle wave voltage. The greyscale plots showed that the use of clipped triangle waves could flatten the centre peak as t_s was increased (Figure 5-10). Optimal results were observed for t_s set between 0.9 to 1.2 seconds. However, a further increase of t_s reintroduces the "valley" as observed in sine waveform sample for t = 1.5s. In addition, the overall width of the deposition area increased with t_s.

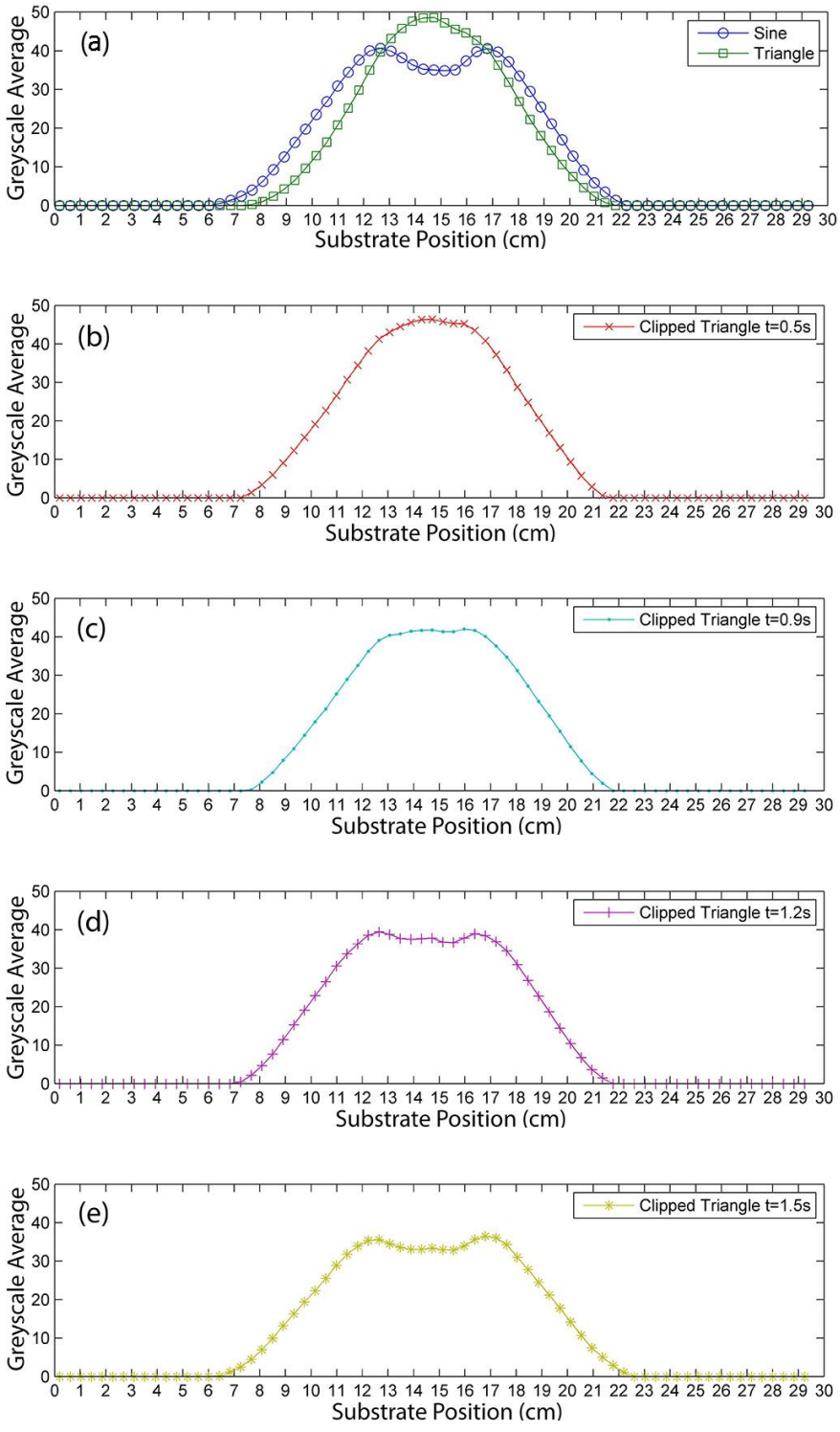

Figure 5-10. Experimental greyscale profiles as a function of position on the substrate when (a) using a sine and a triangle waveform, and (b)-(e) using a clipped triangle waveform with t_s set at 0.5, 0.9, 1.2, and 1.5 s respectively.

Coefficient of variation (COV) was used to measure the uniformity at the centre of the profile between positions of 12.6 and 16.8 cm (Figure 5-11). COV is defined as the ratio of the standard deviation of the greyscale values in that range to its mean (Blum and Rosenblatt, 1972). In this case, the smaller the value of COV, the more uniform the sample. Based on the results, the smallest COV value of 0.02 was exhibited for t_s=0.9s and t_s=1.2s (Table 5-2). Thus, the best uniform coverage of electrospun fibre was achieved by using clipped triangle waves with t_s between 0.9 to 1.2 seconds for the geometrical setup and parameters used in this study.

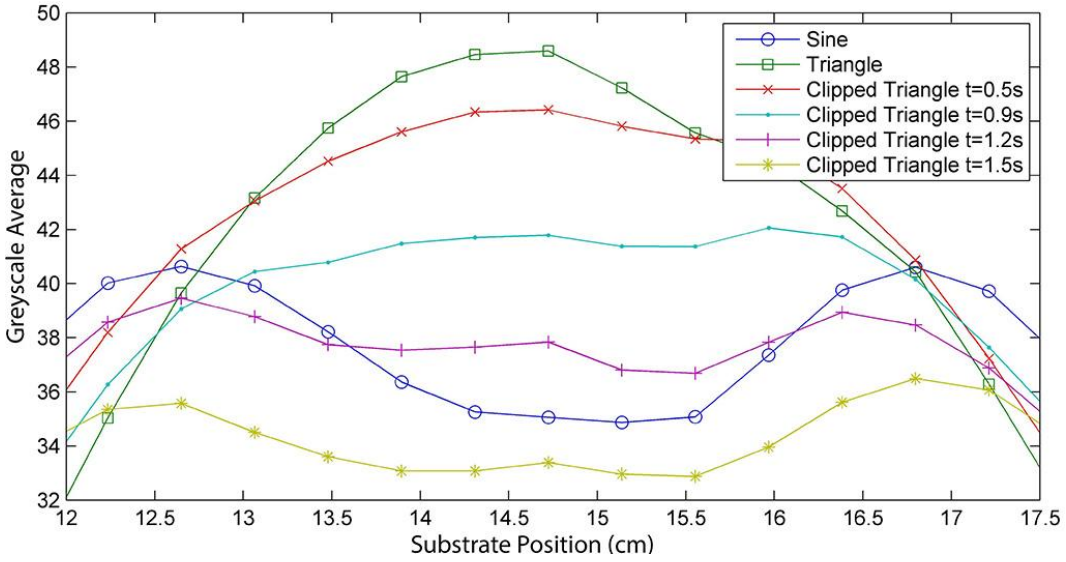

Figure 5-11. A close-up of the centre area of the greyscale plots in Figure 5-10.

Table 5-2. Comparison of coefficient of variation between the samples.

Samples	Sine	Triangle	t = 0.5s	t = 0.9s	t = 1.2s	t = 1.5s
Coefficient of variation	0.06	0.07	0.04	0.02	0.02	0.04

5.3.6 Fibre morphology

Although the deposition time in this experiment (500 seconds) was longer than in Chapter 4 (120 seconds), the amount of fibres found in each image was significantly less compared to Figure 4-9. From the scanning electron micrographs, the A4 paper fibres are clearly visible in the background of all images. The thin deposition was due to using a rotating drum (1 m circumference) used as a collector which means the fibres were distributed over a greater area compared to the stationary collector used in Chapter 4. In addition, the continuous scanning of the jet further reduces the density of the deposited fibres for a given area.

The deposited fibres appeared similar for all of the control, sine and triangle wave voltage samples. Solid, dry PVOH electrospun fibres were observed in a typical randomly orientated pattern. However, there were occasional thicker fibres present in all samples including the control sample. A closer examination reveals that the thicker fibres in some cases are actually folded fibres or more than one fibre bonded together. An interesting example is shown in Figure 5-13(a) where a folded fibre is clearly visible, forming a seemingly thicker fibre (see Appendix 4 for a bigger image). Folded fibres are unlikely to be caused by the continuous scanning of the jet since the folded fibres also appear in the control sample. One possible reason for folded fibres may be due to the sudden change of direction of the fibre due to the moving surface of the drum collector.

When using time-varying voltage of either sine or triangle voltage, the measured fibre diameter was similar across the mat (left, centre, right) with a mean value of ~295 nm (± 44.9 SD). Regardless of type of voltage and location of the samples, the difference in mean diameter is within 2.5% with an actual difference of 7.6 nm between maximum and minimum mean values. Note that the measurement of fibre diameter was carried out without including the thick fibres since the number of thick fibres could vary from one image to another, greatly skewing the final average diameter.

The results showed that the continuous scanning of the electrospinning jet has minimal effects on the whipping instability region and the final fibre diameter was maintained. It is noted that the mean diameter value is slightly smaller compared to the value in the first

experiment (Chapter 4). One possible reason was due to a higher driving voltage used in this study (+16 kV) compared to Chapter 4 (+10 kV). A higher driving voltage causes a higher stretching of the electrospinning jet thus producing a thinner fibres (Ramakrishna et al., 2005).

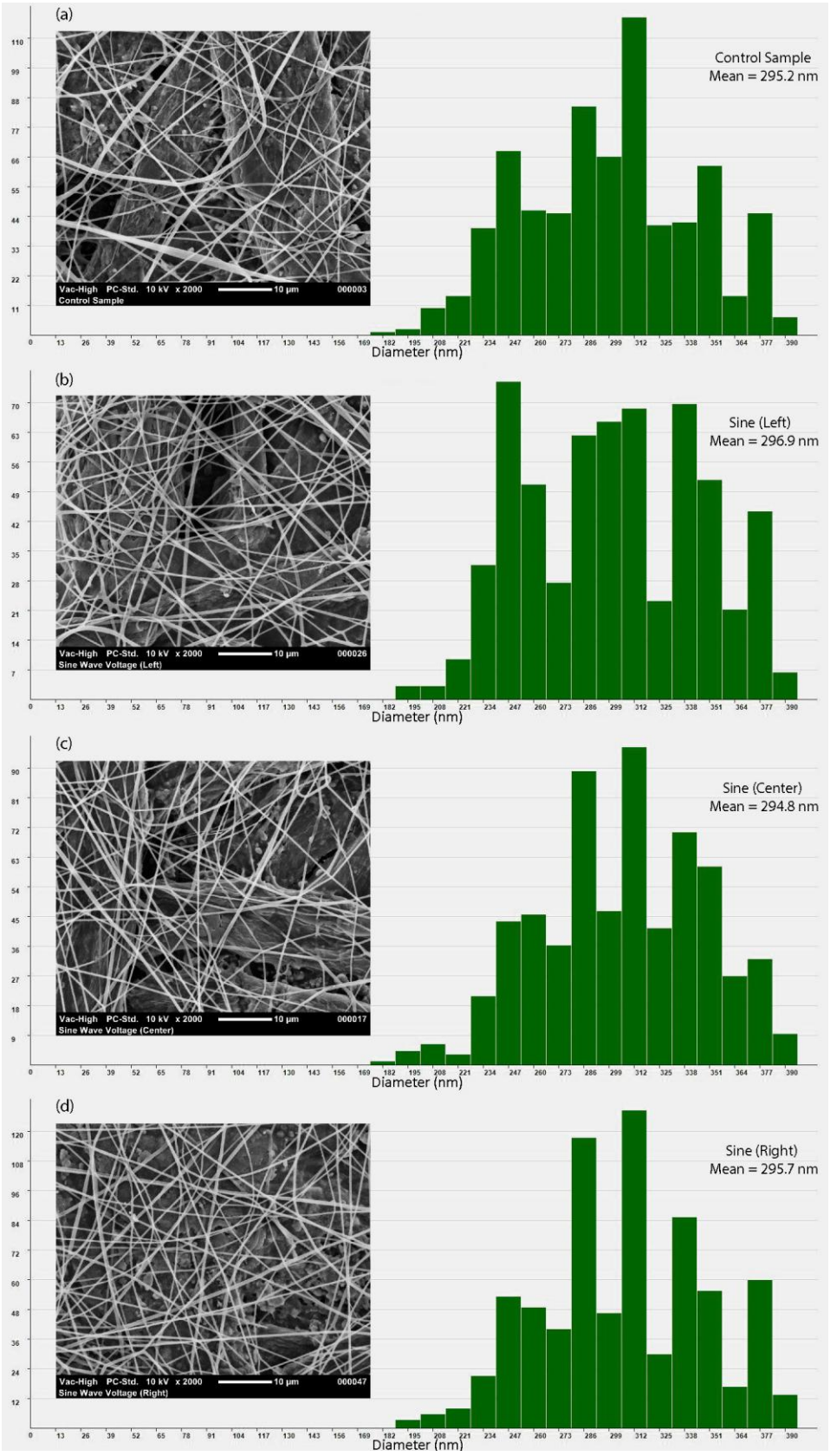

Figure 5-12. The electrospun fibre diameter for the (a) control (b) sine waveform (left) (c) sine waveform (centre) (d) sine waveform (right). Insets show the corresponding scanning electron micrographs of the electrospun mat.

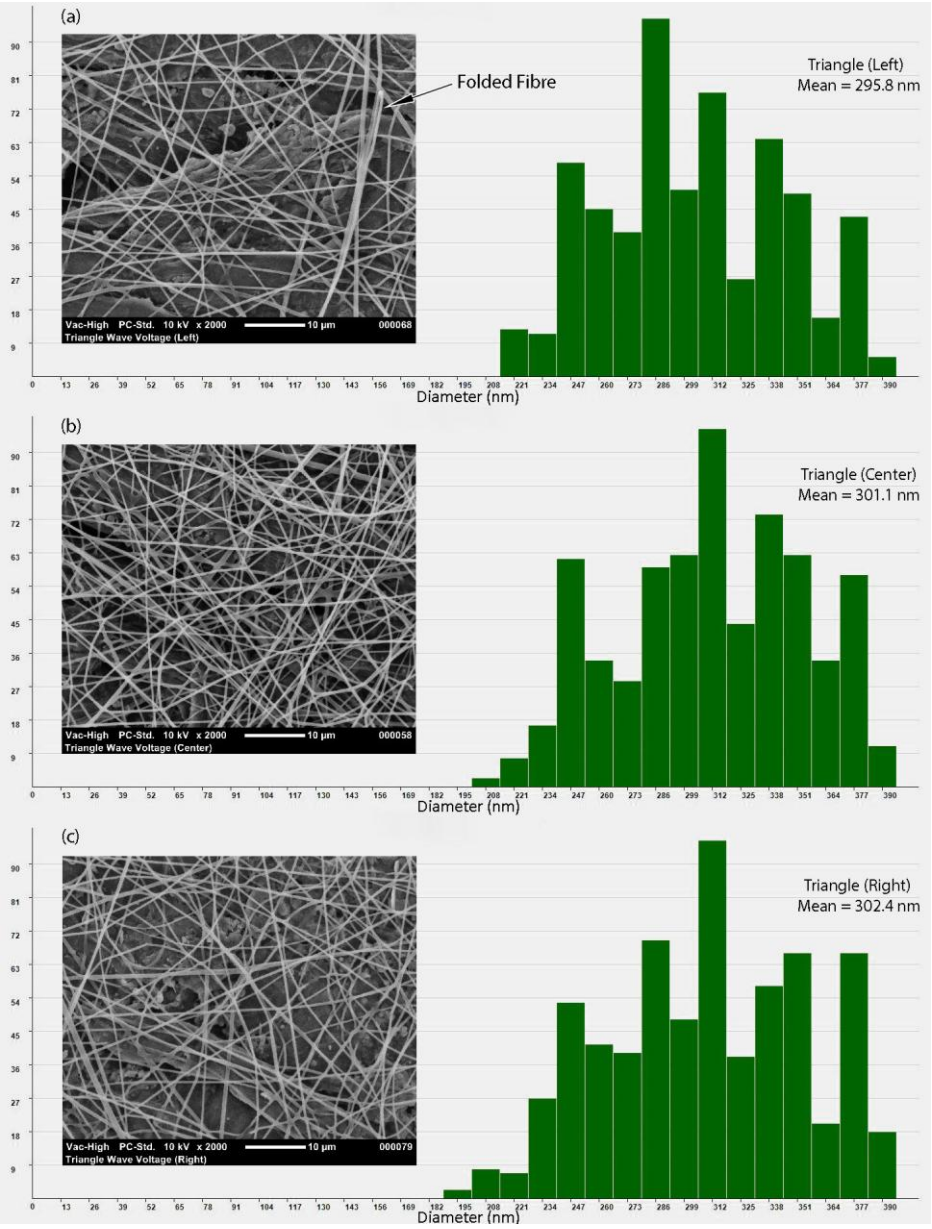

Figure 5-13. The electrospun fibre diameter for the triangle waveform for (a) left (b) centre, and (c) right. Insets show the corresponding scanning electron micrographs of the electrospun mat.

CHAPTER 6

CASE STUDY 1: CONTINUOUS SCANNING OF MULTIPLE ELECTROSPINNING JETS TO ELIMINATE STRIPE APPEARANCE IN A MULTI-SPINNERET ELECTROSPINNING SYSTEM

6.1 Introduction

A common issue when scaling up the electrospinning process through a multi-spinneret system is the repulsive effect between the same charge electrospinning jets (Kim et al., 2006). This effect pushes the jets from each other hindering the formation of a uniform deposited fibre mat (Varesano et al., 2010). Often this effect produces a stripe deposition pattern on a rotating drum, conventionally requiring additional moving mechanisms (as discussed in Chapter 2) to obtain uniform coverage of electrospun fibres (Filatov et al., 2007). Though it was noted that such setups are not be trouble free as the repulsive effect between the jets could still caused a substantial amount of fibres to be deposited off the target (Tomaszewski and Szadkowski, 2005).

The objective of this study is to demonstrate how the method developed in Chapter 5 could be used to eliminate the stripe appearance in a multi-spinneret electrospinning system. A modification was made on the electrospinning apparatus to include a pair of auxiliary electrodes that were positioned adjacent to a four spinneret electrospinning head. The hypothesis is that when the auxiliary electrodes are charged with two antiphase time-varying voltages, the varying voltage difference between the electrodes would cause the electrospinning jets to scan continuously producing a uniform deposition area. This will eliminate the stripe deposition pattern commonly associated with a multi-spinneret electrospinning system.

A similar image analysis technique as described in Chapter 5 is used to examine the uniformity of the deposited mats. In addition, confocal laser scanning microscopy (CLSM) was used to visualize the fibre composition within the deposited mat. CLSM was chosen due to its ability to reconstruct sample structure images based on fluorescent light detection (van de Velde et al., 2003).

6.2 Experimental procedures

6.2.1 Experimental apparatus

Electrospinning was carried out using a modified commercial laboratory scale machine (Model ES4, Electrospinz Ltd., New Zealand). The original single spinneret head was replaced by a four-spinneret spinning head named as SP1, SP2, SP3, and SP4 (Figure 6-1). The spinnerets are standard polypropylene pipette tips (Axygen T-200-Y) as used in single spinneret electrospinning. Based on prior trials, the distance between SP2 and SP3 was set at 50 mm and the distances between SP1 and SP2; and SP3 and SP4 were 15 mm. A longer distance between the inner spinnerets was chosen to minimize the repulsion effect between the inner jets. This also positions the inner spinnerets closer to the auxiliary electrodes, resulting in increased influence over the inner jets. A grounded stainless steel drum measuring 300 mm wide with a circumference of 1 m was used as collector. The distance between the drum and spinnerets was 180 mm and the rotational speed of the drum was set at 25 rev/min.

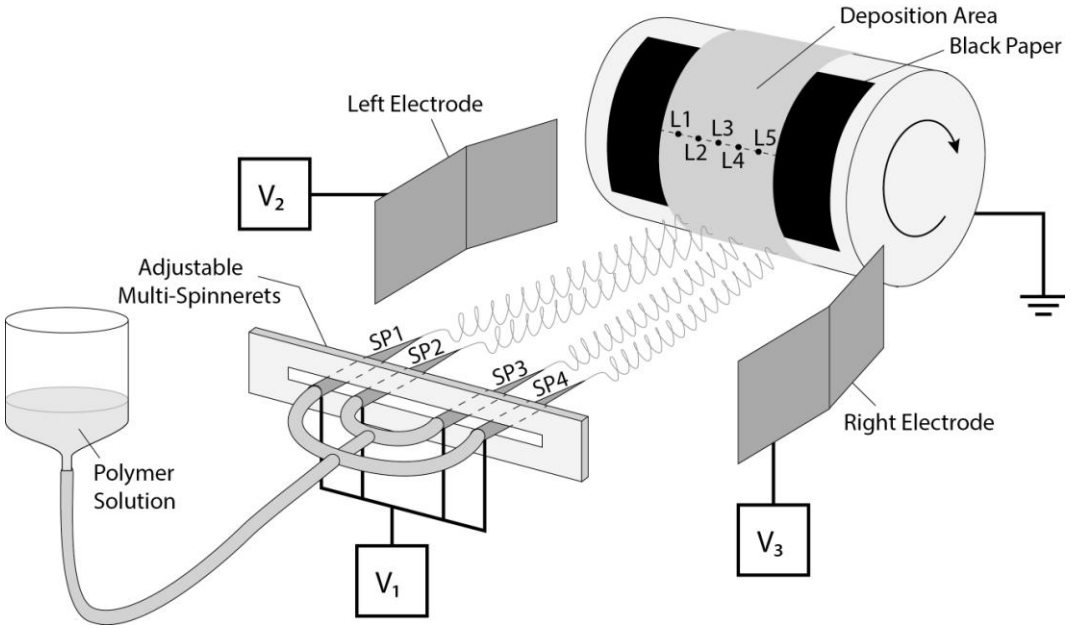

Figure 6-1. A four-spinneret electrospinning setup used in this study.

The spinning voltage V_1 was set at +16 kV (Glassman High Voltage, Inc.) throughout the experiment. Two auxiliary electrodes were placed in position either side of the deposition axis and were independently connected to two high voltage power supplies V_2 and V_3 (Model 4330, EMCO High Voltage, Corp.). Each of the auxiliary electrodes consists of two stainless steel plates (T430, CAMS Ltd., NZ) measuring 100 × 100 × 0.7 mm butted together forming an inside angle of 150°. The distance between the auxiliary electrodes was 300 mm on the spinneret side and 200 mm on the collector side. The distance between the auxiliary electrodes and the collector was 20 mm.

The applied voltages V_1 at the spinneret and V_2 and V_3 at the auxiliary electrodes were controlled using a LabVIEW^{TM} program (Version 10.0, National Instruments) (Appendix 3) and a compactDAQ data acquisition platform (NI cDAQ-9174 with NI9263 module). The experiment utilised one of two varying waveforms, either a sine or triangle wave. The waveforms were antiphased to each other and fed into the power supplies of the auxiliary electrodes. The output voltages at the auxiliary electrodes were two time-varying voltages with a dc offset of +10 kV, amplitude of 8 kV, and period (T) of 10 second (Figure 6-2).

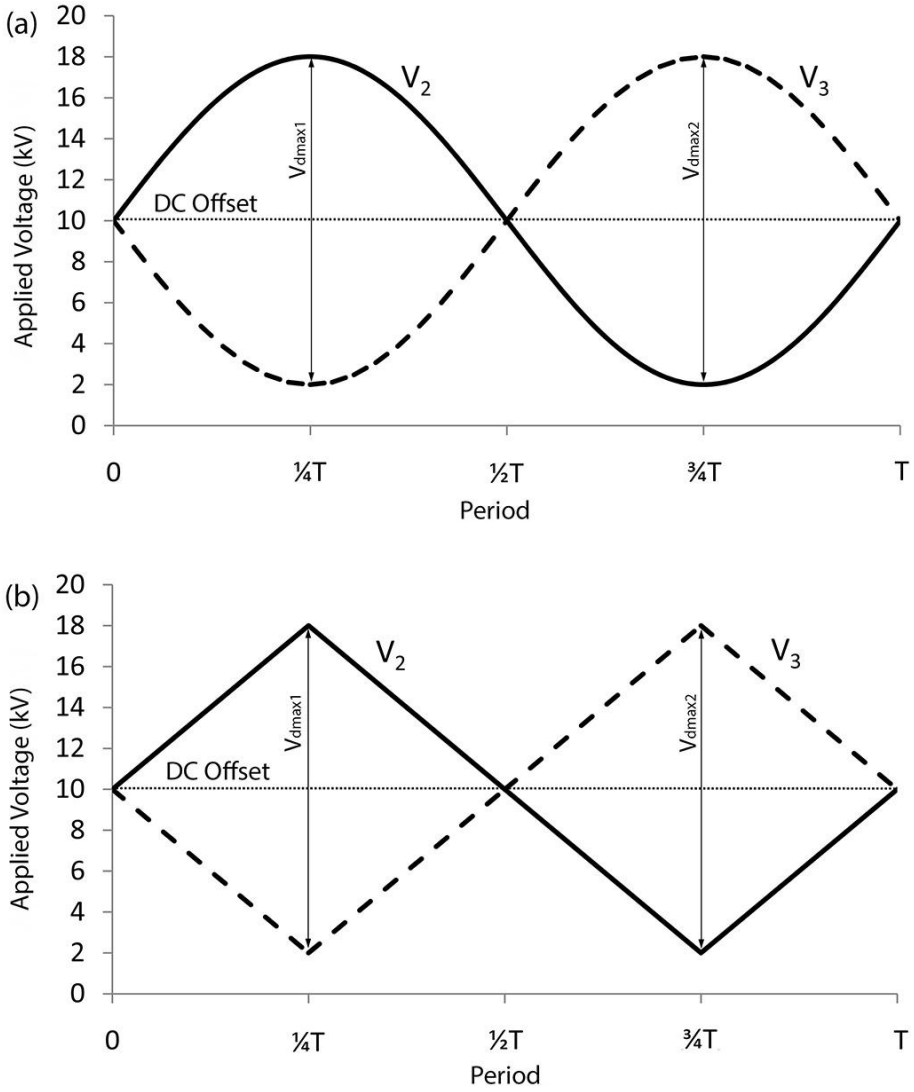

Figure 6-2. Applied voltages V_2 and V_3 (kV) at the auxiliary electrodes as a function of period (*T*) when applying the voltage using a (a) sine waveform and (b) triangle waveform.

6.2.2 Sample preparation

Firstly, experiments were conducted in which all of the spinnerets SP1 to SP4 were fed the same unmodified PVOH solution to examine the uniformity of the deposited mats. Secondly, the same unmodified PVOH solution was fed into SP1, whilst SP2, SP3 and SP4 were each fed three differently colour-dyed PVOH solutions from separate header tanks so as to be able to directly associate fibres observed within the mat with the spinneret of origin.

In the first experiment, sheets of A4 black paper (80 g/m^{2}Kaskad Raven Black 1516RB) were used as substrate and mounted on the surface of the drum (Figure 6-1). Samples were collected for 20 min in triplicate using sine and triangle wave voltages. The samples were named as S1, S2 and S3 when using sine wave voltage, and T1, T2 and T3 for triangle wave voltage. Control samples (C1, C2, C3) were also collected without using the auxiliary electrodes.

In the second experiment, Fluoroscein Sodium Salt (Sigma Chemicals, St. Louis, USA), Rhodamine B (Sigma Chemicals, St. Louis, USA), and Fast Green FCF (G. T. Gurr Ltd., London, UK) were selected as the fluorescent dyes to be used as markers. Three different dyed solutions were prepared by adding 0.5 wt. % of the dye into a 8 wt. % PVOH solution. SP1 was supplied with unmodified PVOH solution, SP2 with Fluoroscein Sodium Salt dyed solution, SP3 with Rhodamine B dyed solution, and SP4 with Fast Green FCF dyed solution. Five microscope slides were mounted on the surface of the drum at L1, L2, L3, L4, and L5; at 2 cm intervals (Figure 6-1). Electrospinning was then carried out for 60 minutes.

6.2.3 Uniformity measurement of the electrospun fibre mats

The uniformity measurement of the first experiment samples was carried out based on the image analysis technique described in Chapter 5.

6.2.4 Determination of fibre composition using confocal laser scanning microscopy

Confocal laser scanning microscopy (CLSM) images of the second experiment samples were taken using a Leica TCS SP5 confocal microscope (Leica Microsystems GmbH, Germany). The excitation wavelengths used for Fluorescein Sodium Salt, Rhodamine B, and Fast Green FCF were 488, 561, and 633 nm, respectively. Three CLSM images were obtained from each slide. The micrographs were then converted into TIFF files measuring 1024 × 1024 pixels.

Photoshop® was used to analyse the micrographs to determine the overlaying composition of the fibres. This was done by summing the number of pixels of each colour using the default

colour filters. The grey fibres representing the unmodified PVOH from SP1, green-yellow fibres representing the Fluoroscein Sodium Salt dyed fibres from SP2, red-magenta fibres representing the Rhodamine B dyed fibres from SP3, and blue-cyan fibres representing the Fast Green FCF dyed fibres from SP4.

6.3 Results and discussion

As described in Chapter 5, it was observed that the introduction of a pair of auxiliary electrodes charged with either sine or triangle wave voltages caused the four jets to scan to-and-fro simultaneously in the horizontal axis. However, some of the fibres tend to drift away and landed on the sides of the rotating drum due to the repulsive effect between the jets. The use of a pair of auxiliary electrodes that are angled inward helps to confine the fibres within the desired location. However, the auxiliary electrodes begin to attract the fibres when the applied voltage is 0 kV. Therefore, a minimum base voltage (V_b) of +2 kV was needed to prevent fibres from being deposited onto the auxiliary electrodes (Figure 6-2(a) and (b)) due to the geometrical limitation of the experimental setup.

Both auxiliary electrodes were charged at +10 kV at t = 0 so that V_d= 0 kV with the jets at their default position (Figure 6-2(a) and (b)). The jets then move to the right as V_d increases until reaching its first maximum deflection point when t = ¼*T* (V_{dmax1} = 16 kV). After ¼*T*, the jets move toward their default position as V_2 decreases and V_3 increases. The jets pass the default position at ½*T* (V_d = 0 kV) and continue moving towards the next maximum deflection point (left) as V_2 decreases and V_3 increases. The deflection continues until reaching the second maximum deflection point at t = ¾*T* when the voltage difference is at another maximum (*i.e.* V_{dmax2}= 16 kV). V_2 increases and V_3 decreases beyond ¾*T*, moving the jets towards the default position at *T* and the cycle then repeats itself.

Electrospun samples exhibited a pattern consisting of four white stripes when using the four-spinneret electrospinning setup without the use of the auxiliary electrodes. These samples served as the control samples (C1, C2 ,C3) (Figure 6-3). In multi-spinneret electrospinning striped patterning is expected due to the mutual repulsion between like-charged jets that prevents the overlap of deposition areas from adjacent spinnerets (Theron et al., 2005). The stripes in C1-C3 appeared to be equally spaced across the substrate surface, although the

width of the two inner stripes were narrower compared to the two outer stripes. A narrower deposition area as observed for the inner jets is also expected when using a multi-spinneret system due to the additional surrounding electric field applied by the neighbouring jets (Varesano et al., 2009). It was noted that increasing the deposition time beyond 20 min did not significantly widen the stripes such that stripe patterns persisted at the end of the process. It was also noted when both of the auxiliary electrodes were charged with equal dc voltage, the stripes do not merge with one another. Instead, the width of each stripe was reduced as the result of additional "squeezing" by the auxiliary electric field generated by adjacent jets.

The changing electric field moved the jets periodically with the use of the auxiliary electrodes that were charged with a time-varying voltage, ensuring that the fibre deposition moved across the substrate. The previously observed striped patterning was eliminated by this process. As previously, the deposition area was found to produce slightly uneven deposition when using a sine wave voltage (S1-S3) compared with a triangle wave voltage (T1-T3) (Figure 6-3).

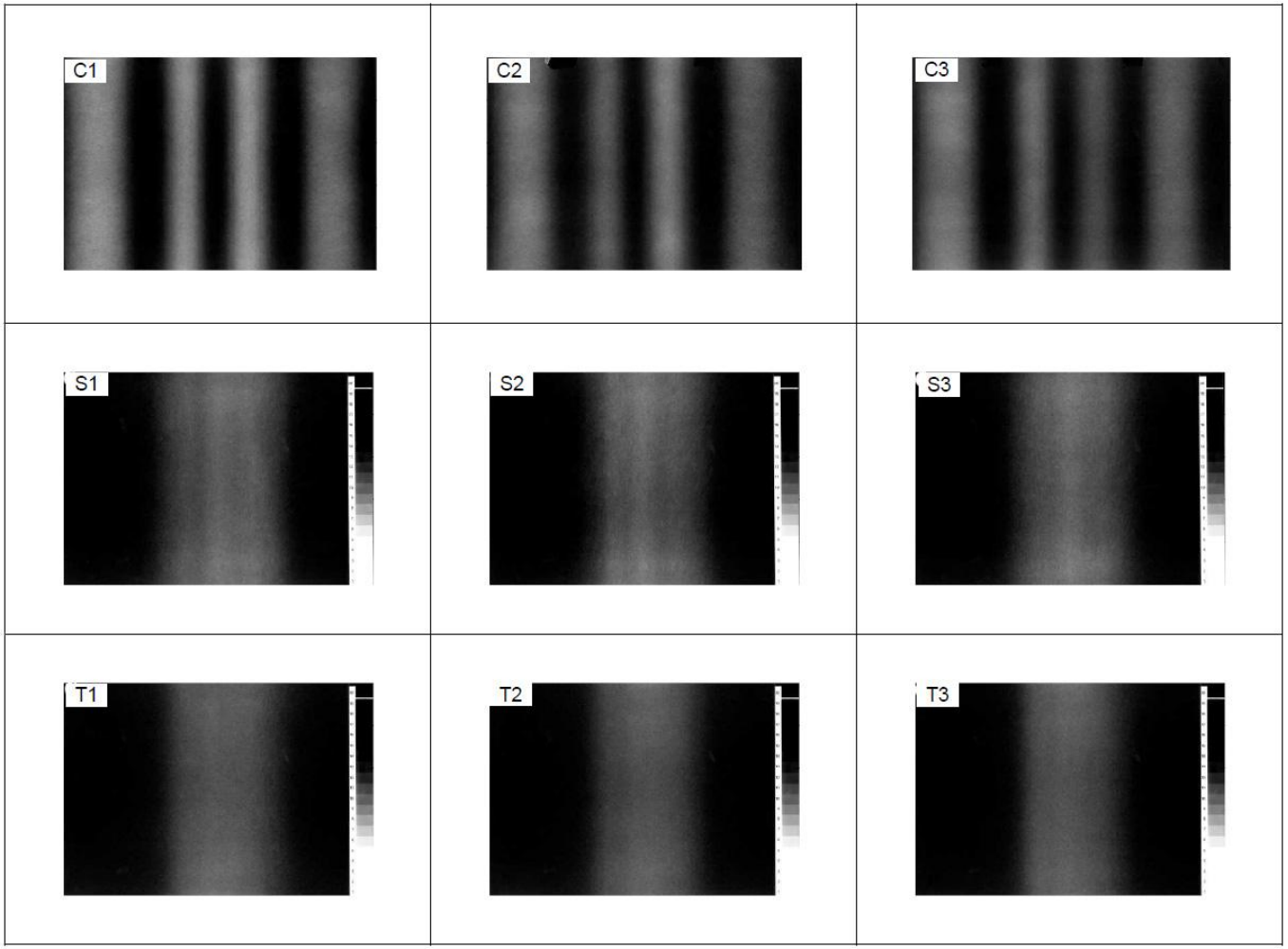

Figure 6-3. Scanned images of the triplicate (i)control samples (C1-C3) (*i.e.* without auxiliary electrodes), (ii)samples produced using auxiliary electrodes set up with a sine wave voltage (S1-S3), and (iii)samples produced using auxiliary electrodes set up with a triangle wave voltage (T1-T3).

Greyscale intensity measurements (see Figure 5-4) provided an approximation of the density of the electrospun fibres across the substrate. The striped patterning observed for samples C1-C3 can be represented by a density profile that reveals the presence of four peaks (Figure 6-4). However, the density profile exhibits only a single peak located at the centre of the substrate when the charged auxiliary electrodes were used. The inferior deposition of samples S1-S3is demonstrated by a less uniform profile at the centre of the curve compared to the smoother density profile of samples T1-T3. The calculated coefficient of variation (COV) of the greyscale intensity of the samples between 12-18 cm position are 0.10 and 0.08 for S1-S3 and T1-T3, respectively. The smaller COV value associated with the triangle waveform confirms that the triangle waveform produces a more uniform coverage of electrospun fibres.

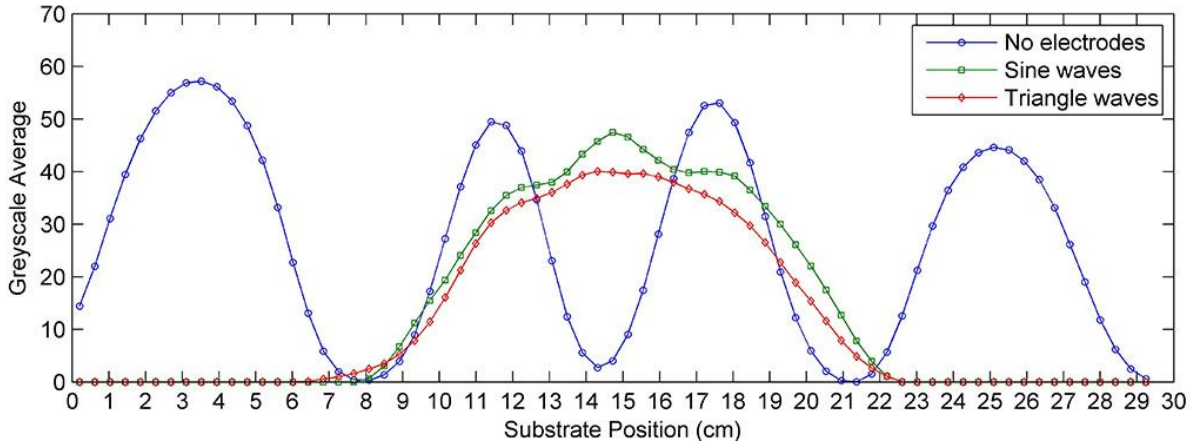

Figure 6-4. Average greyscale levels of C1-C3, S1-S3 and T1-T3 as a function of position on the substrate.

It was observed that compared to using a triangle wave voltage, using a sine wave voltage once again produced an inferior deposition as the result of varying scanning speed of the electrospinning jet. It is therefore concluded that if uniformity of the deposited mat is the priority one should use a triangle wave voltage instead of a sine wave voltage. This is due to the constant rate of voltage change when using triangle wave voltage, as explained in Chapter 5. It is noted that in previous studies, multi-spinneret setups using a rotating drum collector that can oscillate horizontally to the deposition direction has been suggested to achieve uniform depositions (Ding et al., 2004, Anon, 2013b). However, the lateral speed of such

system would necessarily demonstrate a simple harmonic motion which is represented by a sinusoidal function (Halliday et al., 2001). Although there has been no study pertaining the degree of uniformity of such systems, it is reasonable to believe that achieving a uniform coverage of electrospun fibres using such system would still be a challenge.

It can be observed that the overall widths of the deposition areas of S1-S3 and T1-T3 were greatly reduced compared to that of C1-C3 for which fibre deposition spanned across almost the entire width of the substrate (Figure 6-4). However, the observed difference in the overall width of the density profiles was expected due to the (i) geometrical limitation of the setup used and (ii) minimum applied voltage of +2 kV that prevented fibres from depositing directly onto the auxiliary electrodes. The minimum voltage influenced the electric field so that squeezing of the whipping instability occurred, consequently reducing the deposition area.

In the second experiment, it was observed that the additions of differently coloured dyes to the PVOH fed into 3 of the 4 spinnerets (the 1stspinneret contained no dye) had no impact on the electrospinning process. The varying colours of the dyed PVOH fibres across the drum were clearly visible following a deposition time of 60 min (Figure 6-5).

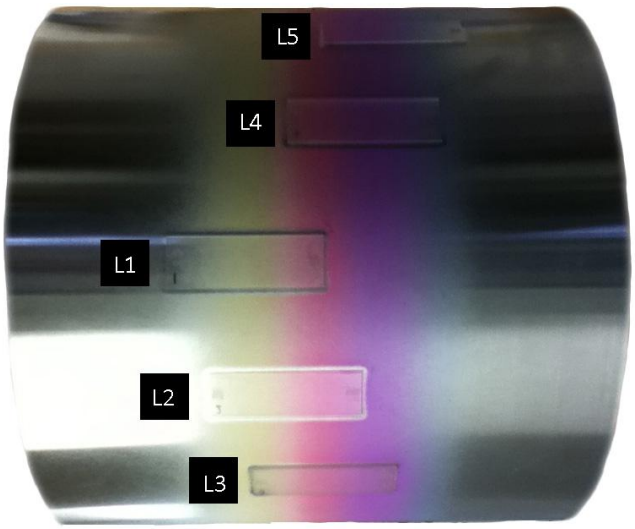

Figure 6-5. Dyed electrospun fibres collected on glass slides at location L1-L5.

The overlaying of fibres from different spinnerets was shown to occur by observing the CLSM images (Figure 6-6). The colour composition varied in step with the locations of the spinnerets SP1 to SP4 as summarized in Table 6-1. For example, fibres were mainly dominated by undid (33%) and green (61%) fibres at L1, with only 6% of red fibres and no blue fibres detectable. The fibre composition changed to plain (31%), green (47%), and red (22%) fibres at L2. There were similar amounts of green (49%) and red (41%) fibres atL3, with only small amounts of plain (7%) and blue (3%) fibres. Red fibres (66%) were dominant at L4, along with approximately the same amount of green (17%) and blue (16%) fibres. Finally, the composition of fibres was dominated by red fibres (61%) at L5, with some blue fibres (38%) and very little or no green (1%) and undyed (0%) fibres detectable.

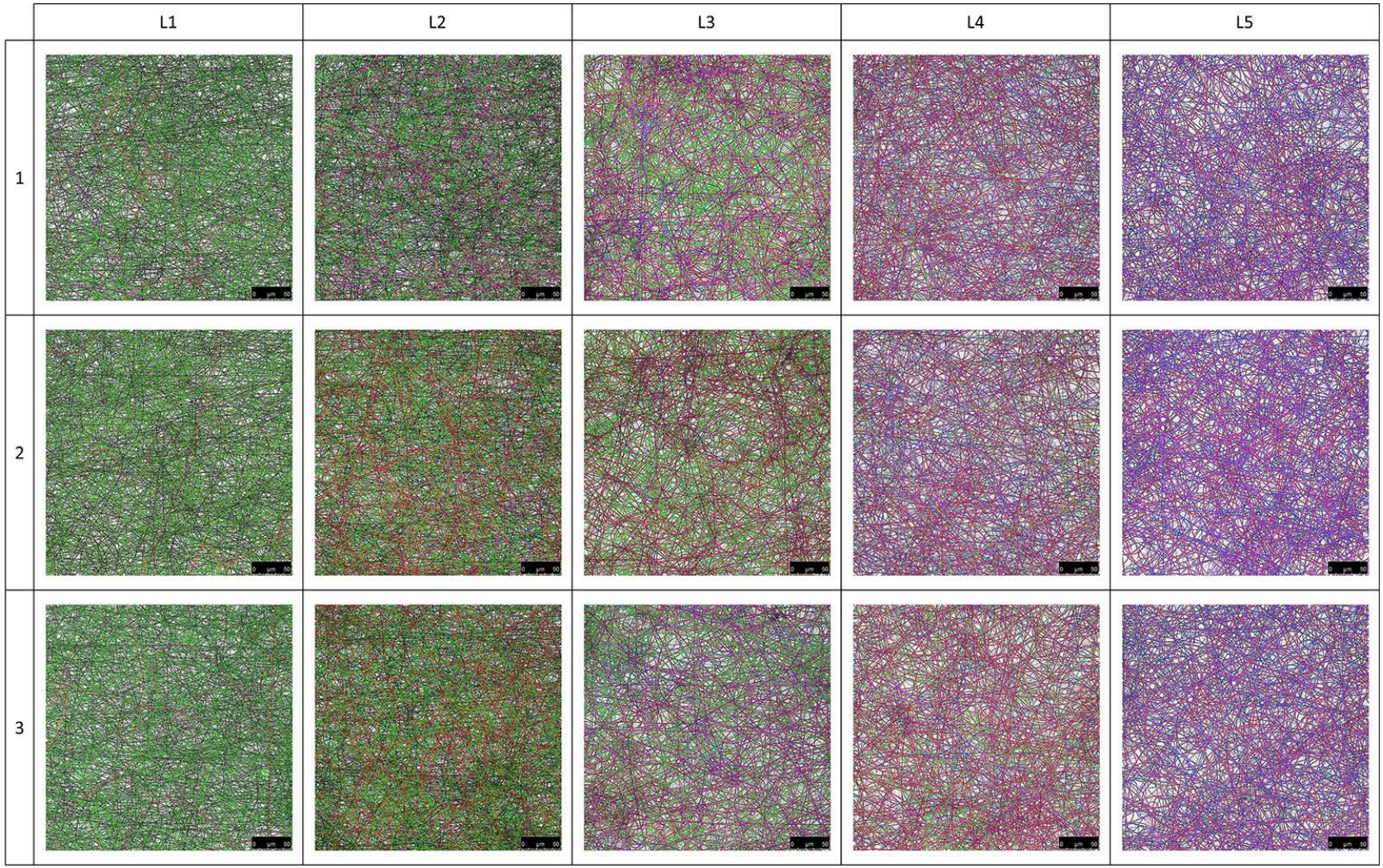

Figure 6-6. Three replicates of confocal microscopy images taken at locations L1-L5.

Table 6-1. Summary of fibre composition (%) at L1-L5 based on the colour pixel count measured from confocal microscopy images.

Colour Composition	Location				
	L1	L2	L3	L4	L5
Grey (%)	33	31	7	0	0
Green-Yellow (%)	61	47	49	17	1
Red-Magenta (%)	6	22	41	66	61
Blue-Cyan (%)	0	0	3	16	38

The results from the CLSM images suggest that the technique is not only capable of producing uniform coverage of electrospun fibres but it can also be used to produce blend of electrospun fibre mats consisting of different materials. In addition, a different percentage of composition at a specific location can be achieved by feeding individual spinnerets with desired materials. Although other techniques which are capable of producing blend of electrospun fibre mats have been described (Filatov et al., 2007, Ding et al., 2004), the main advantage of this technique is that no moving mechanical components are required.

The appearance of the deposited fibres look similar at all locations (L1-L5) based on scanning electron micrographs of the samples (Figure 6-7(a)-(e)). Typical solid and dry fibres characteristic of PVOH electrospun fibres were deposited in a randomly orientated pattern. However, the mean diameters of the fibres varied slightly across the mat. The thickest fibres were produced around the centre of the mat at L2, L3, and L4, with a mean diameter in the range of 338-344 nm (± 59.2 SD). In contrast, thinner fibres were produced at L1 and L5 with a mean diameter of ~315 nm (± 58.5 SD).

In Chapter 5, a more consistent fibre diameter was produced across the mat as there was only one jet used. As might be expected, thicker fibres were produced at the central location due to the squeezing effect by the outside jets that constrains the whipping instability. Although there was slight variation in fibre diameter, the difference between the maximum and minimum mean value is only 30.4 nm (9% increase in fibre diameter) which is less than the actual size of two pixels when conducting the measurement (36.6 nm). In addition, the

difference in fibre diameters is insignificant as it is within the standard deviation values of the measurements. It is therefore reasonable to conclude that the introduction of auxiliary electrodes does not greatly influence the final diameter of the fibres.

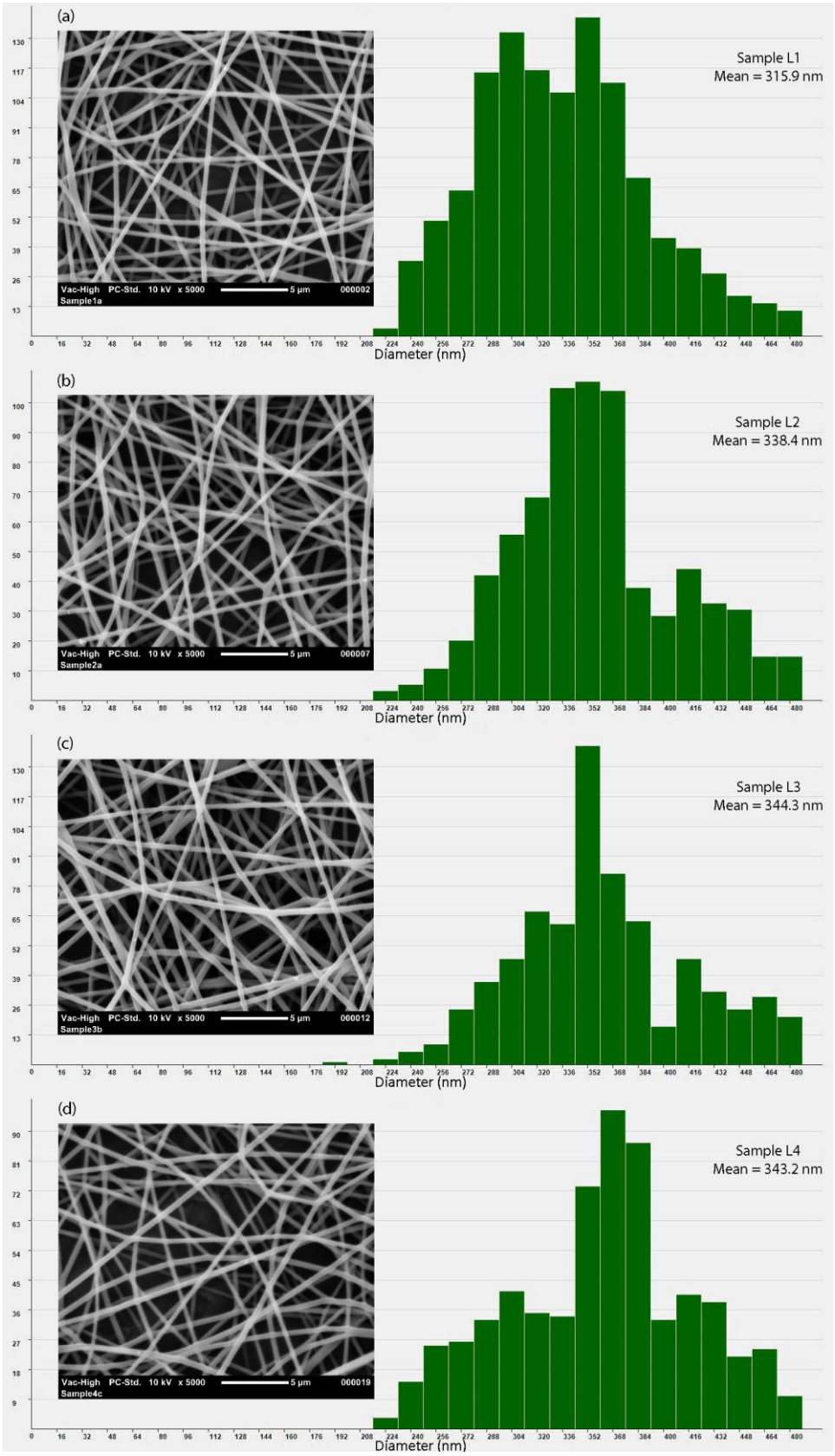

Figure 6-7. Scanning electron micrographs of electrospun fibres collected at locations (a) L1 (b) L2 (c) L3 (d) L4 (e) L5 (continued in the next page).

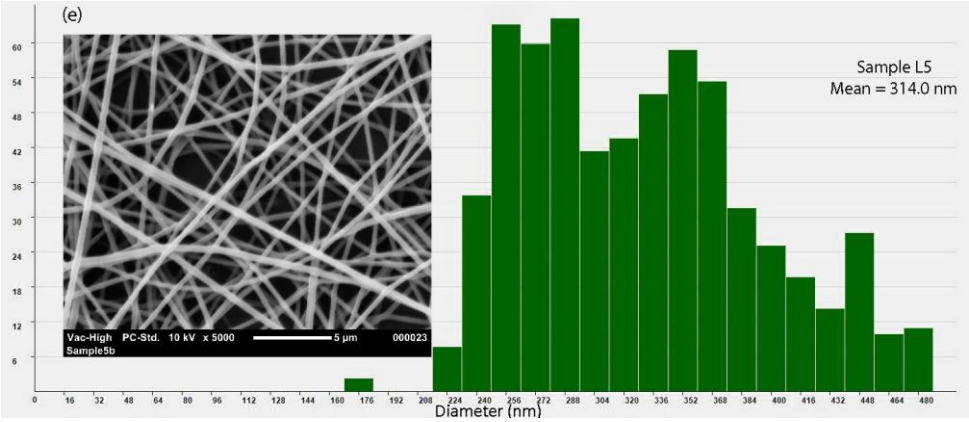

Figure 6-7. (Continued).

CHAPTER 7

CASE STUDY 2: ELECTRODE ASSISTED GAP ELECTROSPINNING (EAGE)

7.1 Introduction

As mentioned earlier in Chapter 2, the electrospinning process produces random orientated fibres due to the occurrence of the whipping instability. However, aligned fibres are sometimes required for certain applications (Boland et al., 2001). One of the widely used methods to produce uniaxially aligned fibres is gap electrospinning (Li et al., 2003). In gap electrospinning, the degree of alignment of the fibres is highly dependent on the geometry of the collector and it is often reported in the form of two parallel grounded collectors with a gap of up to several centimetres in horizontal or inclined plane (Park and Yang, 2011). The alignment of fibres in gap electrospinning can be described by considering an electrospun fibre as a string of charged elements (Figure 2-16). Upon reaching the grounded collectors, the two closest elements to the collectors would be attracted to each side of the collector creating a suspended string of fibre. The subsequent portions of the fibre then repeat the process and as a result uniaxially aligned fibres are produced between the collectors.

One of the issues commonly associated with gap electrospinning is that as the aligned fibres are collected between the electrodes, the difficulty in retrieving the fibres for further processes is problematic without damaging the structure of the fibre. It is preferable to directly deposit the aligned fibres onto a holdable structure which can then be removed from the apparatus after the deposition process. However it is known that by putting a grounded collector in between the parallel collectors it will only accumulates random fibres (Acharya et al., 2008). This is because when the grounded collector is added, the electric field at the

vicinity of the collector is changed and the fibres are now attracted to the shim rather than bridging between the parallel plates.

The objective of this study is to directly deposit uniaxially aligned fibres onto a holdable structure. A grounded window collector is used to capture the aligned fibres between two grounded parallel plates. In achieving this goal, an electrode assisted gap electrospinning (EAGE) system is developed by introducing a pair of auxiliary electrodes charged with time-varying voltages. The hypothesis is that when the auxiliary electrodes are charged, the "squeezing" of the electric field could encourage fibre alignment producing aligned fibres on the grounded window collector. A new method for fabricating a multi-layer aligned fibre construct is also demonstrated.

7.2 Experimental procedures

7.2.1 Experimental apparatus

The Model ES4 electrospinning machine (Electrospinz Ltd., New Zealand) was used in this experiment. The machine was modified to include a pair of auxiliary electrodes, a grounded magnetic holder, and two grounded plates (top and bottom plates) (Figure 7-1). The electrodes were two rods (6061 aluminium alloy, CAMS Ltd., NZ) measuring 10 mm in diameter, 50 mm long and were placed on either side of the magnetic holder. The distance between the electrodes was set at 70 mm. A thin round shim window (304 stainless steel, CAMS Ltd., NZ) was used as substrate and it was grounded through its contact with the magnetic holder. The shim has a thickness of 25 μm and a 30 mm inner diameter. Two grounded plates (430 stainless steel, CAMS Ltd., NZ) measuring 90×300× 0.7 mm were placed 50 mm apart at the top and bottom of the collector to achieve gap electrospinning.

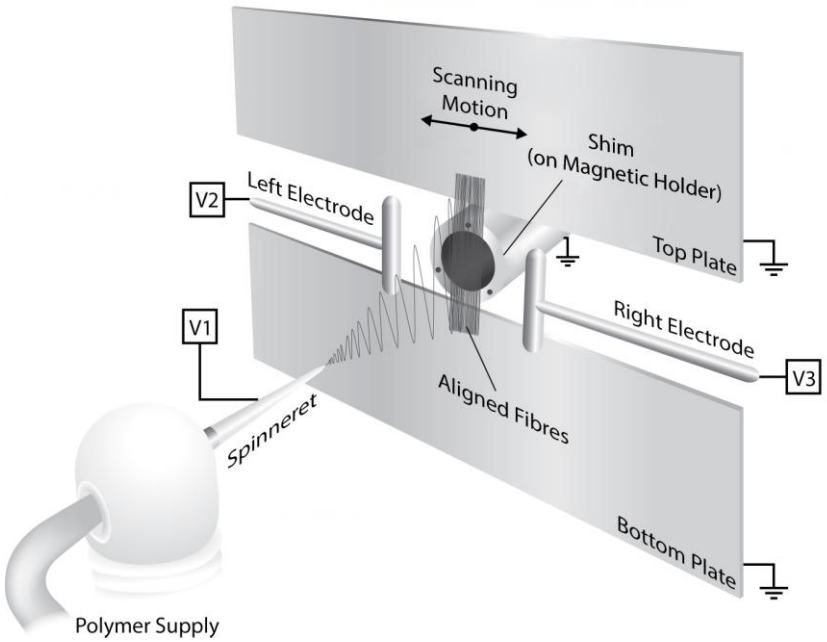

Figure 7-1. A schematic illustrating electrode assisted gap electrospinning (EAGE).

The spinneret was connected to a dc power supply (Glassman High Voltage, Inc.) and placed at 100 mm distance to the collector. The auxiliary electrodes were independently connected to two high voltage power supplies (Model 4330, EMCO High Voltage, Corp.). The applied voltages V_1 at the spinneret and V_2 and V_3 at the auxiliary electrodes were controlled using a LabVIEW^{TM} program (Version 10.0, National Instruments) (Appendix 3) and a compactDAQ data acquisition platform (NI cDAQ-9174 with NI9263 module). The spinneret was charged at +12 kV dc (V_1) whilst the auxiliary electrodes were charged using two antiphase triangle wave voltages (V_2 and V_3) at a frequency of 0.01 Hz. The amplitude of the waveforms was 5.5 kV with a dc offset component of +8.5 kV (Figure 7-2).

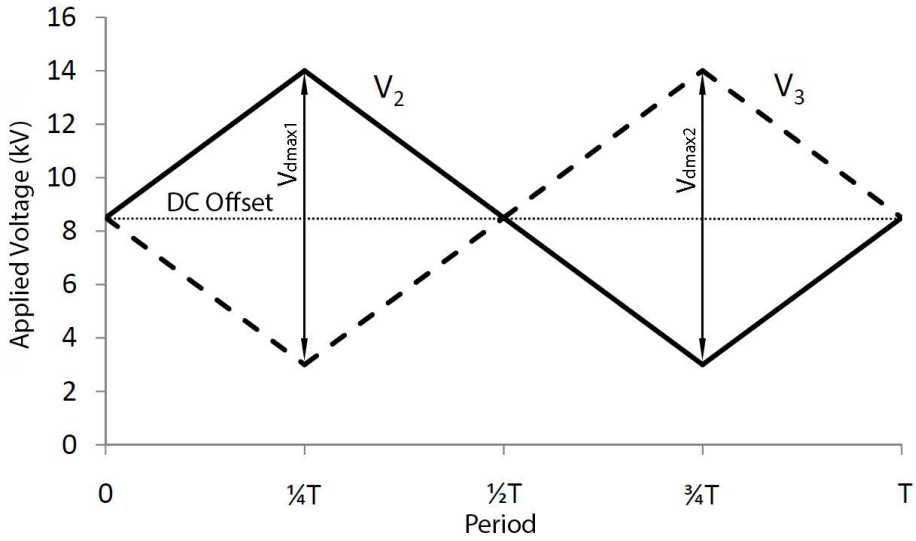

Figure 7-2. The applied triangle wave voltages V_2 and V_3 at the auxiliary electrodes as a function of period (*T*).

7.2.2 Sample preparation

Electrospinning was carried out for 5 min for each sample which was equivalent to three complete cycles of the waveforms. The heat from a soldering iron was used to cut the suspended fibres between the shim and the grounded plates before removing the shim from the apparatus (Figure 7-1). Electrospinning was repeated three times to produce triplicates of shims with uniaxially aligned fibres. The samples were then layered in between a two-piece holder (Figure 7-3). The shims were layered so that the next layer was rotated through an angle of 120˚ anticlockwise to the previous one. The same procedures were repeated without using the auxiliary electrodes to create a control sample.

The mean diameter and orientation of the fibres were observed using a scanning electron microscope. The difference in fibre alignment between the with and without auxiliary electrodes samples was also compared by observing the laser diffraction pattern when a standard green laser pointer (50 mW, 532 nm wavelength, Led Bulbs, NZ) was directed through the samples. Still images of the laser diffraction pattern were captured using a Sony SLT-A77 digital camera.

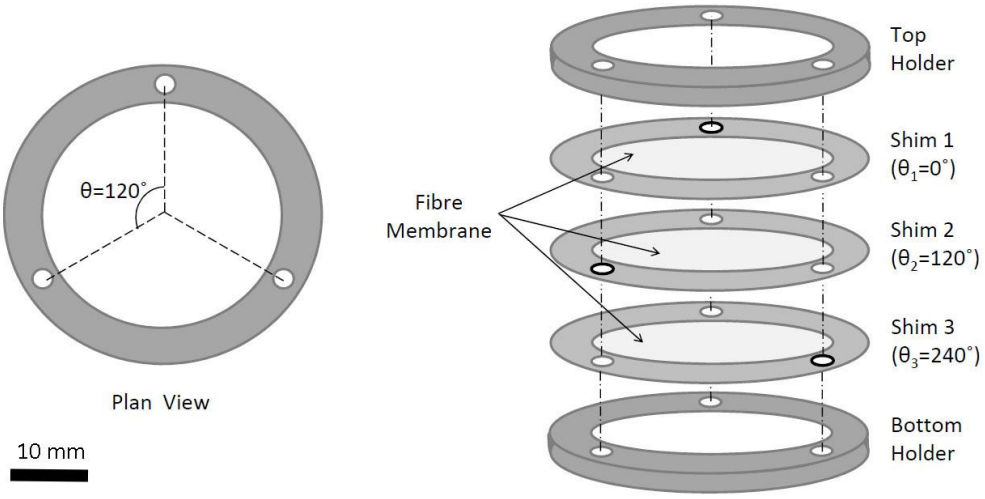

Figure 7-3. A schematic of the assembly of shims between a pair of holders.

7.3 Results and discussion

Initially, electrospinning was carried out without the shim and uniaxially aligned fibres were produced between the two parallel plates. When a shim was placed between the two plates, the deposition pattern was changed and as expected non-aligned fibres were collected on the shim. However, when the auxiliary electrodes were charged at V_2 and V_3 (Figure 7-2), the "squeezing" of the electric field was sufficient to produce uniaxial aligned fibres on the shim.

At t = 0, the deposition started from its default position when both auxiliary electrodes were at +8.5 kV ($V_d = |V_2-V_3| = 0$ kV) (Figure 7-2). Almost instantly a narrow band of aligned fibres (of about 10 mm) was observed at the middle; bridging between the two parallel plates and spanning across the shim (Figure 7-1). Similar to Chapter 5, the deposition area was shifted as the applied voltages V_2 and V_3 changed (in the direction away from the most positive electrode) expanding the coverage area of the aligned fibres. The maximum deflection of the jet occurred twice when the voltage difference between the electrodes was at a maximum (*i.e.* V_{dmax1} or V_{dmax2} = 11 kV at t = ¼*T* and t = ¾*T*, respectively) (Figure 7-2).

The layering of three shims on a two-piece holder at 120˚ angle produced a triaxial aligned fibre construct with fibre orientation angle of -60˚/0˚/+60˚ (Figure 7-4). From the macro photographic image, it is evidenced that a well distributed aligned fibres was produced using EAGE. In this case, the introduction of the auxiliary electric field improved the gap

electrospinning process in two ways. First, the base voltage (V_b) component "squeezed" the whipping instability forcing the fibres to flick up and down (vertically) before reaching the shim as vertically orientated fibres. Secondly, as the voltage difference between the auxiliary electrodes changed, the deposition area moves accordingly improving the distribution of the aligned fibres across the shim.

Figure 7-4. A macro photographic image showing a triaxial aligned fibre construct (-60˚/0˚/+60˚) created by layering three layers of deposited shims onto a two-piece holder

Typical solid and dry fibres characteristic of PVOH electrospun fibres was shown by both with and without EAGE based on scanning electron micrographs of the samples (Figure 7-5(a) and (b)). The fibre orientation angle of -60˚/0˚/+60˚ is clearly visible when using EAGE (Figure 7-5(a)). The uniaxial orientation in each layer is represented by the three peaks in the histogram of fibre orientation angle from SEM Analyser software (Figure 7-5(c)).The histogram suggests that the majority of the fibres are orientated in approximate angles of 300˚, 0˚, and 60˚.

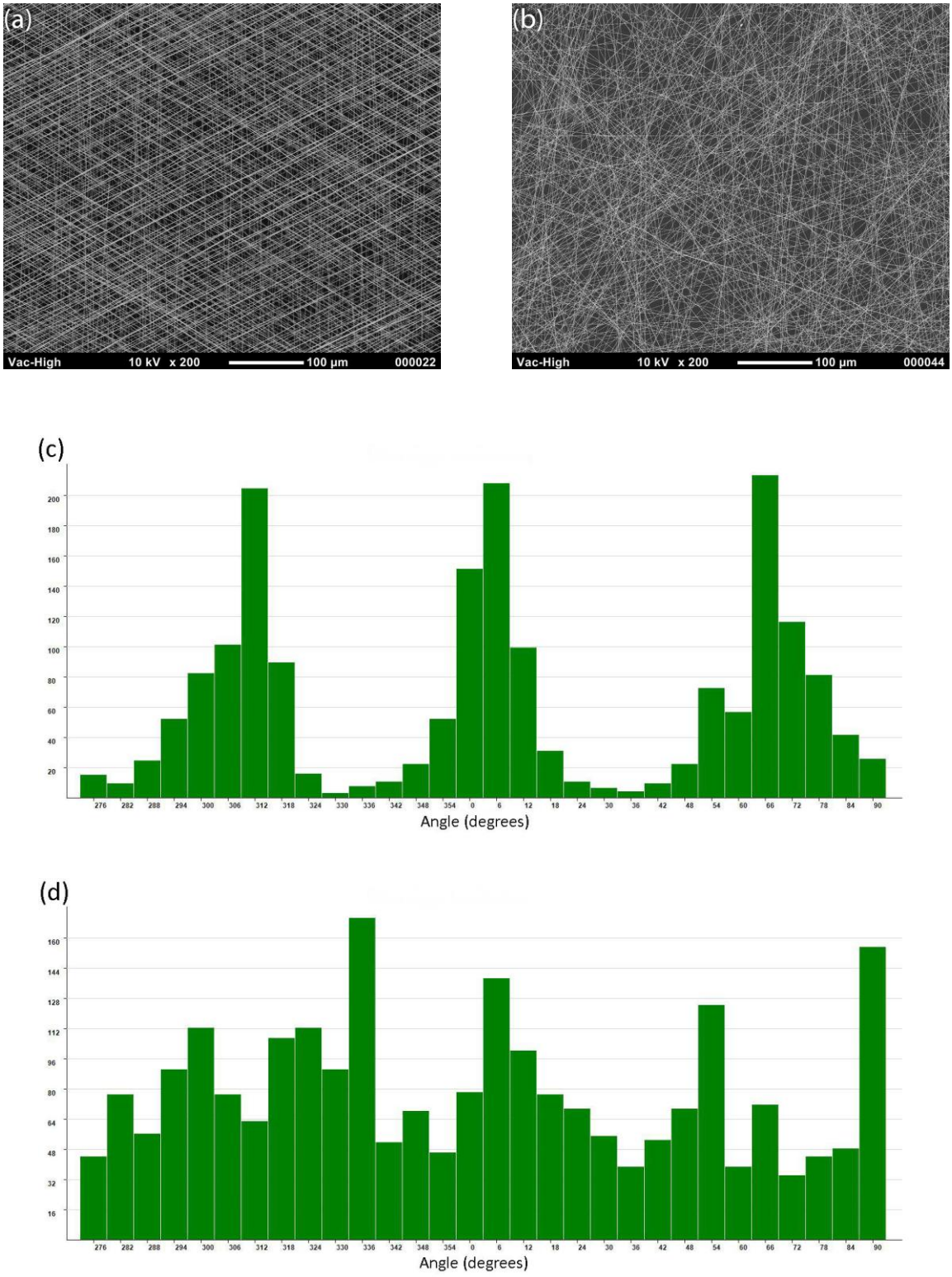

Figure 7-5. Scanning electron micrographs of (a)triaxially orientated fibres with the use of auxiliary electrodes; and (b) random orientated fibres without auxiliary electrodes. The measured fibre orientation angle of sample (a) and (b) are shown in (c) and (d) respectively.

In comparison, samples produced without using the auxiliary electrodes showed layers of random orientated fibres (Figure 7-5(b)). It is worth noting that this fibre structure is different compared to a typical randomly orientated fibre mat. The structure only consists of straight fibres (no bent fibres) which were orientated at random angles (Figure 7-5(b) and (d)). This suggests that gap electrospinning occurs across the shim even without the auxiliary electrodes. In this case, the orientation of the fibres is random due to the shim being circular.

A quick method of inspecting the fibre alignment can also be performed by observing laser-induced diffraction patterns (Section 7.2.2). The sample using the auxiliary electrodes showed a six-point cross denoting the triaxial alignment of the fibres (Figure 7-6(a)). Each line of the cross represents one layer of the aligned fibres. The laser diffraction lines are always perpendicular to the fibre orientation angle; for instance, a horizontal laser diffraction line would indicate vertically orientated fibres. In comparison, the laser diffraction of the control sample showed no particular pattern indicating its random orientation of angles (Figure 7-6(b)).

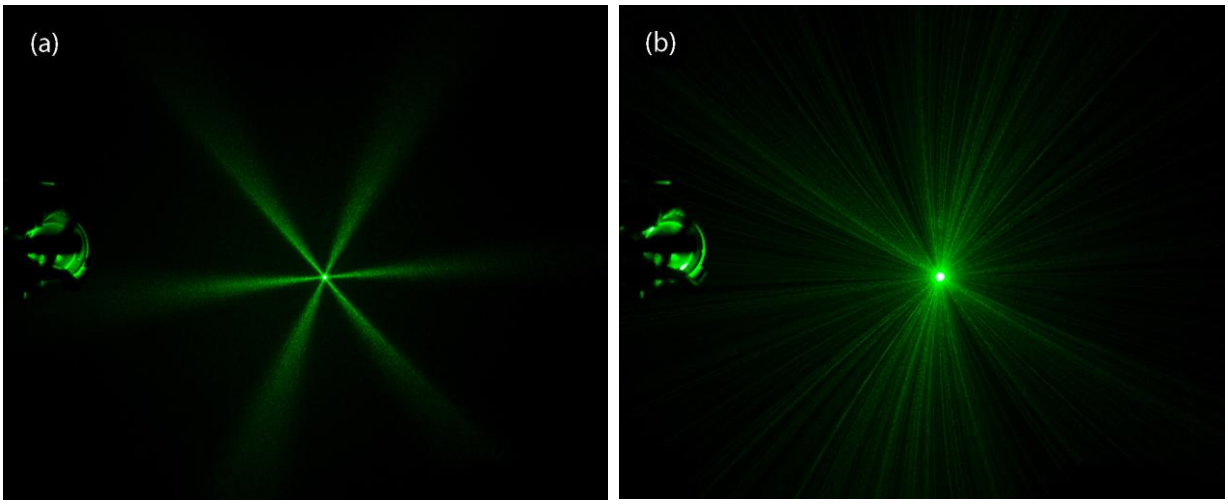

Figure 7-6. Photographic images showing the laser diffraction pattern of the samples exhibiting fibre orientation (a) with and (b) without electrode assisted gap electrospinning.

The mean diameters of the fibres varied slightly between the samples. Thicker fibres were produced when using EAGE with a mean diameter of 352.1 nm (± 82.9 SD) (Figure 7-7(a)). In contrast, thinner fibres were produced without EAGE with a mean diameter of 308.2 nm

(± 70.2 SD) (Figure 7-7(b)). The difference between the mean values is 43.9 nm (14.3% increase in fibre diameter). The increase in fibre diameters when using EAGE is expected due to the dampening of the whipping instability caused by the introduction of the charged auxiliary electrodes. This result is consistent with that in Figure 4-9, although the increase in fibre diameter is not significant when considering the pixel size used in the SEM Analyser software (30.5 nm) and the standard deviation values.

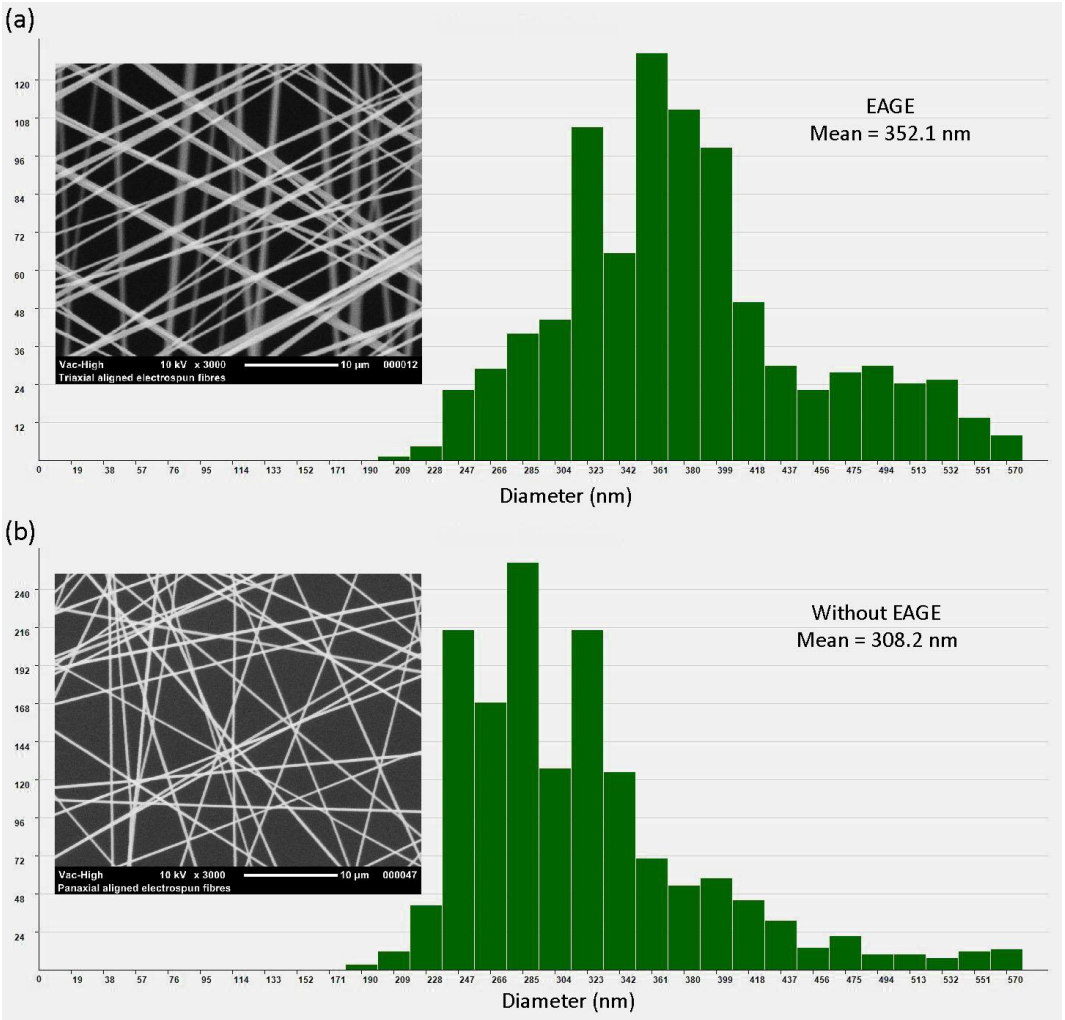

Figure 7-7. Scanning electron micrographs of electrospun fibres collected (a) using EAGE (b) without EAGE.

The results from this study showed that EFM can be used to improve the alignment and distribution of fibres in the gap electrospinning process. It should be noted that the results

reported in this study was dependent on the parameters used in the experiment. The maximum and minimum applied voltage of +14 kV and +3 kV were found to work best with the current apparatus. From the knowledge gained in Chapter 5, voltage with a triangular wave form was chosen in this study in order to obtain a constant scanning speed of the deposition area for obtaining a uniform coverage of aligned fibres across the shim. A uniform coverage of fibres would provide a better prediction of the pore size distribution of the electrospun fibre membrane due to equal spacing between the fibres.

The novel approach of collecting the aligned fibre on shims and stacking these in a two-piece holder opens up the possibility of constructing more complicated 3-D fibre constructs. Although the sample presented in this study has only three layers mounted at 120˚ orientation, the actual possible number of orientations is unlimited and it can be increased simply by increasing the number of layers at different orientations. It is envisioned that this method could be used to extend electrospun fibres to applications which are currently limited by the geometrical constrains of the fibre constructs.

Although a number of studies have proposed methods of producing layer-by-layer orientated fibres (Li et al., 2004, Carnell et al., 2008), the method used in this study has a clear advantage in terms of handling the product. The shims and two-piece holder system allows the fibre constructs to be transferred from one process to another without damaging the delicate structure of the fibres. In addition, the method can be applied to other electrospinnable materials to suit various applications such as filtrations or biomedical applications. Currently, a prototype machine which has a built in programmable control unit is being developed by Electrospinz Ltd to produce electrospun fibre membranes for research purposes.

CHAPTER 8

GENERAL DISCUSSION

To control the flight path of an electrospun fibre it is necessary to cope with considerable physical variation in the fibre itself during flight. The fibre starts life as a near stationary globule of dilute polymer solution. It is then drawn out into a stream of liquid which accelerates off into free space, solidifying into a gel and then a solid, so gaining a modulus whilst losing the property of viscosity. At some stage in flight the path of the fibre diverges from a straight path into an expanding helix, thinning beyond the point of naked eye visibility before finally impacting into the collecting surface and losing some degree of electrical charge. Although the fibre stream is highly charged at all stages of flight it does have a small but significant mass, and thus a degree of inertia to overcome when changing direction.

Due to the changes in state, mechanical, and aerodynamic properties during electrospinning, concern arises if there may be a non-linear response of fibre to the applied electric field when using electric field manipulation (EFM) for controlling the spatial deposition of electrospun fibre. Although a considerable amount of studies based on EFM has been reported previously (Deitzel et al., 2001), to the best of the author's knowledge, there have been no studies conducted to determine if EFM is able to provide a consistent and repeatable result. This study was aimed at filling this gap by developing, validating, and demonstrating the use of EFM for controlling the spatial deposition of electrospun fibre. Manipulation of the electric field was achieved by introducing a pair of charged auxiliary electrodes adjacent and parallel to the line of deposition of the electrospinning jet. Each study was carried out using a specially modified electrospinning apparatus however the working principle behind the examples is the same *i.e.* the applied voltages at the auxiliary electrodes were used as control variables.

8.1 Electric field manipulation is a valid control method

It was observed that the area where the deposited fibres were formed on a collector can be moved in a controlled manner when the auxiliary electrodes were charged at a given voltage combination (Figure 4-4). Based on experimental results, it was evidenced that there was a significant linear relationship ($p < 0.05$) between voltage difference at the auxiliary electrodes (V_d) and the magnitude of shift of the deposition area (L_{exp}) (Figure 4-5). The magnitude of fibre responses were symmetrical and the direction of shift was always away from the most positive electrode. The linear model proved the hypothesis of the experiment in Chapter 4 that the magnitude of fibre response is proportional to the voltage difference at the auxiliary electrodes.

Further analysis was carried out to ascertain if the linear model adequately describes the relationship between L_{exp} in response to V_d (Figure 4-5). Performing a multi-factor polynomial regression analysis on the experimental data, it was found that the introduction of second order terms were not significant ($p > 0.05$). As such, a linear model is the most appropriate to explain the variance in the data. Furthermore, the R^2 values also suggest that the linear models and the data are a good fit.

It was also observed that when both electrodes were charged (E2) the round shape of the deposition area can be reduced in the axis of alignment of the electrodes reducing the aspect ratio of the deposition area (Figure 4-6). The reduction of the aspect ratio was found to have a significant linear relationship ($p < 0.05$) with base voltage (V_b - the lower applied voltage when both the auxiliary electrodes were charged) (Figure 4-7). By performing a cross check between the variables (Figure 4-8(a) and (b)), it was found that the two control variables are independent in their action *i.e.* V_d for shift and V_b for changing the aspect ratio of the deposition area.

Although a simplified particle-model used in simulations was unable to predict the precise location of the fibre deposition position, FEA was useful for broadly describing the movement of electrospun fibres in flight in response to varying electric fields. In conventional electrospinning, the F_z component is the dominant force that draws the fibre toward the collector (Heikkila et al., 2007, Cui et al., 2011). However, in the present study the F_x component has an influence on the deflection of the fibre due to varying electric fields

imposed by the auxiliary electrodes. When the auxiliary electrodes were charged at a given voltage combination, a similar response to the applied electric field as in experiment was observed *i.e.* the particle moved away from the most positive electrode (Figure 4-10(a) and (b)).

Based on simulations, the results showed that the x-axis component of electric field (E_x) which correspond to electric force F_x was responsible for the shift in location and the reduction of aspect ratio of the deposition area (Figure 4-11 and Figure 4-12). Performing the simulations at different voltage combinations, it was observed that when V_d or V_b increased, E_x also increased. The increase in E_x means higher electric forces were subjected to the fibre (Equation 4-1). The results are in coherence with the findings observed in experiments *i.e.* when V_d or V_b increased, the magnitude of shift and aspect ratio of the deposition area respectively also increased (Figure 4-5 and Figure 4-7).

Initially, the simulated shift of the deposition area based on a massless particle was found to correlate closely with the experimental results. This suggests that the path of the electrospun fibre followed the electric field lines. This is in agreement with the remark made by Viswanadam and Chase (2013) who used auxiliary electrodes to control the location of where the fibres landed on a collector. However by repeating the experiment at an extended distance, it was found that the correlation between simulation and experimental results was a coincidence. The extra distance between the spinneret and collector in the simulation allows more time to the massless particle to travel further but in the experiment it only makes the control fields less influential on the electrospun fibre (Figure 4-14). Therefore, it was concluded that the trajectory of the fibres was guided by the electric field but it did not necessarily follow exactly the electric field line.

The results of this study are significant as it proved that EFM can provide a consistent and repeatable method of controlled deposition. The good fit of the linear models in Figure 4-5 suggests that the applied voltage at the auxiliary electrodes is a valid control. These findings can potentially be used as the basis for controlling the deposition area. Within the limits of control, the same outcome can be expected when the same control voltage is used. Furthermore, as V_d and V_b are two separate controls, one can simply sum the effects of the different applied electric fields to achieve the desired response. Therefore, in considering

control of spatial deposition area, one can predetermine the V_d and V_b of the applied voltages to electrospin fibres onto a targeted area at a specified aspect ratio. In addition, it is presumed that a multiple axes control of the deposition area can be achieved simply by adding another set of auxiliary electrodes.

8.2 A wide and uniform deposition area using time-varying electric field

The knowledge gained in Chapter 4 was further developed in Chapter 5 to provide an insight into how the EFM technique using a pair of charged auxiliary electrodes can be applied to achieve a desired deposition pattern. Knowing that the magnitude of shift of the deposition area is proportional to V_d (Figure 4-5), applying a sequence of voltage combinations to the auxiliary electrodes that gives a varying V_d over time would moves the deposition area periodically. The results proved the hypothesis that the application of time-varying voltage at the auxiliary electrodes provides a continuous scanning of the jet producing a wide and uniform distributed electrospun fibre mat (Figure 5-6). It was observed than the default width of a single jet deposition area was doubled when the auxiliary electrodes were charged with either sine or triangle time-varying voltages (Figure 5-5 and Figure 5-6).

Due to the smooth repetitive oscillation of a sine wave voltage, it was first thought it would produce a uniform coverage of electrospun fibres. However, the two-stripe deposition pattern produced when using sine wave voltage was obvious (Figure 5-6(a)) and later confirmed by the greyscale profile Figure 5-6(c). The deposition pattern when using triangle wave voltage appeared to be more uniform however the width of the deposition area was slightly narrower compared to when using sine wave voltage (Figure 5-6). Interestingly, the area under the curve was found to be almost the same for both curves with a percentage difference of 9.4% (Figure 5-6(c)). As the time of deposition is the same, this suggests that to a limit the sum of greyscale intensity correlates with the total fibre deposited.

The difference between the deposition patterns when using a sine or triangle voltage is believed to be caused by a difference in the scanning speeds of the jets. From Equation 5-3 and Equation 5-4, the rate of voltage change which determines the scanning speed of the jet was shown to vary with time when using a sine wave voltage but remained constant when using a triangle wave voltage (Figure 5-7(b)). When using a sine wave voltage, the scanning

speed of the jet was at a maximum when passing the centre area but at a minimum when reaching the edges. Therefore the combination of slow and fast passes of the jet caused the uneven deposition compared to when a using triangle wave voltage. The momentarily stop of the jet at the edges when using a sine wave voltage also caused the deposition area slightly wider compared to when using a triangle wave voltage (Figure 5-6(c)). The experimental results were supported by the simulated greyscale profiles using Matlab. Using a series of greyscale profiles when the auxiliary electrodes were charged at a combination of dc voltages (Table 5-1), the simulated plots using sine and triangle wave voltages also showed similar patterns as observed in experiments.

It was also demonstrated in Chapter 5 that the applied voltages at the auxiliary electrodes can be optimized to produce a more uniform deposition area. By using a clipped triangle wave voltage, controlling the stop time (t_s) during the plateau region allows control of the stop time when the electrospinning jet reaches its maximum deflections. The best results were found when t_s was set at between 0.9 to 1.2 seconds (Figure 5-10(c) and (d)) giving the smallest coefficient of variation (COV) value of 0.02 between 12.6 and 16.8 cm position (Figure 5-11 and Table 5-2). However, when t_s was set at 1.5 seconds the deposition area produced a similar pattern as when using sine wave voltage (Figure 5-10(e)).

8.3 Other potential applications

The two case studies in Chapter 6 and Chapter 7 were presented to demonstrate the applicability of the developed technique in Chapter 5 to solve two common issues in electrospinning.

In Case Study 1 (Chapter 6), the technique was applied in a four-spinneret electrospinning setup to demonstrate its ability to overcome jets repulsion issue when using a multi-spinneret system (Tomaszewski and Szadkowski, 2005). The results in Chapter 6 proved the hypothesis that the continuous scanning of electrospinning jets using time-varying EFM could eliminate the stripe deposition pattern commonly associated with a multi-spinneret electrospinning system (Figure 6-3 and Figure 6-4). The technique could potentially be used for up-scaling the electrospinning process using a multi-spinneret setup without compromising the uniformity of the deposited mats. Furthermore by feeding each spinneret with different

materials, the technique could also be an option for producing blends of electrospun fibre mats; for example a filtration media that consist of different active fibres with specific functionalities (Nurfaizey et al., 2012b).

In Case Study 2 (Chapter 7), an electrode assisted gap electrospinning (EAGE) system was developed by introducing a pair of charged auxiliary electrodes charged with a time-varying voltage. As observed in experiment, random fibres were collected on the shim when no auxiliary electrodes were used (Figure 7-5(b)). However, when the ac charged auxiliary electrodes were introduced, well distributed aligned fibres were deposited between the parallel plates and lying across the shim (Figure 7-5(a)). The results in Chapter 7 proved the hypothesis that the time-varying EFM could be used to improve the alignment and distribution of the aligned fibres in a gap electrospinning system (Figure 7-4). The multi-layer aligned electrospun membrane developed in Chapter 7 can potentially be used to fabricate more complicated 3-D fibre constructs.

8.4 Assumptions and limitations

There were a number of assumptions and limitations that had to be made when conducting this study. The importance of the field strength along the axis of spinning for maintaining consistent electrospinning was considered when positioning the auxiliary electrodes. If the electrodes are located too close to the collector, the resulting electric field in the vicinity of the collector makes the collector less attractive to the charged fibres. The auxiliary electrodes were positioned so that the auxiliary electric field has a minimum effect on the axis field strength; however, it still has sufficient influence on the deposition direction of the fibres. It was observed that the introduction of the auxiliary electrodes did not impede the natural occurrence of bending instability and most importantly, consistent electrospinning process was maintained.

At a given distance between the spinneret and the auxiliary electrodes, the lower limits to the applied voltage at the auxiliary electrodes were investigated. The introduction of a conductor at a potential of 0 kV was found to cause problems, as there is a possibility of this new conductor becoming the effective target electrode. To avoid this, the auxiliary electrodes in Chapter 4 and Chapter 5 were kept at a distance of 100 mm (equivalent to the distance

between the Taylor cone and the collector). For the fibre to deposit on the auxiliary electrode it would either have to leave the Taylor cone at an angle of 90° to the spinning tip or travel a larger distance than to the grounded collector. The jet is unlikely to be ejected at a 90° angle as surface tension in a droplet with a Taylor cone shape would make it energetically favourable to eject the jet from the top of the cone rather than the side. This is only true if the field conditions at 90° to the Taylor cone are of similar or less strength. As designed, the 100 mm distance to the auxiliary electrode use in Chapter 4 and Chapter 5 did not result in any fibre depositing on it at a 0 kV potential.

In conducting the simulations in Chapter 4, several assumptions had to be made. Within the cubic boundary, the simulation is assumed to take place in free space with no atmosphere or gas of any kind so deflection of the particle trajectory which may be caused by friction with air molecules can be neglected. No loss of electric charge to the surroundings occurs and the effect of other geometries in the experimental setup is not considered to be significant.

As mentioned earlier, a linear model adequately describes the relationship between L_{exp} in response to V_d (Figure 4-5). However in simulations, the fitting of polynomial curves appears to improve the fit of relationship between L_{model} in response to V_d slightly (Figure 4-13). A charged particle has a trajectory through space that depends on the applied electric field. As the V_d varies, a higher applied voltage could lead to the charged particle spending less time in the region of higher electric field strength. This is the probable reason for the relationship being slightly non-linear. Nevertheless, the difference between values from the linear and polynomial models is smaller than the maximum standard deviation of the experimental data. Moreover, fitting of linear models to the data produces adjusted R^2 values that already close to unity (0.98-1.00).

Previously, the simulation in Chapter 4 showed that the placement of the auxiliary electrodes at 75 mm from collector produced less traverse electric field at the later stages of fibre flight (Figure 4-11). Therefore in Chapter 5, the auxiliary electrodes were brought forward at about 20 mm from the collector (Figure 5-1). The reason was to maximise the possible magnitude of shift of the deposition area under a certain applied voltage. A minimum 20 mm distance between the electrodes and the collector was found to be adequate to prevent unwanted electrical discharges. The geometry of the electrodes was also changed from cylindrical rods

to flat plates as this shape was found to be more effective in deflecting the jet. One reason would be that the flat shape electrodes caused less divergence of the electric field lines along the axis of deposition (Cui et al., 2011).

Due to geometrical limitation of the experimental setups in Chapter 6 and Chapter 7, exception has to be made on the lower limits to the applied voltage. In Chapter 6, a pair of angled auxiliary electrodes were used to help confine the fibres from depositing on the sides of the rotating drum. This makes the electrodes attractive to the fibres when the applied voltage reaches zero. A minimum base voltage (V_b) of +2 kV was found to be sufficient to prevent the fibres from depositing onto the electrodes. In Chapter 7, the auxiliary electrodes were put close to the collector (15 mm) in order to have enough electric field strength to "squeeze" the deposition area. In achieving this, a minimum base voltage (V_b) of +3 kV was used to prevent the fibres from depositing onto the electrodes.

In Chapter 6, extra caution should be given when considering the minimum distance between inner spinnerets to the auxiliary electrodes, and the distances between adjacent spinnerets. In this study, an adjustable multi-spinneret head was used to give some degree of flexibility to change the distances between spinnerets. At a given voltage, the distance between the inner spinneret and the electrodes must be close enough so that the external electric field imposed by the auxiliary electrodes has a significant influence to the trajectory of the jets. However, adjacent spinnerets need to be kept at an appropriate distance as there is a minimum distance requirement between spinnerets in order to maintain stability in electrospinning.

Previous studies showed that for a particular polymer/solvent system, the final fibre diameter is dependent on concentration/molecular weight irrespective of other processing conditions such as applied voltage, flow rates, and electrospinning distance (Basu et al., 2011, Shenoy et al., 2005). Results from fibre diameter measurement in Chapter 5, Chapter 6, and Chapter 7 are in agreement with the previous finding. When conducting fibre diameter measurements in Chapter 5, Chapter 6, and Chapter 7 the size of a pixel in the SEM image corresponds to an actual size of 30.5, 18.3, 30.5 nm respectively. Whilst, the differences between maximum and minimum mean values were 7.6, 30.4, and 43.9 nm for Chapter 5, Chapter 6, and 7 respectively. Therefore, it is reasonable to assume that any measured variation between

samples that is less than twice of the pixel size could be due to random factors and hence not significant.

However, in Chapter 4 the change in fibre diameter was found significant. The increase in fibre diameter (58.1 nm) was more than double of the pixel size (18.3 nm) and therefore the measured variation cannot be ignored. This seems to be an exclusion from what has been suggested in the previous studies(Basu et al., 2011, Shenoy et al., 2005). In the case when both auxiliary electrodes are charged, the confining of the whipping instability area could cause less thinning resulting in thicker fibres.

Various techniques for measuring the uniformity of fibrous structures have been established in industries ranging from using standard samples to sophisticated image analysis techniques (Chhabra, 2003). In this study, image analysis based on greyscale intensity measurement of a digital image was used to give an approximation of the uniformity of the deposited mats. Previously, the technique has been used in other fields such as nonwoven fibre industries (Bresee et al., 1996) and agricultural (Fant et al., 1994). A greyscale digital image comprises of an array of numbers which represent the intensity of grey shades for each pixel (or picture element which is the smallest addressable element in a digital image) (Russ, 2007). By scanning the samples, the unique information of each sample is converted into the greyscale digital images. To reduce error, the scanned images were calibrated using a photographer's standard grey card (Agfa-Gevaert N.V., Belgium) prior to analysis.

Initially, SEM images were used to investigate the variation of thickness of the deposited mats. Samples were cut using a surgical blade and a guillotine into 10 × 10 mm pieces and put through the standard SEM procedures as mentioned in Section 3.3. A standard SEM tilt jig was used to enable the sample to be viewed from the side. However from the SEM image, it was difficult to make a useful approximation of the deposition thickness as the cutting process changed the structure of the fibres (Appendix 5). SEM samples embedded in epoxy resin were also prepared to preserve the fibre structure. A microtome (Ultrotome 2128, LKB Bromma) was used in order to get a clean cut of the samples. Based on the SEM image, the area where the fibres exist appears as tiny holes due to fibres being partially pulled out during the cutting process and only the area where the fibres intersect with the cutting plane can be

seen (Appendix 5). Therefore it was still difficult to determine the deposited fibre thickness using this method.

A weighing procedure using mass deposition of fibre as a method to predict the density of the deposited mat was also considered. Samples were prepared using the normal procedure but at an extended deposition time of 2 hours to get a significant amount of fibres on the substrate. The substrate were then cut using a special jig into 10 × 210 mm strips with the cutting direction parallel to the drum rotation. The strips were weighed using a four figure balance (Mettler AE200) and compared to control samples (substrate with no fibres). On average, the weight of the strip increased just about 2.5% with the fibres and it was found that the standard deviation of the control strips was too big compared to the actual mass gained due to the fibres. Therefore the weighing method to determine the density of the deposited fibre was inappropriate.

The image analysis technique based on measurements of greyscale value intensities was sufficient for measuring the uniformity of the deposited mats. Even though techniques for measuring the actual thickness of deposited mats have been introduced such as using SEM (Barhate et al., 2006) and contact measurement using a digital micrometer (Aussawasathien et al., 2008), the main concern in this study was to measure uniformity rather than the actual thickness of the deposited mats. In addition, techniques based on SEM and micrometer as demonstrated by Barhate et al. (2006) and Aussawasathien et al. (2008) require such handlings which could damage the delicate structure of the fibres. A non-destructive method such as using white light profilometry technique was preferable (Affandi et al., 2010). However, this method requires the sample to be deposited on a glass surface which in turn will drastically change the deposition pattern of the fibres.

8.5 The advantages of the developed EFM techniques

Compared to conventional methods, there are a number of advantages to using the techniques used in this study:

- Design simplicity - since the method developed in this study is based on EFM the basic equipment required includes auxiliary electrodes and additional power supplies.

Therefore, the design of this system is simple without the need for mechanical componentry.

- Low development and maintenance cost - due to its simplicity in design, the method should require less cost to develop and maintain compared to a mechanical based system.
- Wide operating speed range - without moving component the speed of response of the system is only limited by the speed at which the electrical field can be manipulated (Nurfaizey et al., 2012a). Therefore, it can be operated at a low speed for slow scanning of the deposition area or at a high speed to match the speed of deposition to produce aligned fibres.
- Variability of option - other than sine or triangle wave voltages there are numerous of options available for controlling the applied voltage at the auxiliary electrodes.
- Ease of handling - the method of collecting aligned fibres in Chapter 7 eases the handling of as-spun fibres for further processes without damaging the fibre structure.
- 3-D fibre construct - the method introduced in Chapter 7 also provides the possibility to produce a complex multi-layer aligned fibres at various orientation angles.
- Fibre diameter - based on the results, the method produces fibres within the typical fibre diameter of the material used. This is because the introduction of the auxiliary electrodes does not interfere with the thinning and solidifying process of the fibres.
- Blend of fibres - the method introduced to achieve continuous scanning of multiple jets (Chapter 6) not only capable of eliminating the stripe deposition pattern of a multi-spinneret electrospinning but also capable of producing blends of fibres from different materials.

CHAPTER 9

CONCLUSIONS AND RECOMMENDATIONS FOR FUTURE WORK

9.1 Conclusions

The development, validation, and demonstration of the use of electric field manipulation (EFM) technique to achieve control of spatial location and size of the deposition area were the focus of this study. The main conclusions from this study are as follows:

- The magnitude of shift of the deposition area was found to increase linearly with voltage difference (V_d) between the auxiliary electrodes (Figure 4-5);
- The aspect ratio of the deposition area (ratio of width over height) was found to decrease linearly with the base voltage, V_b i.e. lower of the two auxiliary electrode voltages (Figure 4-7);
- The good fit of the linear models suggest that the magnitude of fibre response to the applied voltage was consistent and repeatable which indicate that EFM is a valid control method (Figure 4-5);
- Simulation results also showed that the x-axis component of the electric field (E_x) which corresponds to electric force F_x was responsible for the shift and reduction of aspect ratio of the deposition area (Figure 4-12(a) and (b));
- A wide and uniform deposition area can be produced from a single jet electrospinning by applying time-varying voltages at the auxiliary electrodes (Figure 5-6);
- The rate of voltage change was found to vary with time when using a sine wave voltage causing the jet to scan at a varying speed within a cycle (Figure 5-7(b)). The variability of the jet's scanning speed produced a two peak distribution pattern. However, the scanning speed of the jet remained at a constant throughout a cycle when using triangle wave voltages producing a single peak distribution pattern;

- It was found that the uniformity of the deposited area can be further improved by using clipped triangle wave voltages. The use of clipped waves enables a controlled stop time at the edges whilst maintaining a constant scanning speed when the jet moves between the edges (Figure 5-10);
- Continuous scanning of the jets using auxiliary electrodes charged with time-varying voltages was able to prevent the formation of a stripe deposition pattern in a multi-spinneret electrospinning system (Figure 6-3);
- The EFM technique using auxiliary electrodes charged with time-varying voltages can also be applied in a gap electrospinning system to improve the alignment and distribution of the fibre (Figure 7-4);
- Finally, the results proved the hypothesis that EFM through a pair of charged auxiliary electrodes could provide a consistent and repeatable control of the deposition area. The future of this technique is promising as there are numerous options available in terms of controlling the applied voltage at the auxiliary electrodes.

9.2 Recommendations for future work

It is recommended that a higher precision positioning of the auxiliary electrodes are used in future research. Due to the symmetry of the applied control field it was expected that the amplitude of the response would be equivalent regardless of which of the two electrodes was held at a higher voltage. As samples in Chapter 4 were collected for both directions, it allows the symmetrical of the applied electric field to be tested. It was found that the field was not perfectly symmetrical and the optimal linear fits to the data did not intersect the origin (Figure 4-5). Within the limits of statistical significance ($p < 0.05$) the gradients of a linear model fitted to either direction of response were equivalent, unlike the intercepts. The lack of symmetry was likely to be due to the imprecision inherent in the method of positioning the auxiliary electrodes (laboratory clamp stands). This is a limitation of the equipment available at the time and the use of a higher precision positioning of the auxiliary electrodes such as using a mechanical linear track system should result in the same deflection response regardless of direction.

It might be expected that modelling a charged particle with mass would give an improved approximation to L_{exp}. However, L_{model} of the charged particle with mass was ~80% less than L_{exp} (Figure 4-13(a) and (b)). The most obvious reasons are the limitations of the current model used in this study. Therefore, it is recommended that if the control algorithm is to be refined then a more complex model is required, considering other factors such as solvent loss and the nature of the whipping instability. Although modelling the electrospun fibre as a charged particle provides sufficient insight into the process to produce a practical control algorithm, it is clearly insufficient to replicate the detailed behaviour of a continuous charged jet of polymer molecules. The magnitude of shift of the deposition area in an actual electrospinning process is also thought to be magnified by the existence of the whipping instability. In the instability region, the helical-like flight path of the fibre presents itself as a number of individual loops travelling towards the collector. An initial offset between the loops due to lateral electric forces will be magnified by the repulsive forces of like charges, meaning that each loop will also push the others away resulting in a greater deflection of the electrospun fibres. Clearly, a single charged particle-type model does not account for this behaviour.

It is recommended that for future research the same study to be conducted using different waveforms. The results in Chapter 5 showed that one can not only change the deposition area using EFM but how the control voltage could be manipulated to improve the deposition area. In Chapter 5, sine and triangle waves were chosen due to simplicity of replicating the waveforms. The use of interface equipment that can execute a control signal to the power supplies would give an unlimited number of possibilities on how the EFM technique can be applied. For example, two special type waveforms with different phases and frequencies can be used depending on the magnitude of shift of deposition area and the jet's scanning speed that are required to suit one's objective.

The results in Chapter 6 showed that the application of time-varying voltage at the auxiliary electrodes can be used to avoid the stripe deposition pattern in a multi-spinneret electrospinning system. It is presumed that it is possible to introduce more spinnerets in the system beyond that of a four-spinneret head as successfully reported with the geometries and parameters used in this work. However, as mentioned earlier an extra caution should be given when considering the distances between the spinnerets and the location of the auxiliary

electrodes. One of the options to increase productivity would be by applying the existing system in arrays to multiply the number of spinneret. However, further investigation is required to exploit this concept in mass production of electrospun fibre.

The multi-layer aligned electrospun membrane developed in Chapter 7 can potentially be used as tissue engineering scaffolds. Studies indicate that aligned electrospun fibres are advantageous as it allow cells to grow and elongate along the fibre orientation directions (Wang et al., 2009, Sundararaghavan et al., 2013). To date, several methods have been demonstrated to produce aligned electrospun 3D scaffolds such as by using patterned collectors (Wang et al., 2010) or in a direct-writing method using melt electrospinning (Dalton et al., 2013). However, cell infiltration through these scaffolds is still a problem due to dense packing of the fibres (Sundararaghavan et al., 2013). The technique developed in Chapter 7 could be a solution to the problem as it allows an initial cell culturing to take place in a single layer before layering the scaffolds into a 3D structure. In addition, the spacing between each layer can easily be controlled depending on the thickness of the shim used to collect the fibre.

In Chapter 7, a minimum gap of 50 mm between the parallel plates is required to achieve gap electrospinning. A wider gap between the plates is favourable as this would allow the use of a bigger shim (currently limited to 30 mm inner diameter) to collect aligned fibres. However, a wider gap between the plates could cause random fibres to be deposited directly on the surface of the plates rather than bridging between them. Another modification on the current apparatus is needed in order to encourage fibre alignment in a wider distance. It is recommended for future research that these parallel plates to be charged with a time-varying high voltage. At an appropriate frequency and voltage, the repulsive and attractive forces generated by the charged plates would be sufficient to encourage the fibres to bridge between the parallel plates even at a wider distance between the plates.

In this study, standard A4 black paper was used as substrate as it gave good contrast for measuring the size and location of the deposited fibres during image analysis. It also cheap, having good dimensional tolerance, and provide ease of handling of the samples. The placement of the black paper in front of the collector had no noticeable effect to the electrospinning process. The conclusion was based on the normal formation of the Taylor

cone, the occurence of the whipping instability, and measured fibre diameters; similar to the ones observed using a stainless steel plate or an aluminium foil as collector. This is in agreement with a previous study by Stanger et. al. (2009) which concluded that a collecting material will only effect the mass deposition rate if it acts completely as an insulator. Another issue that have not been studied in this work is the effect of EFM on the mass deposition rate. Although it was not the focus of this study to quantitatively measure the effect of different substrate materials and EFM on mass deposition rate, however it would be an interesting topic for future research.

The EFM technique is thought to be applicable to all polymer/solvent systems that allow normal electrospinning process to occur. This is due to the fact that fibres are still carrying an amount of electric charge and therefore will get deflected if the electric field is manipulated. In this study, poly(vinyl alcohol) (PVOH) was used as the model material due to simplicity of using an aqueous polymer solution for electrospinning. Preliminary studies also indicated that a similar fibre response to the applied auxiliary electric field was achieved when using polyvinyl butyral (PVB) 15 wt.% in ethanol and Nylon 6 20 wt.% in formic acid. However, more studies are required before a conclusion can be made. Therefore, it is recommended that for future research the same study to be conducted using other polymer/solvent systems.

REFERENCES

ACHARYA, M., ARUMUGAM, G. K. & HEIDEN, P. A. 2008. Dual electric field induced alignment of electrospun nanofibers. *Macromolecular Materials and Engineering,* 293**,** 666-674.

AFFANDI, N. D. N., TRUONG, Y. B., KYRATZIS, I. L., PADHYE, R. & ARNOLD, L. 2010. A non-destructive method for thickness measurement of thin electrospun membranes using white light profilometry. *Journal of Materials Science,* 45**,** 1411-1418.

ANGAMMANA, C. J. & JAYARAM, S. H. 2011. The Effects of Electric Field on the Multijet Electrospinning Process and Fiber Morphology. *Ieee Transactions on Industry Applications,* 47**,** 1028-1035.

ANON. 2011. *DuPont™ Hybrid Membrane Technology* [Online]. DuPont. Available: http://www2.dupont.com/Separation_Solutions/en_US/assets/downloads/DHM702_HMTSheetRev_me05.pdf [Accessed 10 January 2011].

ANON. 2013a. *Nanosan* [Online]. SNS Nano Fiber Technology. Available: http://www.snsnano.com/ [Accessed 10 July 2013].

ANON. 2013b. *Nanospinner24* [Online]. Inovenso. Available: http://www.inovenso.com/portfolio-view/nanospinner24/ [Accessed 10 July 2013].

ARRAS, M. M. L., GRASL, C., BERGMEISTER, H. & SCHIMA, H. 2012. Electrospinning of aligned fibers with adjustable orientation using auxiliary electrodes. *Science and Technology of Advanced Materials,* 13.

AUSSAWASATHIEN, D., TEERAWATTANANON, C. & VONGACHARIYA, A. 2008. Separation of micron to sub-micron particles from water: Electrospun nylon-6 nanofibrous membranes as pre-filters. *Journal of Membrane Science,* 315**,** 11-19.

BARHATE, R. S., LOONG, C. K. & RAMAKRISHNA, S. 2006. Preparation and characterization of nanofibrous filtering media. *Journal of Membrane Science,* 283**,** 209-218.

BASU, S., AGRAWAL, A. K. & JASSAL, M. 2011. Concept of Minimum Electrospinning Voltage in Electrospinning of Polyacrylonitrile N,N-Dimethylformamide System. *Journal of Applied Polymer Science,* 122**,** 856-866.

BAUMGARTEN, P. K. 1971. Electrostatic Spinning of Acrylic Microfibers. *Journal of Colloid and Interface Science,* 36**,** 71-79.

BELLAN, L. M. & CRAIGHEAD, H. G. 2006. Control of an electrospinning jet using electric focusing and jet-steering fields. *Journal of Vacuum Science & Technology B,* 24**,** 3179-3183.

BELLAN, L. M. & CRAIGHEAD, H. G. 2011. Applications of controlled electrospinning systems. *Polymers for Advanced Technologies,* 22**,** 304-309.

BLUM, J. R. & ROSENBLATT, J. I. 1972. *Probability and statistics,* Saunders.

BOLAND, E. D., WNEK, G. E., SIMPSON, D. G., PAWLOWSKI, K. J. & BOWLIN, G. L. 2001. Tailoring Tissue Engineering Scaffolds Using Electrostatic Processing Techniques: A study of Poly(glycolic acid) Electrospinning. *Journal of Macromolecular Science-Pure and Applied Chemistry,* 38**,** 1231-1243.

BOYLESTAD, R. L. 2000. *Introductory Circuit Analysis,* New Jersey, Prentice Hall International.

BRESEE, R. R., DANILUK, T. S., TECH ASSOC, P. & PAPER, I. N. D. 1996. Characterizing nonwoven web structure using image analysis techniques. *1996 Nonwovens Conference.*

BROWN, T. D., DALTON, P. D. & HUTMACHER, D. W. 2011. Direct Writing By Way of Melt Electrospinning. *Advanced Materials,* 23**,** 5651-+.

BURG, J. 2008. *The Science of Digital Media,* Prentice Hall/Pearson Education.

CARNELL, L. S., SIOCHI, E. J., HOLLOWAY, N. M., STEPHENS, R. M., RHIM, C., NIKLASON, L. E. & CLARK, R. L. 2008. Aligned Mats from Electrospun Single Fibers. *Macromolecules,* 41**,** 5345-5349.

CHANG, C., LIMKRAILASSIRI, K. & LIN, L. W. 2008. Continuous Near-field Electrospinning for Large Area Deposition of Orderly Nanofiber Patterns. *Applied Physics Letters,* 93**,** 123111-1-3.

CHHABRA, R. 2003. Nonwoven Uniformity- Measurements Using Image Analysis. *International Nonwovens Journal,* Spring**,** 43-50.

COOLEY, J. F. 1900. *Improved Methods of and Apparatus for Electrically Separating the Relatively Volatile Liquid Component from the Component of Relatively Fixed Substances of Composite Fluids*. United Kingdom patent application 6385.

CUI, X. J., LI, L. M. & XU, F. 2011. Controlled assembly of poly(vinyl pyrrolidone) fibers through an electric-field-assisted electrospinning method. *Applied Physics a-Materials Science & Processing,* 103**,** 167-172.

DALTON, P. D., GRAFAHREND, D., KLINKHAMMER, K., KLEE, D. & MOLLER, M. 2007. Electrospinning of polymer melts: Phenomenological observations. *Polymer,* 48**,** 6823-6833.

DALTON, P. D., JOERGENSEN, N. T., GROLL, J. & MOELLER, M. 2008. Patterned melt electrospun substrates for tissue engineering. *Biomedical Materials,* 3.

DALTON, P. D., VAQUETTE, C., FARRUGIA, B. L., DARGAVILLE, T. R., BROWN, T. D. & HUTMACHER, D. W. 2013. Electrospinning and additive manufacturing: converging technologies. *Biomaterials Science,* 1**,** 171-185.

DEITZEL, J. M., KLEINMEYER, J. D., HIRVONEN, J. K. & TAN, N. C. B. 2001. Controlled Deposition of Electrospun Poly(ethylene oxide) Fibers. *Polymer,* 42**,** 8163-8170.

DERSCH, R., LIU, T. Q., SCHAPER, A. K., GREINER, A. & WENDORFF, J. H. 2003. Electrospun Nanofibers: Internal Structure and Intrinsic Orientation. *Journal of Polymer Science Part a-Polymer Chemistry,* 41**,** 545-553.

DING, B., KIMURA, E., SATO, T., FUJITA, S. & SHIRATORI, S. 2004. Fabrication of blend biodegradable nanofibrous nonwoven mats via multi-jet electrospinning. *Polymer,* 45**,** 1895-1902.

DOSHI, J. & RENEKER, D. H. 1995. Electrospinning Process and Applications of Electrospun Fibers. *Journal of Electrostatics,* 35**,** 151-160.

DOVE, S. B. 2002. *UTHSCSA ImageTool* [Online]. UTHSCSA. Available: http://compdent.uthscsa.edu/dig/itdesc.html.

DROZIN, V. G. 1954. The Electrical Dispersion of Liquids as Aerosols. *Journal of Colloid Science,* 10**,** 158-164.

EARNSHAW, S. 1842. On the Nature of the Molecular Forces which Regulate the Constitution of the Luminiferous Ether. *Trans. Camb. Phil. Soc.,* 7**,** 97-112.

FANT, E., CASADY, W., GOH, D. & SIEBENMORGEN, T. 1994. GRAY-SCALE INTENSITY AS A POTENTIAL MEASUREMENT FOR DEGREE OF RICE MILLING. *Journal of Agricultural Engineering Research,* 58**,** 89-97.

FILATOV, Y., BUDYKA, A. & KIRICHENKO, V. 2007. *Electrospinning of Micro and Nanofibers: Fundamentals and Applications in Separation and Filtration Processes,* New York, Begell House Inc.

FORMHALS, A. 1934. *Process and Apparatus for Preparing Artificial Threads*. United States patent application US1975504.

GILBERT, W. 1600. *De Magnete, Magneticisque Corporibus, et de Magno Magnete Tellure (On the Magnet and Magnetic Bodies, and on That Great Magnet the Earth),* London, Peter Short.

GRAHAM, K., GOGINS, M. & SCHREUDER-GIBSON, H. 2003. Incorporation of Electrospun Nanofibers into Functional Structures. *2003 International Nonwovens Technical Conference.* Baltimore, Maryland.

GRASL, C., ARRAS, M. M. L., STOIBER, M., BERGMEISTER, H. & SCHIMA, H. 2013. Electrodynamic control of the nanofiber alignment during electrospinning. *Applied Physics Letters,* 102.

GREINER, A. & WENDORFF, J. H. 2007. Electrospinning: A Fascinating Method for the Preparation of Ultrathin Fibres. *Angewandte Chemie-International Edition,* 46**,** 5670-5703.

HALLIDAY, D., RESNICK, R. & WALKER, J. 2001. *Fundamentals of Physics,* New York ; Chichester, Wiley.

HEIKKILA, P., SODERLUND, L., UUSIMAKI, J., KETTUNEN, L. & HARLIN, A. 2007. Exploitation of electric field in controlling of nanofiber spinning process. *Polymer Engineering and Science,* 47**,** 2065-2074.

HELLMANN, C., BELARDI, J., DERSCH, R., GREINER, A., WENDORFF, J. H. & BAHNMUELLER, S. 2009. High Precision Deposition Electrospinning of nanofibers and nanofiber nonwovens. *Polymer,* 50**,** 1197-1205.

HUANG, Z. M., ZHANG, Y. Z., KOTAKI, M. & RAMAKRISHNA, S. 2003. A review on polymer nanofibers by electrospinning and their applications in nanocomposites. *Composites Science and Technology,* 63**,** 2223-2253.

HUEBNER, W. C. 1948. *Method and Means of Producing Threads or Filaments Electrically*. United States patent application.

HUTMACHER, D. W. & DALTON, P. D. 2011. Melt Electrospinning. *Chemistry-an Asian Journal,* 6**,** 44-56.

JAEGER, R., BERGSHOEF, M. M., BATLLE, C. M. I., SCHÖNHERR, H. & JULIUS VANCSO, G. Electrospinning of ultra-thin polymer fibers. Macromolecular Symposia, 1998. Wiley Online Library, 141-150.

JAFARI, A., JEON, J. H. & OH, I. K. 2011. Well-aligned Nano-fiberous Membranes Based on Three-pole Electrospinning with Channel Electrode. *Macromolecular Rapid Communications,* 32**,** 921-926.

JIRSAK, O., SANETRNIK, F., LUKAS, D. & KOTEK, V. 2005. *A method of nanofibres production from a polymer solution using electrostatic spinning and a device for carrying out the method*. International patent application WO2005024101.

KAMEOKA, J., ORTH, R., YANG, Y. N., CZAPLEWSKI, D., MATHERS, R., COATES, G. W. & CRAIGHEAD, H. G. 2003. A Scanning Tip Electrospinning Source for Deposition of Oriented Nanofibres. *Nanotechnology,* 14**,** 1124-1129.

KESSICK, R., FENN, J. & TEPPER, G. 2004. The use of AC potentials in electrospraying and electrospinning processes. *Polymer,* 45**,** 2981-2984.

KIM, G., CHO, Y. S. & KIM, W. D. 2006. Stability Analysis for Multi-jets Electrospinning Process Modified with a Cylindrical Electrode. *European Polymer Journal,* 42**,** 2031-2038.

LARRONDO, L. & MANLEY, R. S. J. 1981. ELECTROSTATIC FIBER SPINNING FROM POLYMER MELTS .1. EXPERIMENTAL-OBSERVATIONS ON FIBER

FORMATION AND PROPERTIES. *Journal of Polymer Science Part B-Polymer Physics,* 19**,** 909-920.

LI, D., WANG, Y. L. & XIA, Y. N. 2003. Electrospinning of Polymeric and Ceramic Nanofibers as Uniaxially Aligned Arrays. *Nano Letters,* 3**,** 1167-1171.

LI, D., WANG, Y. L. & XIA, Y. N. 2004. Electrospinning Nanofibers as Uniaxially Aligned Arrays and Layer-by-layer Stacked Films. *Advanced Materials,* 16**,** 361-366.

LIU, L. H. & DZENIS, Y. A. 2008. Analysis of the effects of the residual charge and gap size on electrospun nanofiber alignment in a gap method. *Nanotechnology,* 19.

MELCHER, J. R. & WARREN, E. P. 1971. Electrohydrodynamics of a Current-Carrying Semi-Insulating Jet. *Journal of Fluid Mechanics,* 47**,** 127-&.

MORTON, W. J. 1902. *Method of Dispersing Fluids* United States patent application US705691.

NAYAK, R., PADHYE, R., KYRATZIS, I., TRUONG, Y. B. & ARNOLD, L. 2012. Recent advances in nanofibre fabrication techniques. *Textile Research Journal,* 82**,** 129-147.

NIU, H., WANG, X. & LIN, T. 2011. Needleless electrospinning: developments and performances. *In:* LIN, T. (ed.) *Nanofibers - Production, Properties and Functional Applications.* InTech.

NIU, H. T. & LIN, T. 2012. Fiber Generators in Needleless Electrospinning. *Journal of Nanomaterials.*

NIU, H. T., LIN, T. & WANG, X. G. 2009. Needleless Electrospinning. I. A Comparison of Cylinder and Disk Nozzles. *Journal of Applied Polymer Science,* 114**,** 3524-3530.

NORTON, C. L. 1936. *Method of and apparatus for producing fibrous or filamentary material*. United States patent application US2048651.

NURFAIZEY, A. H., STANGER, J., TUCKER, N., BUUNK, N., WALLACE, A. & STAIGER, M. P. 2012a. Manipulation of electrospun fibres in flight: the principle of superposition of electric fields as a control method. *Journal of Materials Science,* 47**,** 1156-1163.

NURFAIZEY, A. H., STANGER, J., TUCKER, N., BUUNK, N., WOOD, A. R. & STAIGER, M. P. In press. Control of spatial deposition of electrospun fibre using electric field manipulation. *Journal of Engineered Fibers and Fabrics,* 9.

NURFAIZEY, A. H., TUCKER, N., STANGER, J. & STAIGER, M. P. 2012b. Functional nanofibers in clothing for protection against chemical and biological hazards. *In:* WEI, Q. (ed.) *Functional nanofibers and their applications.* Cambridge: Woodhead Publishing.

OGATA, N., SHIMADA, N., YAMAGUCHI, S., NAKANE, K. & OGIHARA, T. 2007. Melt-electrospinning of poly(ethylene terephthalate) and polyalirate. *Journal of Applied Polymer Science,* 105**,** 1127-1132.

PARK, S. H. & YANG, D. Y. 2011. Fabrication of Aligned Electrospun Nanofibers by Inclined Gap Method. *Journal of Applied Polymer Science,* 120**,** 1800-1807.

PETRAS, D., MALY, M., POZNER, J., TRDLICKA, J. & KOVAC, M. 2010. *Rotary Spinning Electrode*. United States patent application 20100034914. Feb 11 2010.

PETRAS, D., MARES, L. & STRANSKA, D. 2008. *Method and device for production of nanofibres from the polymeric solution through electrostatic spinning*. United States patent application US20080307766.

PETRÍK, S. 2011. Industrial Production Technology for Nanofibers. *In:* LIN, T. (ed.) *Nanofibers - Production, Properties and Functional Applications.* InTech.

RAMAKRISHNA, S., FUJIHARA, K., TEO, W. E., LIM, T. C. & MA, Z. 2005. *An introduction to electrospinning and nanofibers,* Hackensack, NJ ; London, World Scientific.

RENEKER, D. H. & CHUN, I. 1996. Nanometre diameter fibres of polymer, produced by electrospinning. *Nanotechnology,* 7**,** 216-223.

RENEKER, D. H., HOU, H. Q., RANGKUPAN, R. & LENNHOFF, J. D. 2003. Electrospinning polymer nanofibers in a vacuum. *Abstracts of Papers of the American Chemical Society,* 226**,** U425-U425.

RENEKER, D. H., YARIN, A. L., FONG, H. & KOOMBHONGSE, S. 2000. Bending instability of electrically charged liquid jets of polymer solutions in electrospinning. *Journal of Applied Physics,* 87**,** 4531-4547.

RUSS, J. C. 2007. *The image processing handbook,* Boca Raton, Fla., CRC ; London : Taylor & Francis [distributor].

SARKAR, S., DEEVI, S. & TEPPER, G. 2007. Biased AC electrospinning of aligned polymer nanofibers. *Macromolecular Rapid Communications,* 28**,** 1034-1039.

SCHREUDER-GIBSON, H., GIBSON, P., SENECAL, K., SENNETT, M., WALKER, J., YEOMANS, W., ZIEGLER, D. & TSAI, P. P. 2002. Protective Textile Materials Based on Electrospun Nanofibers. *Journal of Advanced Materials,* 34**,** 44-55.

SHENOY, S. L., BATES, W. D., FRISCH, H. L. & WNEK, G. E. 2005. Role of chain entanglements on fiber formation during electrospinning of polymer solutions: good solvent, non-specific polymer-polymer interaction limit. *Polymer,* 46**,** 3372-3384.

SHIN, Y. M., HOHMAN, M. M., BRENNER, M. P. & RUTLEDGE, G. C. 2001. Electrospinning: A Whipping Fluid Jet Generates Submicron Polymer Fibers. *Applied Physics Letters,* 78**,** 1149-1151.

STANGER, J., TUCKER, N., FULLICK, S., SELLIER, M. & STAIGER, M. P. 2012. Insights into the power law relationships that describe mass deposition rates during electrospinning. *Journal of Materials Science***,** 1113-1118.

STANGER, J., TUCKER, N. & STAIGER, M. 2009. *Electrospinning*, iSmithers Rapra Publishing.

SUN, D. H., CHANG, C., LI, S. & LIN, L. W. 2006. Near-field Electrospinning. *Nano Letters,* 6**,** 839-842.

SUNDARARAGHAVAN, H. G., SAUNDERS, R. L., HAMMER, D. A. & BURDICK, J. A. 2013. Fiber alignment directs cell motility over chemotactic gradients. *Biotechnology and Bioengineering,* 110**,** 1249-1254.

SUNDARAY, B., SUBRAMANIAN, V., NATARAJAN, T. S., XIANG, R. Z., CHANG, C. C. & FANN, W. S. 2004. Electrospinning of Continuous Aligned Polymer Fibers. *Applied Physics Letters,* 84**,** 1222-1224.

TAYLOR, G. 1964. Disintegration of Water Drops in an Electric Field. *Proceedings of the Royal Society of London A: Mathematical, Physical & Engineering Sciences,* 280**,** 383-397.

TAYLOR, G. 1969. Electrically Driven Jets. *Proceedings of the Royal Society of London A: Mathematical, Physical & Engineering Sciences,* 313**,** 453-475.

TEO, W. E., KOTAKI, M., MO, X. M. & RAMAKRISHNA, S. 2005. Porous Tubular Structures with Controlled Fibre Orientation Using a Modified Electrospinning Method. *Nanotechnology,* 16**,** 918-924.

THERON, A., ZUSSMAN, E. & YARIN, A. L. 2001. Electrostatic Field-assisted Alignment of Electrospun Nanofibres. *Nanotechnology,* 12**,** 384-390.

THERON, S. A., YARIN, A. L., ZUSSMAN, E. & KROLL, E. 2005. Multiple Jets in Electrospinning: Experiment and Modeling. *Polymer,* 46**,** 2889-2899.

TOMASZEWSKI, W. & SZADKOWSKI, M. 2005. Investigation of electrospinning with the use of a multi-jet electrospinning head. *Fibres & Textiles in Eastern Europe,* 13**,** 22-26.

VAN DE VELDE, F., WEINBRECK, F., EDELMAN, M. W., VAN DER LINDEN, E. & TROMP, R. H. 2003. Visualisation of biopolymer mixtures using confocal scanning laser microscopy (CSLM) and covalent labelling techniques. *Colloids and Surfaces B-Biointerfaces,* 31**,** 159-168.

VARESANO, A., CARLETTO, R. A. & MAZZUCHETTI, G. 2009. Experimental Investigations on the Multi-jet Electrospinning Process. *Journal of Materials Processing Technology,* 209**,** 5178-5185.

VARESANO, A., ROMBALDONI, F., MAZZUCHETTI, G., TONIN, C. & COMOTTO, R. 2010. Multi-jet nozzle electrospinning on textile substrates: observations on process and nanofibre mat deposition. *Polymer International,* 59**,** 1606-1615.

VISWANADAM, G. & CHASE, G. G. 2013. Modified electric fields to control the direction of electrospinning jets. *Polymer,* 54**,** 1397-1404.

WANG, Y. & SANTIAGO-AVILES, J. COMSOL-Based Numerical Analysis of The Electric Field Distribution During Electrospinning and Piezo-response Imaging of Ultra-Fine Lead Zirconate Titanate Fibers. Comsol Conference, 2007 Boston.

WANG, Y., WANG, G., CHEN, L., LI, H., YIN, T., WANG, B., LEE, J. C. & YU, Q. 2009. Electrospun nanofiber meshes with tailored architectures and patterns as potential tissue-engineering scaffolds. *Biofabrication,* 1**,** 015001.

WANG, Y. Z., LI, H., WANG, G. X., YIN, T. Y., WANG, B. C. & YU, Q. S. 2010. Electrospinning of Polymer Nanofibers with Ordered Patterns and Architectures. *Journal of Nanoscience and Nanotechnology,* 10**,** 1699-1706.

XIE, S. & ZENG, Y. C. 2012. Effects of Electric Field on Multineedle Electrospinning: Experiment and Simulation Study. *Industrial & Engineering Chemistry Research,* 51**,** 5336-5345.

YARIN, A. L. & ZUSSMAN, E. 2004. Upward needleless electrospinning of multiple nanofibers. *Polymer,* 45**,** 2977-2980.

ZELENY, J. 1917. Instability of Electrified Liquid Surfaces. *The Physical Review,* 10**,** 1-6.

ZHENG, G. F., LI, W. W., WANG, X., WU, D. Z., SUN, D. H. & LIN, L. W. 2010. Precision Deposition of a Nanofibre by Near-field Electrospinning. *Journal of Physics D-Applied Physics,* 43**,** 1-6.

ZHMAYEV, E., ZHOU, H. & JOO, Y. L. 2008. Modeling of non-isothermal polymer jets in melt electrospinning. *Journal of Non-Newtonian Fluid Mechanics,* 153**,** 95-108.

Electrospinz
nanofibre engineering

Model ES4

Double 200mm Laboratory Electrospinning Platform.

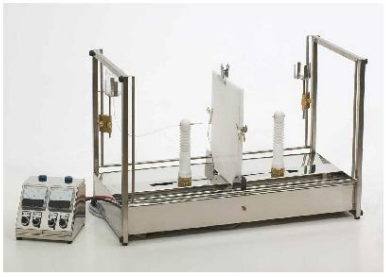

Operation and Maintenance Manual

Specifications

Description:
The ES4 is designed to be used by competent operators in a laboratory environment, using an aqueous solution. Other solutions may be spun but the materials of the hose and spinning tip may need to be changed.

The ES4 is a two-part bench top machine with a solid, easy to clean base. The constant head system is adjustable and has both coarse and fine adjustment. The moveable Spinning head can be set from zero to 200mm from the fixed target plane; this can be adjusted during operation. The power to the spinning heads is adjustable from zero to + or - 33,000 VDC from the separate control box.

Materials:
Base and control box are constructed from stainless steel.
Insulating materials are acetal.
Target plane 300mm x 350mm x 10mm polyethylene (PE)
Electrical connection fittings are brass.
Header tank is glass.
Hose is Polyurethane.
Spinning tip is high density polypropylene.

Power Supply:
Single phase 100 to 240 VAC, 1 amp maximum.
Power supply socket is a DIN standard fitting; most computer cords will fit this.

Contact:
Electrospinz Limited

44 Lee Street
Blenheim 7301
New Zealand

Email: neil_buunk@xtra.co.nz

Phone +64 3578 8092

Safety

High voltage power can present a serious risk of personal injury if not used in accordance with these safety instructions. All users of this equipment must have read and understood the contents of this manual before operation is begun.

The ES4 complies with the relevant New Zealand standards and has been constructed to the electrical part of the BS EN 50 059: 1991 specification for hand-held spraying equipment for non-flammable material for painting and finishing. Although the output voltage can be as high as 33,000 Volts, the maximum output current cannot exceed 0.3mA. No conducting parts of the machine that are not earthed can be touched by the operator during normal operation, provided that these instructions are correctly followed.

Caution:
Static charges may be present on insulated components, even when the equipment is turned off. Users **MUST ALWAYS** earth themselves by holding the metal frame of the ES4 before touching any other part of the equipment.
Electrospun fibres are charged during manufacture, some of this charge is transferred to the depositing area. This charge is very low and provided the user is earthed, is safe to handle.

After the equipment is turned off, the high voltage system will take about two seconds to discharge; do not touch the spinning bush during this time.

Do not use this equipment unless the spinning tip and the feed hose are in place.

Always ensure that there are no volatile gasses near the ES4 during operation as a static discharge could cause ignition.

The high voltage power supplies fitted to the ES4 are rated at 10 Watts, do not overload them. They are designed to be used for electrospinning and are not intended for other uses.

Initial Assembly

Parts check list:

1. ES4 spinning platform and Control box

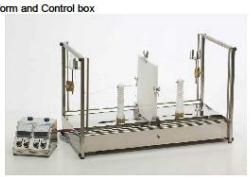

3. Earthing jumper leads 2 off
4. Power cable. 1 off
5. Constant head system. 2 off
6. Hose 2 m
7. Glass header tank 2 off
8. Toolbox containing 1 x allen key set, 1 x 10 / 11mm spanner.

A. Unpack and check that the parts are all present.

B. If the target plane is shipped unmounted. Remove the four machine screws and mount the target plane to the Mounting brackets in the middle of the spinning platform, do not over tighten the screws.

C. Install the constant head system to one of the rods as shown .

D. Plug the spinning platform leads into the back of the control box, the one coded Black is the negative spinning head and the one coded Red is the positive spinning head. These may be connected either way to reflect the current orientation of the machine.

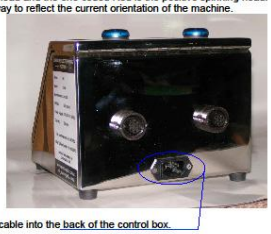

E. Plug the power cable into the back of the control box.

F. Check that the earthed power outlet has a good earth by plugging in the power lead with the switch OFF and checking for Voltage to another earthed point. This check is very important and should be repeated each time the ES4 is used.

G. Turn on the power to the ES4 at the wall, ensure that the HV Adj. Knobs are turned to Zero and turn on one side of the ES4, the blue light for that side on top of the control box should light up.

H. Turn the HV Adj. knob slowly to full power and back, the meter should smoothly move from zero to 33KV and back to zero, repeat steps G and H for the other side.

I. Turn off the ES4, it is ready to use.

Operation

1. Perform assembly tests F. to I. Inclusive before steps 3 & 4 are followed.

Assembly Tests
F. Check that the earthed power outlet has a good earth by plugging in the power lead with the switch OFF and checking for Voltage to another earthed point. This check is very important and should be repeated each time the ES4 is used.
G. Turn on the power to the ES4 at the wall, ensure that the HV Adj. Knob is turned to Zero and turn on the ES4, the blue light on top of the control box should light up.
H. Turn the HV Adj. knob slowly to full power and back, the meter should smoothly move from zero to 33KV and back to zero.
I. Turn off the ES4, it is ready to use.

2. Place the glass header tank in the constant head system.

3. Connect the hose from the header tank to the spinning bush.

4. Insert the spinning tip over the spigot on the other end of the spinning bush.

5. Earth the target area; if this is not done then the fibre will be drawn to the nearest earthed thing. This is not necessarily the ES4; it may be any structure within reach.

6. Pour the prepared polymer into the header tank.

7. Raise the header tank with the course adjustment to the priming position.

8. When the polymer is seen to be almost at the spinning tip lower the header tank to provide a head of about 20mm. This will need to be adjusted once spinning has begun.

9. With the HV Adj. knob turned to zero, turn on the switch. While watching closely; raise the voltage until the Taylor cone appears this is normally visible with the naked eye. Normally only a very slight increase in voltage will initiate the spinning process.

10. Maintain the header tank to hold a small droplet of polymer at the spinning tip. Every now and then, a small droplet will fall from the spinning tip, this is quite normal. A piece of paper may be placed on the ES4 bed between the spinning tip and the target plane to assist with cleaning.

11.If spinning is continued too long then the build up of fibre on the target can be such as to insulate the target and fibre may be deposited in other areas.

Maintenance

Cleaning

A. Remove the header tank, hose and spinning tip. Move these to the cleaning area.

B. Remove the spinning bush as shown, use the 10mm spanner if required.

Do not remove the brass spinning bush holder!
The spinning bush is made from stainless steel and should be thoroughly washed and dried before reassembly.
The spinning tip may be cleaned but is designed as a disposable item.

C. Clean the base of the ES4 with a damp cloth or a cloth dampened with a little solvent. Be careful with solvents around the plastic components as these may be damaged by some solvents.

D. Reassemble in the reverse order, be careful not to over tighten the nut on the spinning bush, finger tight is usually enough.

Servicing

The ES4 has been designed to be serviced without returning it to Electrospinz Limited.

The electrical system must be serviced only by qualified personal and must be maintained in compliance with the relevant local legislation. Replacement components are available world wide and should be obtained locally.

The mechanical components should be serviced by a competent person, any required special parts can be ordered from Electrospinz Limited.

Circuit Diagram

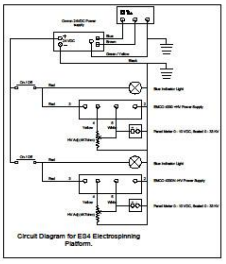

Circuit Diagram for ES4 Electrospinning Platform.

Wire numbers shown are for the Plug, socket, multi-core cable and HV power supply.

Appendix 2 Poly(vinyl alcohol) (PVOH/PVA) material specification

CHANG CHUN PETROCHEMICAL CO., LTD.

NO. 301 SONGKIANG ROAD 7FL., TAIPEI 10477 TAIWAN

TEL: 886-2-25001800 , FAX: 886-2-250333

PVA Grades and Specifications

Revised date : Oct. 20, 2004

By lsshi

1. Standard Grades

Grade	Viscosity[1] (cps)	Hydrolysis (mole %)	Volatile (wt%)	Ash[2] (wt%)	pH[3]
Fully Hydrolyzed					
BF-26	70-80	98.5-99.2	<5	<0.7	5-7
BF-24	58-68	98.5-99.2	<5	<0.7	5-7
BF-24E	58-66	97-98.5	<5	<0.7	5-7
BF-17H	25-30	99.4-99.8	<5	<0.7	5-7
BF-17	25-30	98.5-99.2	<5	<0.7	5-7
BF-17E	25-30	97-98.5	<5	<0.7	5-7
BF-17W	25-30	95-97	<5	<0.7	5-7
BF-14	13-16	98.5-99.2	<5	<0.7	5-7
BF-14W	13-16	95-97	<5	<0.7	5-7
BF-08	8-10	98.5-99.2	<5	<0.7	5-7
BF-05	5-6	98.5-99.2	<5	<0.7	5-7
BF-04	4-5	98-98.8	<5	<1	5-7
BF-03	3-4	98-98.8	<5	<1	5-7
Partially Hydrolyzed					
BP-28	60-70	86-89	<5	<0.5	5-7
BP-26	50-58	86-89	<5	<0.5	5-7
BP-24	44-50	86-89	<5	<0.5	5-7
BP-20	27-33	86-89	<5	<0.5	5-7
BP-20H	27-33	90-93	<5	<0.5	5-7
BP-17	21-26	86-89	<5	<0.5	5-7
BP-14	11-14	86-89	<5	<0.5	5-7
BP-08	8-10	86-89	<5	<0.5	5-7
BP-05	5-6	86-89	<5	<0.5	5-7
BP-04	4-5	86-89	<5	<0.5	5-7
BP-03	3-4	86-89	<5	<0.5	5-7
Sub- Partially Hydrolyzed (* For PVC)					
BC-24*	44-52	78.5-81.5	<5	<0.3	5-7

BC-24P*	38-44	75.5-77.5	<5	<0.3	5-7
BC-20*	36-42	78.5-81.5	<5	<0.3	5-7
BC-20P*	28-33	74-76	<5	<0.3	5-7
TC-07H*	5.5-6.5	76-79	<5	<1	5-7
TC-07P*	5.5-6.5	69-72	<5	<1	5-7
BC-05	5-6	72-76	<5	<0.5	5-7
Low Ash					
BP-17G	21-26	86-89	<5	<0.3	5-7
BP-05G	5-6	86-89	<5	<0.3	5-7

2. Low Foaming Grades

BP-05A	Specification is same as BP-05, and with better defoaming property.
BP-17A	Specification is same as BP-17, and with better defoaming property.
BP-14A	Specification is same as BP-14, and with better defoaming property.
BP-20A	Specification is same as BP-20, and with better defoaming property.
BP-24A	Specification is same as BP-24, and with better defoaming property.

3. Tackified Grades

Grade	Viscosity(4) (cps)	pH
AW-401	4,200 ~ 6,000	4.0 ~ 4.8
AW-201	1,200 ~ 2,000	4.0 ~ 4.8

4. Fine Particle(5) Grades, S-grades

BF-17S	Specification is same as BF-17, and with particle pass 80 mesh screen
BP-05S	Specification is same as BP-05, and with particle pass 80 mesh screen
BP-17S	Specification is same as BP-17, and with particle pass 80 mesh screen
BP-20S	Specification is same as BP-20, and with particle pass 80 mesh screen
BP-24S	Specification is same as BP-24, and with particle pass 80 mesh screen

Remark:

(1) Viscosity of a 4.00 wt % standard grade PVA solution at 20.0 ℃ which is determined by Brookfield Viscometer LVF mode with UL adapter.

(2) Calculated as Na_2O.

(3) pH is determined by pH meter at 20℃

(4) Viscosity of a 10 wt % tackified grade PVA solution which is determined by Brookfield Viscometer at 25℃

(5) Particle size of standard grades is all passes through 10-mesh screen.

Appendix 2 Poly(vinyl alcohol) (PVOH/PVA) material specification

Molecular Weight and Degree of Polymerization of CCP PVA

Grade	Degree of Polymerization	Molecular Weight
BF-26	2,500-2,600	110,000-120,000
BF-24	2,400-2,500	107,000-112,000
BF-24C	2,400-2,500	108,000-113,000
BF-20	2,000-2,100	89,000-95,000
BF-17H	1,700-1,800	75,000-80,000
BF-17	1,700-1,800	75,000-80,000
BF-17C	1,700-1,800	76,000-81,000
BF-17W	1,700-1,800	77,000-82,000
BF-14	1,100-1,200	50,000-55,000
BF-14W	1,100-1,200	50,000-55,000
BF-08	800-900	35,000-40,000
BF-05	500-600	22,000-27,000
BF-04	400-500	18,000-22,000
BF-03	300-400	13,000-18,000
BP-26	2,500-2,650	124,000-130,000
BP-24	2,400-2,500	118,000-124,000
BP-20	2,000-2,100	99,000-104,000
BP-20H	2,000-2,100	99,000-100,000
BP-17	1,700-1,800	84,000-89,000
BP-14	1,100-1,200	54,000-60,000
BP-08	800-1,000	40,000-50,000
BP-05	550-650	27,000-32,000
BP-04	420-550	21,000-27,000
BP-03	300-420	15,000-21,000
BC-24	2,500-2,700	132,000-140,000
BC-20	2,300-2,500	120,000-132,000

Appendix 2 Poly(vinyl alcohol) (PVOH/PVA) material specification

Physical Properties of GCP PVA

- *Appearance:* White to ivory granule or powder
- *Specific Gravity:* 1.23–1.31
- *Bulk Density:* 0.5 –0.7 g/ml
- *Storage Stability:* Indefinite in dry storage
- *Refractive Index at 20°C:* 1.52–1.55 (anhydrous polymer)
- *Specific Heat:* 1.65–1.67 J/g°C (0.1 cal/g°C)
- *Heat of Combustion:* 5.6 kcal/g
- *Mean Coefficient of Thermal Expansion:* 7–10*10^-5/°C
- *Glass Transition Temperature:* 60°C(BP type)–85°C(BF type)
- *Melting Point:* 180 ~ 90°C(BP type), 230°C(DP type)
- *Heat Sealing Temperature(dry, unplasticized):* 165-210°C
- *Compression-Molding Temperature(plasticized):* 100-150°C
- *Heat Stability:* The color turns yellowish gradually when heated above 100°C, turns dark rapidly above 160°C. Decomposes above 200-220°C.
- *Flammability:* Burn at about the rate of paper.
- *Light Stability:* Excellent
- *Effect of Strong Acids:* Dissolves or decomposes
- *Effect of Strong Alkalies:* Softens or dissolves
- *Effect of Weak Acids:* Softens or dissolves
- *Effect of Weak Alkalies:* Softens or dissolves
- *Effect of Organic Solvents:* Resistant to most solvent
- *Gas Permeability:* Effectively resist permeation of gases such as oxygen, nitrogen, and carbon dioxide.
- *Hygroscopicity:* Less sensitive to humidity than other water-soluble resins.
- *Toxicity:* Non-toxic to human and animal.

Appendix 3 LabVIEW™ programs

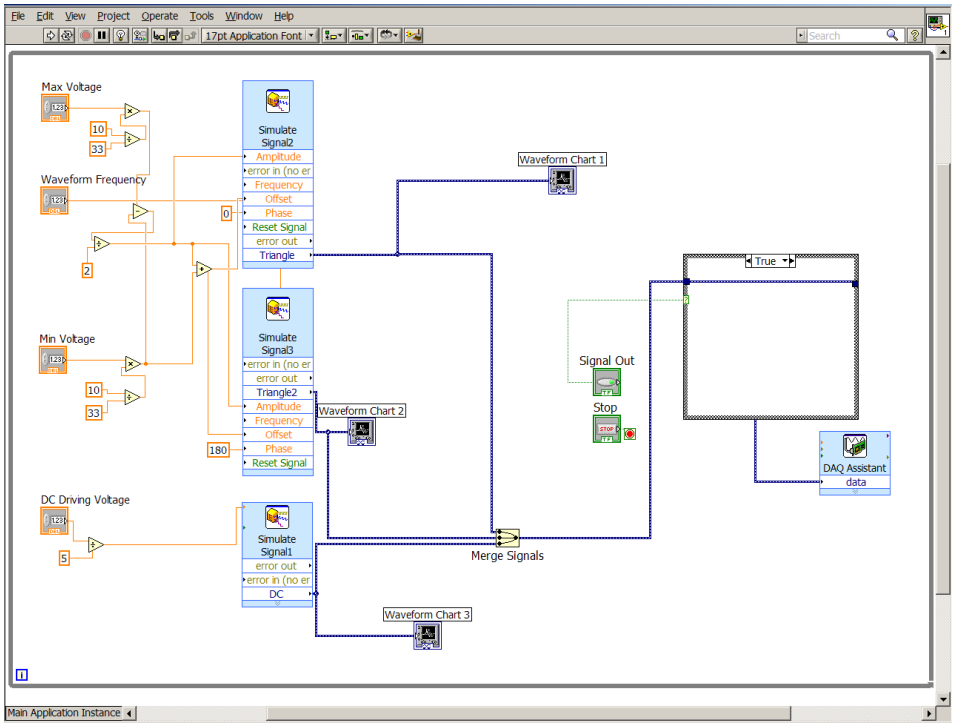

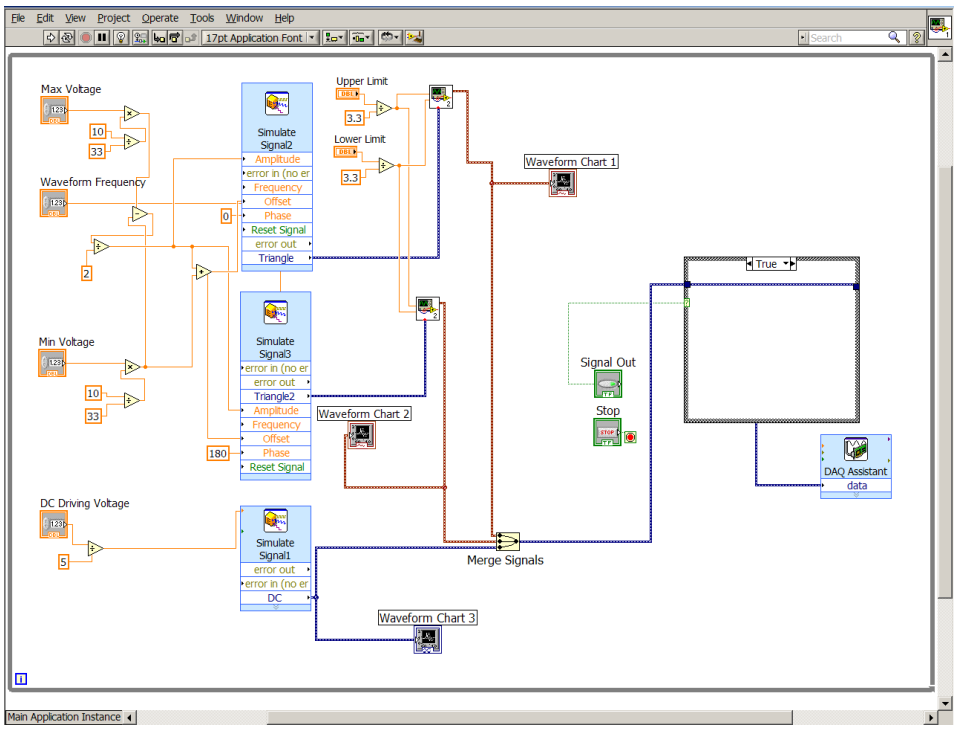

The LabVIEW™ programs used to control the output voltages at the spinneret (V_1) and the auxiliary electrodes (V_2 and V_3). The program used for either a sine or triangle wave voltage (top) and the program used for a clipped triangle wave (bottom).

Appendix 4 Folded fibre

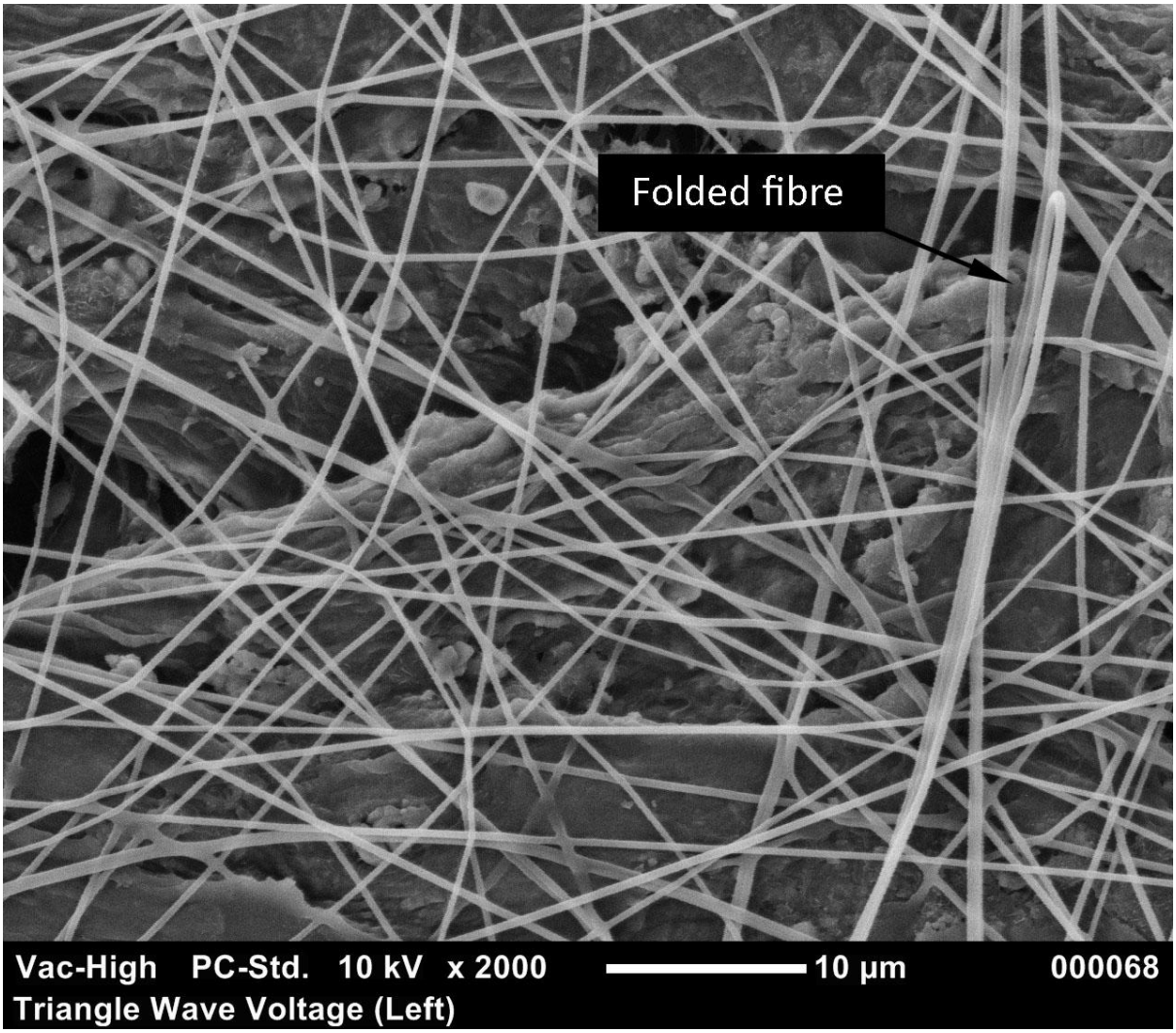

Scanning electron micrograph showing a folded fibres (as seen in Figure 5-13(a))

Appendix 5 Scanning electron micrographs of samples taken from the side

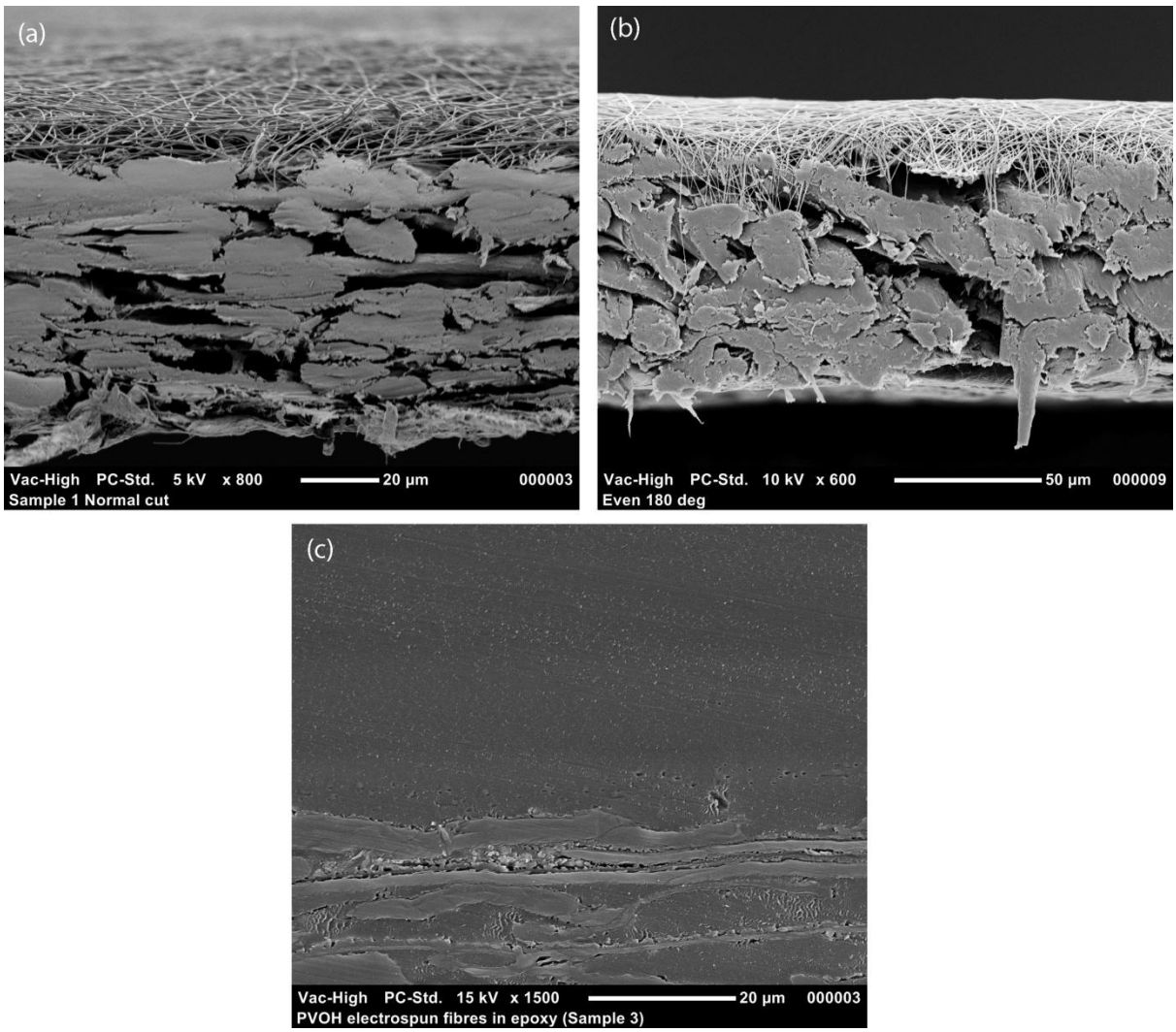

Scanning electron micrograph of PVOH electrospun fibres taken from the side using different methods of sample preparation. Samples were deposited on a paper substrate and cut using (a) a surgical blade, and (b) a guillotine. In (c) sample was embedded and cured in epoxy resin before cut using a microtome machine.